Tapestries Revealed: Novel methods of characterisation, conservation and presentation

A Thesis submitted to The University of Manchester for the degree of Doctor of Philosophy in the Faculty of Engineering and Physical Sciences

2011

Ruth Perkins

School of Materials

Table of Contents

WORD COUNT: 52448

(INCLUDING MAIN TEXT, TABLES AND FIGURES BUT EXCLUDING APPENDICES)

List of Figures

List of Tables

List of Equations

$$\begin{bmatrix} X \\ Y \\ Z \end{bmatrix} = \begin{bmatrix} X_{r,\max} & X_{g,\max} & X_{b,\max} & X_{w,\max} \\ Y_{r,\max} & Y_{g,\max} & Y_{b,\max} & Y_{w,\max} \\ Z_{r,\max} & Z_{g,\max} & Z_{b,\max} & Z_{w,\max} \end{bmatrix} \begin{bmatrix} R \\ G \\ B \end{bmatrix}$$

EQUATION 20 178

$$\begin{bmatrix} X \\ Y \\ Z \end{bmatrix} = \begin{bmatrix} 0.6567 & 0.3306 & 0.1441 & 0.3102 \\ 0.3324 & 0.6408 & 0.0557 & 0.3523 \\ 0.0109 & 0.0286 & 0.8002 & 0.3375 \end{bmatrix} \begin{bmatrix} R \\ G \\ B \end{bmatrix}$$

EQUATION 21 180

Abstract

Ruth Perkins
The University of Manchester
PhD
Tapestries Revealed: Novel methods of characterisation, conservation and presentation
2011

The digital conservation of cultural heritage has received significant attention in recent years. This active area of research endeavors to digitally conserve culturally significant items. The digital archives produced serve as an important resource for conservators. These records allow the accurate tracking of the degradation of the materials used in the construction of these artefacts.

This project outlines the digital conservation and subsequent presentation of a historically significant tapestry held by the Royal Collection at Hampton Court Palace. The tapestry is one of *The Story of Abraham* set constructed by Willem de Kempeneer in Brussels in the 1540s. These tapestries were commissioned by King Henry VIII and were displayed as a reflection of his wealth and power. The materials used in their construction included wool, silk, silver and gold threads.

The objectives of the Thesis are as follows:

1) To digitally conserve the tapestry, the *Oath and Departure of Eliezer*.
2) To produce a colorimetrically accurate projection system. This system will be used to project an accurate representation of the original tapestry colours onto the current photofaded version.
3) To investigate the photo-fading properties of the natural dyes used to produce the *Oath and Departure of Eliezer* and their interactions with the metallic threads woven within the tapestry.

The work presented in this Thesis contributed to a visitor exhibition called "Henry VIII's Tapestries Revealed" held at Hampton Court Palace between April 2009-October 2010 as part of Historic Royal Palaces' celebrations of the 500th anniversary of Henry VIII's accession to the throne.

Declaration

No portion of the work referred to in this thesis has been submitted in support of an application for another degree or qualification of this or any other university or other institute of learning.

Copyright Statement

i. The author of this thesis (including any appendices and/or schedules to this thesis) owns certain copyright or related rights in it (the "Copyright") and she has given The University of Manchester certain rights to use such Copyright, including for administrative purposes.

ii. Copies of this thesis, either in full or in extracts and whether in hard or electronic copy, may be made only in accordance with the Copyright, Designs and Patents Act 1988 (as amended) and regulations issued under it or, where appropriate, in accordance with licensing agreements which the University has from time to time. This page must form part of any such copies made.

iii. The ownership of certain Copyright, patents, designs, trademarks and other intellectual property (the "Intellectual Property") and any reproductions of copyright works in the thesis, for example graphs and tables ("Reproductions"), which may be described in this thesis, may not be owned by the author and may not be owned by third parties. Such Intellectual Property and Reproductions cannot and must not be made available for use without the prior written permission of the owner(s) of the relevant Intellectual Property and/or Reproductions

iv. Further information on the conditions under which disclosure, publication and commercialisation of this thesis, the Copyright and any Intellectual Property and/or Reproductions described in it may take place is available in the University IP Policy (see http://www.campus.manchester.ac.uk/medialibrary/policies/intellectual-property.pdf), in any relevant Thesis restriction declarations deposited in the University Library, The University Library's regulations (see http://www.manchester.ac.uk/library/aboutus/regulations) and in The Univeristy's policy on presentation of Theses.

Publications & Awards

Museums + Heritage Awards for Excellence 2011. *Henry VIII's Tapestries Revealed* was the winner of the Innovations Award, 11 May 2011.

ICOM-CC (International Council of Museums – Committee for Conservation) Triennial 16th Conference, Lisbon, September 2011. Cultural Heritage/Cultural Identity – The Role of Conservation. **Paper accepted**

Perkins, R. M., Owens, H.C., Carr, C. M., Hallett, K., and Gibb, I. 2011. Investigation into the nature of thermal and photo-ageing of tapestry materials. *Journal of Materials Science* (In Preparation, 2011)

The Daily Telegraph – 'Just like new: Henry VIII's tapestry 'virtually restored' to its brilliant best', pg 10, 10 April 2009, plus online article at http://www.telegraph.co.uk/culture/culturenews/5131200/Henry-VIIIs-500-year-old-tapestry-gets-21st-century-makeover.html

The Times – 'New light cast on Tudor tapestry', pg 26, 10 April 2009, plus online article at http://www.timesonline.co.uk/tol/news/uk/article6069988.ece

The Guardian – 'Digital technology makes light of Tudor glory', pg 4, 10 April 2009, plus online article at http://www.guardian.co.uk/artanddesign/2009/apr/10/tudor-tapestry-restoration-digital-photography

BBC – 'Henry VIII's tapestries on show' TV film clip and interview appeared on BBC1 'News at One' television programme, 9 April 2009 with video clip and text online at http://news.bbc.co.uk/1/hi/england/london/7992153.stm. The project was also featured in a programme about Henry VIII shown on BBC4

Manchester University – 'Scientists 'virtually restore' 16th century tapestry at Hampton Court Palace', press release and online article, 10 April 2009, at http://www.manchester.ac.uk/aboutus/news/display/?id=4568 and cover story and article in UniLife, the University's monthly magazine, May 2009

Acknowledgements

I would like to express my deep and sincere gratutide to my supervisors Dr Huw Owens and Professor Chris Carr for their continuous support of my PhD studies, for their patience, understanding, motivation, enthusiam and immense knowledge.

I am indebted to them and to Kathryn Hallett for her knowledge and guidance and her hard work in developing and promoting the recolouration project. I also want to thank Ian Gibb, Constantina Vlachov and the staff of Conservation and Collection Care at Hampton Court Palace for their warm welcome and all their help during my time with them.

This project would not have been possible without the support of the Royal Collection and Historic Royal Palaces and the funding provided by The Clotherworkers' Foundation, The Charles Hayward Foundation and The Dyers' Company.

I must thank Marei Hacke for providing the model tapestry samples which were invaluable to this research, Trevor Jones for SEM/EDX analysis and Alison Harvey for her help with XPS.

I am grateful to my fellow students in Mezz 3 for tea breaks, parties and entertaining conversations and to all those who have been a friend during the completion of this project.

I would particularly like to thank all my family and my amazing friends for their unwavering encouragement, support and love without which I could never have achieved anything. Especially my wonderful parents Austin and Claire Perkins to whom I dedicate this thesis.

1 Introduction

1.1 Hampton Court Palace tapestries

The *Story of Abraham* tapestries at Hampton Court Palace comprises of a set of 10 Flemish tapestries which were commissioned by Henry VIII circa 1541. Each of the tapestries measures approximately 8 metres across by 5 metres high and all are highly detailed, depicting scenes from the Old Testament. The tapestries are some of the most valuable pieces in The Royal Collection. Six are currently displayed in the Great Hall of Hampton Court Palace.

The tapestries are constructed from wool and silk and highly embellished with large areas of silver and gold threads which are woven into the design to enhance the magnificence of the images. Unfortunately the tapestries have lost much of their original visual impact due to physical and environmental degradation. The dyed wool and silk fibres have photo-faded and the metallic threads have tarnished with the result that the overall visual impression of the tapestries has diminished.

1.2 Henry VIII's Tapestries Revealed

'Henry VIII's Tapestries Revealed' was a ground-breaking exhibition that was launched in 2009 as part of Historic Royal Palaces' celebrations of the 500th anniversary of Henry VIII's accession to the throne. The show was conceived to raise public awareness of the important tapestry collections at Hampton Court Palace, their fragile state and the essential conservation work that is carried out to ensure their survival.

The show involved projecting a digitally recoloured image of one of the *Story of Abraham* set, *The Oath and Departure of Eliezer,* onto the tapestry as it hung in The Queen's Guard Chamber of the palace. This digital restoration gave the visitors an impression of how the tapestry would have originally appeared, nearly 500 years ago, before photo-fading of the dyes and tarnishing of metallic threads had occurred.

In order to discover the original appearance of the tapestry, colour measurements were taken of the front and reverse of the tapestry and of model tapestry fabric which had been dyed using natural dyestuffs from the 16th century. This information was used to create a digitally recoloured image that was projected onto the front of the hanging tapestry, restoring it to the original magnificent appearance.

This project demonstrates the use of scientific research in a heritage application to develop an exciting and entertaining way of communicating the important work of conservators.

1.3 Digital conservation

The digital conservation of cultural heritage has received significant attention in recent years. This active area of research endeavors to digitally conserve culturally significant items. The digital archives produced serve as an important resource for conservators; these records allow the accurate tracking of the degradation of the materials used in the construction of these artefacts. The colorimetric information collected during the imaging process can also be used to match prospective restoration materials to portions of the piece which are damaged or degraded. In addition, electronic resources of heritage collections are a modern and safe way of displaying items to the public that would otherwise not be available, without risk of damage.

1.4 Objectives of the research

This project seeks to digitally capture, conserve and "virtually" restore an image of one of *The Story of Abraham* tapestries; *The Oath and Departure of Eliezer.*

In order to secure the support of the Royal Collection it was necessary to ensure that all work on the tapestry was carried out within stringent conservation standards. This involved controlling the amount of light to which the tapestry was exposed throughout the project, complying with the annual light budget for the tapestry that was calculated by the conservators. It was also necessary to carry out all colour measurement and imaging of the tapestry using non-invasive methods, without removing any material or damaging the tapestry in any way.

1.4.1 Determine the original appearance of the tapestry

The *Story of Abraham* set of tapestries has been exposed to extended periods of optical radiation leading to loss of vibrancy and intensity of the coloured yarns. The metallic threads have tarnished, leaving large areas of dark grey that once would have been shimmering gold. In order to determine the original appearance of the tapestry, the ageing characteristics of the materials were investigated.

The reverse of *The Oath and Departure of Eliezer* tapestry has experienced relatively low levels of photo-fading in comparison to the front due to the thickness of the fabric and the lining material stitched to the back that had protected against light exposure. Figure 1.4.1 shows images of the front and reverse of a section of the tapestry, demonstrating the difference in colour due to exposure to light. An impression of the original appearance was gained by taking colour measurements of the reverse and the corresponding areas on the front using a telespectroradiometer (Photo Research PR-655, see Section 5.1). Inspection of the tapestry's reverse revealed substantial areas of colour that were very vibrant but had completely photo-faded to a neutral shade on the front. These areas corresponded to certain dyes that are very sensitive to light, having lost most of their colour within a short period of time. The most significant dye that was completely photo-faded was brazilwood, which can be seen in the loss of pink in the faces of the figures in Figure 1.4.1 and in the wall between the figures. Also the metallic threads were relatively untarnished on the reverse and revealed the large areas of glittering gold that would have amazed viewers of the tapestry during Henry VIII's time. The large areas of dark grey visible in the image on the left in Figure 1.4.1 are tarnished metallic thread whereas they are still gold in the image on the right. The effect of this tarnishing is very detrimental to the subtle colour balance of the design. The gold areas on the reverse were imaged in order to later reproduce them during the projection onto the front.

Figure 1.4.1 Images of a section of the front and reverse of the tapestry *The Oath and Departure of Eliezer*

The photo-fading properties of the natural dyes used to produce *The Oath and Departure of Eliezer* and their interactions with the metallic threads woven within the tapestry were investigated. Reproduction tapestry samples were constructed as part of a previous project, 'Monitoring of Damage in Historic Tapestries'. Wool and silk yarns were dyed using the natural dyes and ingredients that would have been employed in the 16th century, using recipes reformulated from medieval texts. The yarns were then woven into a tapestry structure. The colours of the model dyed samples are indicative of the shades producible at the same time that the *Story of Abraham* tapestries were woven. Model metallic threads were also constructed using gilt-silvered-copper filament wrapped around a silk core.

Accelerated ageing was performed on a selection of the samples in order to determine the fading profiles of each dye, the ageing characteristics of the metallic thread and to discover if metallic thread degradation was affected by its proximity to certain dyestuffs. Photo-ageing was performed for a total of 500 hours in a Xenotest machine and samples were thermally aged using the Oddy test method. Corrosion on the metallic threads was analysed using Scanning Electron Microscopy (SEM), Energy Dispersive X-Ray spectroscopy (EDX) and X-Ray Photoelectron Spectroscopy (XPS). Colour measurement of the unaged and aged fabric samples was performed using a spectrophotometer (Datacolor SF600) to determine the fading profiles of each dye. The total of 500 hours of high intensity radiation in the

Xenotest equates to around 500 years of exposure in typical museum lighting conditions.

The areas of colour on the tapestry were matched to the natural dyes used for the model tapestry samples by comparing the colour difference between the front and reverse to the gradual fading profiles of the dyes. This information was used in the recolouration process to identify distinct areas of dyes and to shift the colour distribution information of these areas towards the original colours of the dyes. It was particularly important to identify those areas on the front of the tapestry that were completely photo faded and to recolour them according to the colour data of the corresponding area on the reverse.

1.4.2 Digital recolouration of the tapestry

One aim of the recolouration project was to provide the visitors with as realistic an impression of the original tapestry appearance as possible so that they might gain a better understanding of how the *Story of Abraham* tapestries would have been perceived at the time.

The display of the tapestry in a dedicated exhibition room has provided the opportunity to highlight the tapestry collection and has stimulated renewed interest in tapestries and their conservation. Visitors can appreciate the size and magnificence of the tapestry when viewed in isolation as well as learning much more about the history and significance of Henry VIII's tapestries than is usually possible. The 'Henry VIII's Tapestries Revealed' show was extremely popular with visitors; it was extended for nine months to a total of 18 months and was seen by over a million people.

The front of the tapestry was imaged while hanging in the Queen's Guard Chamber where the exhibition was held. This image was recoloured using image processing software (Photoshop) and MATLAB. The distinct areas of different dyes within the image were automatically and manually masked and the colour distribution information (in three planes, L*, a* and b*) of these areas was adjusted/shifted to the distributions of the original dyed colour. The areas of tarnished metallic thread were replaced with a sample of an area of unaged metallic thread. The image was projected onto the tapestry and the results were measured using the PR-655 to

ensure that the combination of the colours still present on the front of the tapestry and the over-projection gave the correct result.

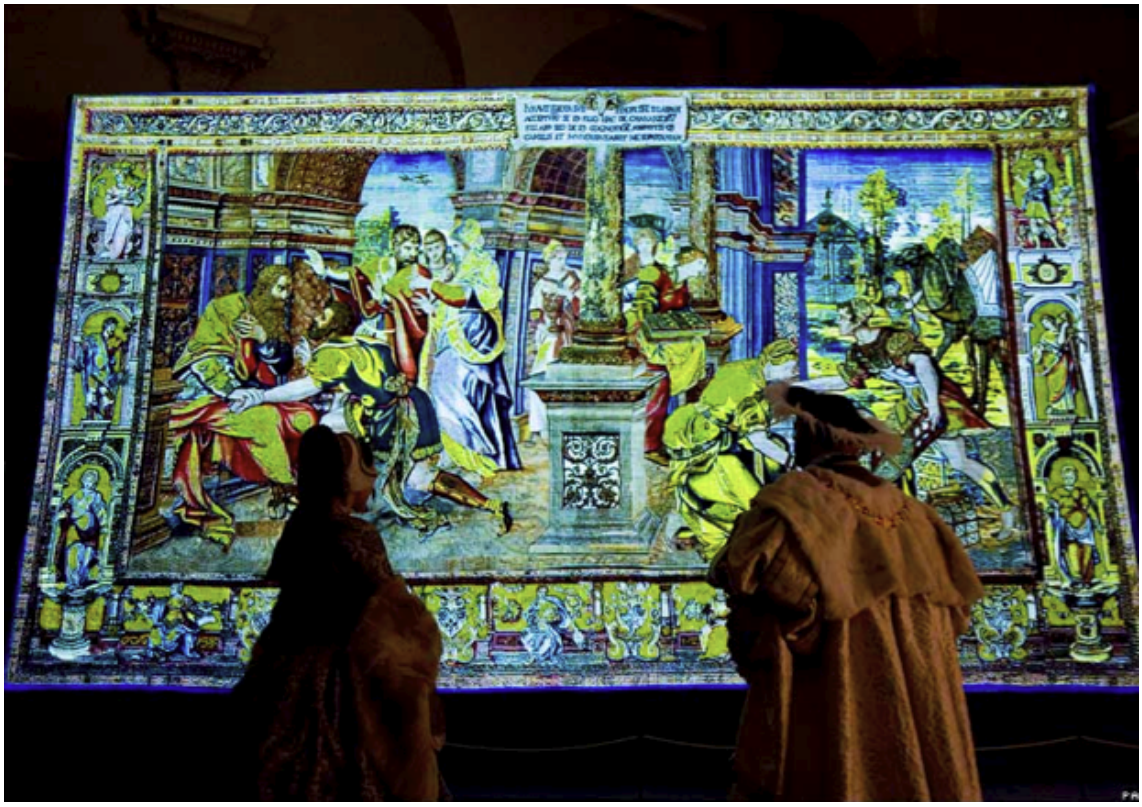

Figure 1.4.2 An image of the recoloured tapestry during the 'Henry VIII's Tapestries Revealed' show

1.4.3 Digital conservation of a colorimetrically accurate image of the tapestry

The digital conservation of the tapestry involved taking high resolution, colour-calibrated hyperspectral images of sections of the front of the tapestry that provided a digital archive of the current colour appearance and condition of the tapestry. The development of an imaging system that captures the spectral information of the tapestry at each pixel produced a more complete and detailed set of data than is possible using a three-channel RGB system.

The hyperspectral imaging system comprised a scientific grade monochromatic 12-bit CCD digital camera, a micro NIKKOR 55mm Nikon lens, and a narrow bandwidth liquid crystal tuneable filter in controlled lighting conditions. The front of the tapestry was imaged from above in 170 sections each with an image size of 50 cm x 50 cm (4.19 megapixels). The hyperspectral imaging system produced 31 monochromatic images taken at a spectral resolution of 10 nanometre (nm) wavelength intervals over the 400 – 700 nm visible range that were subsequently

calibrated and collated to generate precise spectral reflectance data for every pixel. Each component of the imaging system has been calibrated to ensure accurate results and reproducibility. The system as a whole has also been calibrated using the PR-655 telespectroradiometer, which is traceable to NPL standards.

The whole of the front of the tapestry and sections of the reverse were imaged using the hyperspectral imaging system. The digital archives produced serve as an important resource for conservators; the colorimetric data could be applied to future deterioration studies to allow the accurate tracking of the degradation and colour shifts of the materials used in the construction of these culturally significant artefacts.

This project has advanced the conservation application of scientific grade hyperspectral imaging systems and methodologies, generating precise spectral reflectance data of a textiles surface. The imaging methodology was developed in a complex environment where temperature, humidity and light conditions were uncontrolled and variable. As such the methodology can be reproduced in many environments where historic collections are commonly on display.

The data archive on historic dyestuffs for wool and silk has been expanded, providing a range of colour measurements of unfaded and photo faded natural dyes. In addition, information on the corrosion of metallic threads within the tapestry environment has been collected. This research into the fading characteristics of historic tapestries and their materials has led to further knowledge and understanding of these complex processes.

2 Tapestries

2.1 Introduction

"Tapestry is a pictured cloth in which the design is an integral part of the fabric, and not an embroidery stitched on a basic tissue" (Candee, 1935). The oldest tapestries to be found were discovered in ancient Egypt and date back as far as 1400BC. The common understanding of a tapestry, as a large pictoral weaving, developed in Northern regions as a way of decorating and warming cold rooms. The technique spread from the Middle East to France where it became an established industry in which the quality of the materials and labour was highly regulated (Geijer, 1979). This form of art is very costly and time consuming and was therefore restricted to commissions from churches and the nobility. The centre of the tapestry making trade shifted from Paris to the city of Arras and then onto Flanders in the 14th and 15th centuries. The tapestry designs were often painted by renowned artists of the day and these designs were converted into cartoons; templates for the weavers to follow when constructing the tapestries.

At the time of Henry VIII's reign, Brussels was the city where the master weavers had their workshops and the King's advisers dealt directly with the merchants there. During this time, the possession of tapestries was a point of rivalry amongst the monarchs and princes of the European courts and palaces and they became important status symbols (Marillier, 1931). Sets of tapestries were ordered from renowned workshops for usage as decorative furniture which could be easily transported between the different residences of the court. The tapestry designs were often utilised to produce several copies of the tapestries which is evident from records of the time and by the surviving items which exist around the world. For example, it is known that at least six duplicate sets of the *Story of Abraham* tapestries were woven; there is strong evidence to suggest that Henry VIII's set was the first weaving of this design, however, two more sets were produced in the mid sixteenth century, one of which partially survives in the Spanish Royal Collection and the other in the Kunsthistorisches Museum in Vienna (Campbell, 2003). The Hampton Court set and these other two sets carry the mark of one of the most prominent master weavers in Brussels at the time, Willem de Kempeneer (a.k.a.

Pannemaker). The production of a set of tapestries of such fine quality and complexity of design required immense skill and would have taken at least two years to weave, being delivered to the Great Wardrobe of Hampton Court between 1543 and 1544 (Campbell, 2003). The enormous scale and complexity of the tapestries is further enhanced by the finest quality of materials used in their construction as they contain a large percentage of silk and gilt-metallic threads. The richness of the Hampton Court set surpasses the copies which are woven only in wool and silk and do not contain the vast amount of gold and silver threads. This fact contributes to the belief that Henry VIII owned the first weaving of this design and that by commissioning such a sumptuous set of tapestries, the Tudor Court sought to proclaim its magnificence to the rival European courts.

2.2 Historical aspects

It was not only the sheer opulence of the tapestry set, denoting Henry VIII's wealth and power, which reflected upon the English King and the Tudor Court. The iconography of the designs intended to portray Henry as a patriarch to his people during the English Reformation by comparing him to one of the great figures of the Old Testament, Abraham.

The *Story of Abraham* set is made up of ten scenes depicting important events of Abraham's life as written in chapters 12 to 24 of the book of Genesis (Appendix A). The focus of the tapestry designs is on Abraham's role as the founder of the Hebrew nation, God's covenant with Abraham, the birth of his son Isaac and the continuation of Abraham's agreement with God through Isaac. The names of the tapestries are given in Table 2.2.1.

Table 2.2.1 Order of the Story of Abraham tapestries in accordance with the Book of Genesis

1	Departure of Abraham
2	Return of Sarah
3	Separation of Abraham and Lot
4	Meeting of Abraham and Melchizedek
5	God Appears to Abraham
6	Circumcision of Isaac
7	Sacrifice of Isaac
8	Purchase of the Fields of Ephron
9	Oath and Departure of Eliezer
10	Eliezer and Rebekah at the Well

These themes are very significant to Henry's life during the 1530s and 1540s when the Tudor court was separating itself from Rome, after the divorce from Catherine of Aragon, with Henry's assertion that he was the head of the English church rather than the Pope. Henry sought to establish a new Church of England and the model of Abraham leading his people into a new land served as propaganda for this cause.
The story of God appearing to Abraham to promise him a son and successor is resonant with the birth of Henry's long-awaited son Edward in 1537. Henry finally had an heir to carry on the Tudor line and to continue as the spiritual and secular leader of his people (Campbell, 2003). Although it cannot be conclusively proven that the designs were conceived at Henry's request, the subject and patriarchal analogies of the designs were certainly resonant for Henry, his son Edward and the Tudor court at the time.

The *Abraham* tapestries were very important to the King's collection as they were extremely expensive to commission due to their scale, gold and silver content and number. They have been noted throughout the centuries for their beauty and magnificence above all other sets in England and Europe. The tapestries were utilized on the grandest occasions such as the signing of the peace treaties with France in 1546 and Spain in 1630. It is believed that the set was intended for use on ceremonial occasions in the Great Hall of Hampton Court and possibly for use during the coronation of Henry's son Edward VI based on evidence that the tapestries were subsequently hung in Westminster Abbey for the coronations of Charles II and James II. Succeeding Henry VIII, the set was highly prized amongst

the following monarchs and was regularly transported to London on barges to decorate Whitehall Palace for example (Band, 2006).

The intermittent usage of the *Story of Abraham* tapestries during Henry's reign have contributed to their relatively well maintained condition since they were not subjected to damaging light radiation or environmental effects continuously. The court of Henry VIII moved between many different residences and so the tapestries would be packed up and only displayed when Henry was entertaining guests of the highest nobility. This practice of removing the tapestries from display reduced the amount of light which the tapestries were subjected to but would increase the chance of physical damage as the pieces were taken on and off the wall.

2.3 Environmental conditions

The conditions that a historic tapestry has endured since its production, and not just its age, will determine the level of degradation which it has suffered. The amount and quality of light, temperature and humidity to which the tapestry has been subjected, how much it has been handled, any washing or conservation treatments applied and how it has been displayed will all contribute to the degraded state of the materials. Due to the inconsistency of records, it is not usually possible to establish the history of a tapestry; however, the significance of the *Story of Abraham* tapestries has resulted in a fairly comprehensive account of this set of historic tapestries over the years. Records exist of an inventory of Henry VIII's tapestry collection that was taken after his death in 1547. Details of any work carried out on the collection were noted in the annual accounts of the Great Wardrobe and in inventories that were taken when a new keeper of the houses was appointed. These sources record the contents of the collection and sometimes the condition of the tapestry pieces.

The condition of the King's tapestries was assessed and recorded in the Great Wardrobe and if a piece began to degrade then the keeper of the wardrobe would evaluate the tapestry with regard to its financial and artistic value and also its contribution to the overall splendor of the court. The records from the wardrobes indicate that significant levels of time and money were invested in the upkeep of the King's tapestry collection.

In addition, many of the tapestry conservation methods in use today were already well established within the royal household in the 16th century such as brushing to remove surface dirt, lining and woven repairs which were carried out by specialist craftsmen (Hayward, 2006).

In subsequent centuries, the *Abraham* set of tapestries became more frequently displayed due to it still being regarded as the highest quality set in England. The *Abrahams* remained in the royal collection after being reserved by Cromwell when much of the country's valuable items were sold after Charles I's execution. Once the monarchy was restored, the tapestries were displayed during the Coronation ceremonies of Charles II, James II and George II. The almost permanent display of the set at Hampton Court since the early 1700s unfortunately has resulted in the accelerated tarnishing of the metallic threads. From the Victorian era onwards, restoration of the tapestries has been suspended and replaced with conservation treatments to impede further deterioration using scientific research and innovative techniques.

The main cause of degradation in textile fibres is exposure to light resulting in discolouration of the material, fading of dyestuffs and loss of mechanical strength of the fibres (Hacke, 2006). In addition, pollutants in the atmosphere can cause chemical degradation of the materials and corrosion of any metallic components. Displaying the tapestries hanging inflicts a tremendous amount of strain on the vertical weft threads resulting in yarn breakages and holes appearing in the tapestry. To combat this effect, linings are stitched to the reverse of the tapestry from which the pieces are hung, reducing the tension on the historic threads (Hayward, 2006).

2.4 Tapestry materials and construction

The *Story of Abraham* tapestries are constructed from a wool warp at 18 ends per inch woven with wool, silk and silver and gilt-metallic threads. Each of the ten tapestries measures approximately 8 metres in width and 5 metres in height with *The Oath and Departure of Eliezer* covering 853 x 487cm (Figure 2.4.1). The design of each tapestry in the series comprises a central scene relating to an event from Abraham's life surrounded by an ornate border depicting symbolic figures which

relate to the story. There is an inscription above the main scene which describes the story as from the book of Genesis.

"And the servant put his hand under the thigh of Abraham his master, and sware to him that he would take a wife for Isaac not from among the daughters of the Canaanites, but of his own kindred. And the servant took ten camels, and the goods of his master, and went to Mesopotamia" (Genesis 24, 9-10).

Figure 2.4.1 The Oath and Departure of Eliezer, from The Story of Abraham, c. 1541-1541, Willem de Kempeneer (Brussels). Wool, silk and gilt-metallic thread, 487 x 853cm. Hampton Court Palace, Royal Collection.

The tapestries woven in Brussels in the sixteenth century were manufactured using two different techniques; a high-warp or *haute lisse* loom wherein the warps are held vertically or the low-warp or *basse lisse* loom having a horizontal warp. The undyed woollen warp threads form the support structure onto which the design is built up by weaving coloured weft threads in only the required areas. This means that the weft threads do not continue across the entire width of the fabric resulting in the appearance of slits where two distinct coloured areas meet. The slits run parallel to the warp and are sewn up with needle and thread on completion of the tapestry which imparts more strength in the fabric (Hunter, 1925; Candee, 1935).

The warp yarns are held under high tension during weaving with the consequence that, when removed from the loom, the fabric will contract along its length. The designs are adapted to suit this effect whereby the pattern is woven perpendicular to the warp direction. In this case, upon shrinkage, the figures in the design will appear to become slimmer and lengthened which is more desirable than the

alternative; a shortening and widening of the figures. Therefore it occurs that most large-scale tapestries are in the landscape format with a horizontal warp direction. The disadvantage of this system is that, being hung from the top edge, the weft yarns are subjected to the weight of the tapestry. Consequently the stitches which hold the slits together are strained and can break causing holes in the tapestry while the weft yarns themselves are subjected to large strains which can result in loss of structural integrity. The addition of a lining to the reverse of the tapestry, stitched at small intervals over the whole area, supports the weft threads by reducing the amount of strain on them, a practice that has been carried out on the *Story of Abraham* tapestries at Hampton Court.

The Hampton Court set of *Abraham* tapestries are woven with wool, silk and metallic thread wefts. This variation of materials is used artistically to provide a contrast in texture between different areas of the design. Wool was often used for weaving the areas of dull and dark colours while the delicate yellows, blues, greens and pinks were in silk (Hunter, 1925). The silk adds a lustre to the coloured areas which serves to enhance the beauty and impact of the tapestry. Metallic threads woven into the tapestries add glinting effects, being used especially in the garments of the figures in the designs. In some areas of the borders, metallic threads pass over up to 3 warp ends, creating areas of intense shine sumptuously glittering in the light.

The metallic threads were constructed by wrapping a very thin strip of metal foil, typically ≈300 micrometers (μm) wide, around a core silk yarn. The silk core was yellow or white, depending on whether the final thread would be gold or silver respectively. The lengths of metal foil were produced by drawing a gilt silver and copper rod then flattening the resulting wire between two pressured rollers to create a thin strip. The lengths of metal were then spun around the silk core. This method of winding metal filaments about a fibre core came into practice in about the fifth century BC in the Middle East and Eastern Mediterranean regions. The resulting threads were more flexible and easier to manage than the simple lengths of metal filaments woven directly into fabric previously (Rogerson & Garside, 2006). A study of the structure of 110 samples of metallic threads from one of the

Story of Abraham tapestries found 7 samples which had two layers of metal filament wrapped around the silk core (Hacke *et al*., 2003).

2.5 Natural dye properties

The range of dyes which were used during the sixteenth century to dye the fibres used in tapestry weaving were derived from many plant sources, insects, lichen, fungi and molluscs. Their properties varied widely so that the tapestries as we see them today contain some colours which are close to the originals in shade and strength whereas some of the dyes have faded more significantly. The properties of a selection of commonly used natural dyes are shown in Table 2.5.1; however, the success and fastness of the dyeing often depended as much on the skill of the dyer and the dye recipe as the properties of the dyestuff (Geijer, 1979).

Table 2.5.1: Origin, shades and fastness of natural dyes commonly used to dye tapestry materials (Hacke 2006)

Dye	Origin	Colours Attained	Fastness	Dyestuff Group
Madder	Root of madder plant	Reds	Good with mordanting	Anthraquinones
Cochineal	Dried insects	Reds	Good with mordanting	Anthraquinones
Brazilwood	Heartwood of brazilwood tree	Reds	Poor	Neoflavanoids
Dyer's Greenweed	Plant leaves, flowers and twigs	Yellow	Moderate	Flavonoids
Weld	Plant	Bright Yellow	Moderate	Flavonoids
Young Fustic	Heartwood of plant	Deep Yellow	Poor	Flavonoids
Woad/Indigo	Leaves of woad plant	Blues	Very Good	Indigoids
Oak Gall	Growths on oak tree	Used as a mordant or with iron (II) sulphate to give black dyes	Good	Gallotannins
Alder Bark	Bark	Brown or with iron (II) sulphate to give black dyes	Good	Tannins/ Flavonoids

Green shades were obtained by over-dyeing a yellow material with blue dye to produce a wide range of green shades, unfortunately the inferior fastness properties

of yellow dyes results in these green areas ultimately turning blue. This effect is noticeable in the *Abraham* tapestries where the areas of grass and trees appear blue.

Upon inspection of the tapestries, the fastness properties of natural dyes can be detected; the red and blue shades are still strong while there is little evidence of the bright yellows and greens known to be producible using the sources of dyes available at the time.

Hacke (2006) studied accelerated aged wool and historic wool samples. The chemical deterioration of wool was characterised by the loss of sulphur, nitrogen and the 18-methyl eicanosoic (MEA) lipid. The loss of sulphur occurs when the covalent disulphide bonds oxidize and break leading to reduced fibre cohesion and therefore loss of tensile strength that leads to the increased fragility of historic tapestries (Carr *et al.,* 2004). Photo-degradation of silk is symptomised by the loss of amino acids such as tyrosine due to oxidation and hydrolysis reactions which release nitrogen containing gases and result in loss of tensile strength. Yellowing of silk is caused by exposure to light in 'real' and 'simulated' environments (Howell *et al.,* 2007). Hacke (2006) also found that alum mordanting had a strengthening effect on wool fibres whereas dyeing with weld, dyers greenweed, oak gall mordanting and black dyeing weakened the fibres.

2.6 Corrosion of metallic threads

Corrosion of metallic threads in tapestries depends largely on the tapestry's history and its exposure to atmospheric and environmental conditions which would cause chemical deterioration. Degradation of metallic threads can also be of a physical nature whereby the gilt layer may be abraded and metal filaments may break due to handling and tension during display. Gold has a very low reactivity and is therefore resistant to corrosion; however, the layer of gilding is thin so that any faults in or abrasion of the gold layer will result in exposure of the silver and copper underneath (Tronner *et al.*, 2002). Silver ions are also highly mobile so that over time they can move through the outer gold layer to the surface, silver corrosion will occur and can spread over the surface of the gold layer.

The corrosion of silver and copper will occur only in the presence of oxygen and water. The main corrosion products contain sulphur which is found in atmospheric pollution and from the degradation of wool. Corrosion products containing chlorine arise from salt in the atmosphere, salt used in dyeing and from contamination from perspiration during handling. Silver sulphide corrosion in the metallic threads results in a dark grey or black product on the surface while copper corrosion products are firstly reddish-brown turning greenish-blue (Hacke, 2006). The detrimental effect of metallic thread corrosion in the *Abraham* tapestries can be seen in Figure 2.6.1 where the areas of once sparkling gilt-silver threads have corroded resulting in dull grey patches on the shoulder, arm and leg of the left-most figure, Abraham.

Figure 2.6.1: Detail from *The Oath and Departure of Eliezer* showing grey patches of metallic thread corrosion

2.7 Light budgets

The amount of light to which the *Abraham* tapestries are exposed must be controlled in order to limit the further photo-fading and degradation of the materials as much as possible. Many institutions compose light budgets for their artifacts, by which a maximum level of radiation is designated to an object for a period of time, to which the museum conditions can be adapted. The conditions at Hampton Court Palace in which the tapestries are displayed are closely monitored using light sensitive equipment to measure the amount and variability of light in the Great Hall where the tapestries have been traditionally displayed, however, the location is inherently difficult to control. Displaying the tapestries in their original position allows the visitors to gain a better impression of their historical significance but the hall is far from museum conditions. There are many windows around the hall through which natural sunlight passes through coloured stained

glass. The light varies greatly throughout the day and around the year. Measurements taken in the Great Hall at midday on 22/01/2008 using a spectroradiometer (PR-655, see Section 4.5.1.2) found that the light that fell on the tapestries on the North and South walls varied greatly. The luminance and colour temperature of the light on the South wall were 28 $cd.m^{-2}$ and 2812 K respectively whereas on the North wall the values were 82 $cd.m^{-2}$ and 4700 K. There are artificial lights situated around the hall also which serve to illuminate both the tapestries and the surrounding architectural features. This combination of sources renders a controlled environment unobtainable, despite which the conservators at Hampton Court aim to manage light levels as effectively as possible.

The issues regarding the light budget of The Oath and Departure of Elizer tapestry as part of this project relate to the illumination of the tapestry during imaging and of the projection system casting light onto the tapestry during the exhibition. Illumination of the tapestry was unavoidable in order to maintain good imaging practice in which the optimal conditions are to have a single known light source in a light controlled environment. Exposure to increased radiation was inevitable but was kept to the minimum level possible, as with the projecting system. The projection of the colour-modified tapestry image onto the hanging tapestry was an intermittent event which was scheduled to occur five times per day, at carefully scheduled intervals, for a duration of around five minutes each.

The conservators at the Palace formulated an annual light budget for the tapestry which is 150,000 lux.hours. During the planning of the exhibition thorough calculations of the light budget ensured the annual light dose that the tapestry was going to receive would comply with that limit. These calculations included the light exposure from the projector along with the ambient light in the Queen's Guard Chamber. The light monitoring during the original length of the exhibition, from April 2009 to January 2010, showed that the actual light exposure was 100,000 lux.hours which was 50,000 less than the acceptable light level. This lower-than-predicted exposure, combined with the popularity of the show led to the exhibition being extended until the end of October 2010.

3 Physical Characterisation of tapestry materials

The *Story of Abraham* tapestries are constructed from wool and silk and highly embellished with large areas of silver and gold threads, which are woven into the design to enhance the magnificence of the images. Unfortunately the tapestries have lost much of their original visual impact due to physical and environmental degradation. The dyed wool and silk fibres have photo-faded and the metallic threads have tarnished with the result that the overall impression of the tapestries has diminished. The nature of the tapestry materials and their ageing characteristics have been investigated in order to model their degradation and subsequently predict the original appearance of *The Oath and Departure of Eliezer.*

The photo-fading properties of the natural dyes used to produce *The Oath and Departure of Eliezer* and their interactions with the metallic threads woven within the tapestry were simulated using tapestry reproductions. Hacke constructed the model samples as part of a European Commission funded project, *Monitoring of Damage in Historic Tapestries* (MODHT) (Hacke 2006). Model tapestry fabric was woven from wool and silk yarns representative of historic tapestry materials. The yarns were dyed using the natural dyes and ingredients that would have been used at the time of the *Abraham* tapestries construction, using recipes re-formulated from medieval texts. Model metallic threads were also constructed using gilt-silvered-copper filament wrapped around a silk core.

Accelerated ageing was carried out on a selection of the samples in order to determine the fading profiles of each dye, the ageing characteristics of the metallic thread and to discover if metallic thread degradation was affected by its proximity to certain dyestuffs. Previous investigation of the model tapestry fabrics found that dyeing and mordanting procedures produce alterations in the physical and chemical properties of the threads while the stiffness and crystallinity of fibres is reduced after photo-ageing (Odlyha *et al.,* 2005).

3.1 Tapestry materials

3.1.1 Wool

A summary of the morphology of the wool fibre and its chemical composition is given here as a basis for investigation into the ageing characteristics of model dyed tapestry fabrics.

Fine wool fibres consist of two types of cell; the bulk of the fibre is made up of cortical cells and the cuticle cells form the outer layer surrounding the core, see Figure 3.1.1. The cuticle cells form the overlapping scales on the wool fibre and comprise an enzyme-resistant exocuticle and an enzyme-digestible endocuticle surrounded by a thin hydrophobic membrane, the epicuticle. The cuticle is generally only one cell thick and is separated from the cortical cells by the cell membrane complex, often called intercellular cement for its adhesive properties (Maclaren & Milligan, 1981).

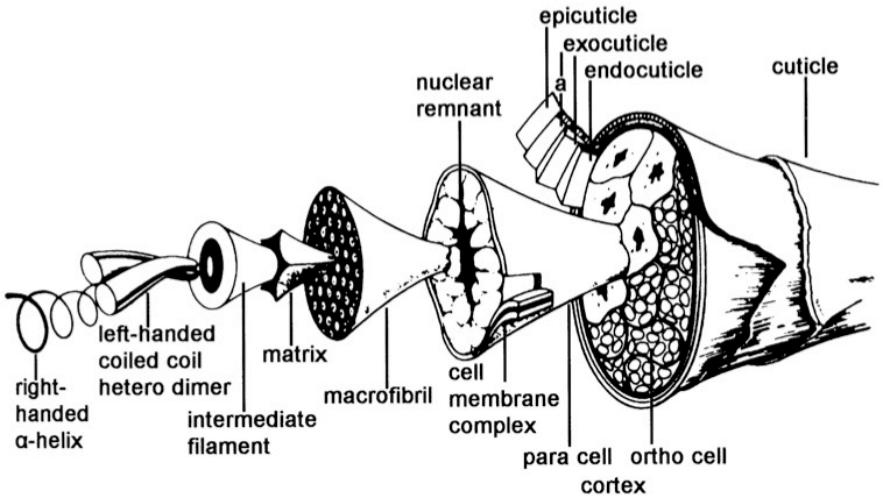

Figure 3.1.1 Morphology of a wool fibre (Rippon, 1992)

Figure 3.1.2 shows a model of the layers that make up a cuticle cell; the outermost layer comprises a lipid monolayer (18-MEA) covalently bound to the outer β-layer and epicuticle beneath that are rich in cysteine, cystine, lysine and glutamine (Hacke, 2006). The thickness of the epicuticle has been measured at ≈7 nanometres (nm) and the lipid layer ≈1 nm although dimensions of the cuticle layers are not generally agreed upon.

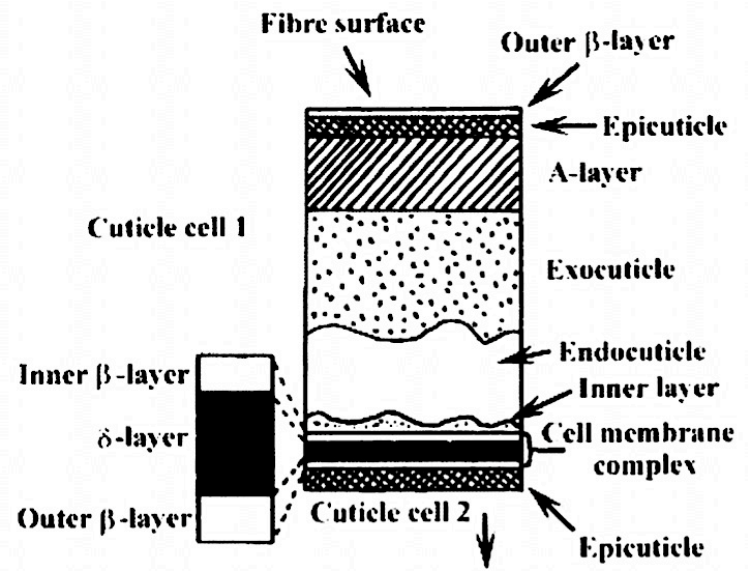

Figure 3.1.2 Schematic of the layered structure of wool cuticle cell (Swift & Smith, 2001)

Wool is a keratinous fibre, composed of approximately 97% of proteinaceous material, which is made up of 21 amino acids. Fatty acids, in particular the 18-methyl eicanosoic (18-MEA) lipid, present on or near the fibre surface account for approximately 2% of the wool by weight and impart the wool's hydrophilic nature. Removal of the outer layer of lipids increases the wettability and therefore dyeability of wool (Rippon, 1992; Zahn, 1997). Wool fibres, and their amino acid content show great variation depending upon breed of sheep, diet, climate and other influences (Maclaren & Milligan, 1981). A selection of data for the amino acid composition is given in Table 3.1.1 and the range of bonds that exist between the amino acid groups is illustrated in Figure 3.1.3. The fibre properties, such as tensile strength and insolubility, are controlled by these crosslinks, most important of which is the disulphide cystine links. The cuticle cells are sulphur rich and contain a large amount of disulphide crosslinking with the measured percentage compositions of amino acids in the cuticle comprising 35% cysteine (Hacke, 2006). The fatty acid composition at the surface of the fibre has about 68% 18-MEA lipid, which binds to the cysteine residues in the outer layers of the cuticle by thioester linkage.

The physical and chemical properties of the fibre are governed by the cell membrane complex, which separates the cuticle cells from the cortex and isolates individual cortex cells. This intercellular cement structure, around 25 nm thick, contains low levels of protein.

Table 3.1.1 Amino acid compositions of wool fibres

Amino acid	**Residue percentage**			
Alanine	5.2	4.5	5.4	5.8
Arginine	6.2	6.5	6.9	7.7
Aspartic acid (a)	5.9	5.4	6.6	6.9
Glutamic acid (b)	11.1	11.1	11.9	12.1
Glycine	8.6	7.5	8.2	7.0
Cysteine (c)	13.1	10.2	10.0	10.7
Histidine	0.8	0.6	0.8	0.7
Isoleucine	3.0	2.5	3.1	3.3
Leucine	7.2	6.3	7.7	7.9
Lysine	2.7	2.1	2.8	3.4
Methionine	0.5	0.4	0.4	0.6
Phenylalanine	2.5	2.7	2.8	2.6
Proline	6.6	6.9	7.2	6.4
Serine	10.8	9.4	10.5	10.0
Threonine	6.5	6.0	6.3	6.0
Tryptophan	(d)	(d)	(d)	(d)
Tyrosine	3.8	3.8	3.7	3.2
Valine	5.7	4.6	5.7	5.8
NH_3	(e)	9.6	(e)	(e)
Reference	Jones *et al.,* 1998	Maclaren & Milligan, 1981	Leeder & Marshall, 1982	Gillespie *et al.,* 1969

(a) Includes asparagine

(b) Includes glutamine

(c) Contributes to cystine

(d) The value cannot be obtained by acid hydrolysis method

(e) NH_3 was not included

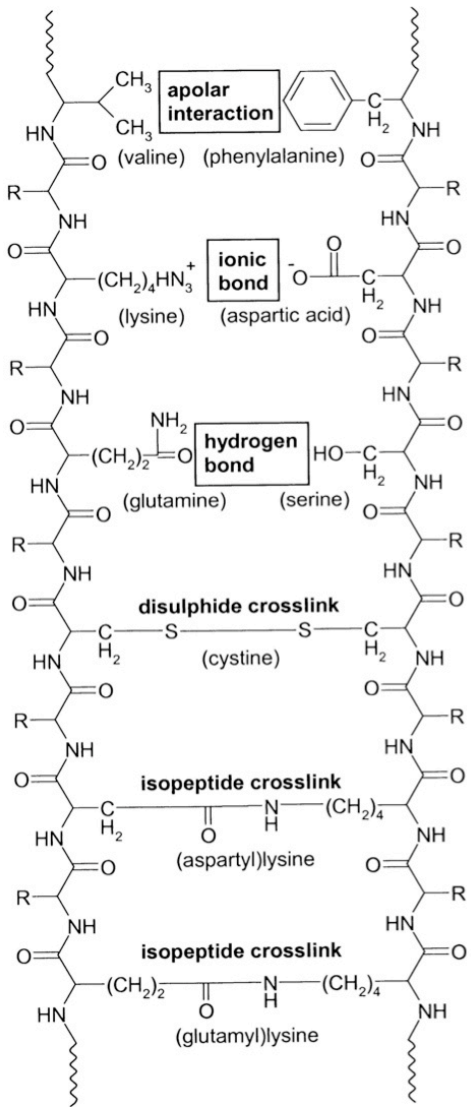

Figure 3.1.3 Amino acid bond formation in wool (Rippon, 1992)

The different effects of UV and visible light irradiation of wool are caused by specific wavelength distributions of incident light; wavelengths between 290 nm and 310 nm are mainly responsible for photo-yellowing while photo-bleaching occurs at wavelengths between 400 nm and 460 nm and photo-tendering is mainly caused by radiation below 300 nm (Maclaren & Milligan, 1981). Radiation causes the degradation of amino acid tryptophan, producing a yellow product that is responsible for the photo-yellowing effect in wool. The photo-bleaching mechanism is less well understood, however, it is known to be caused by exposure to blue light (400 – 460 nm). The absorbance of blue light will be greater for yellower wool samples that will lead to an increased photo-bleaching effect.

UV and simulated sunlight irradiation of the wool surface removes the covalently bound 18-MEA fatty acid.

The breakage of disulphide crosslinks of cystine and peptide bonds in irradiated wool fibres are responsible for loss of strength. This photo-tendering effect is caused by photo-oxidation of cystine residues to cysteic acid by the mechanisms illustrated in Figure 3.1.4.

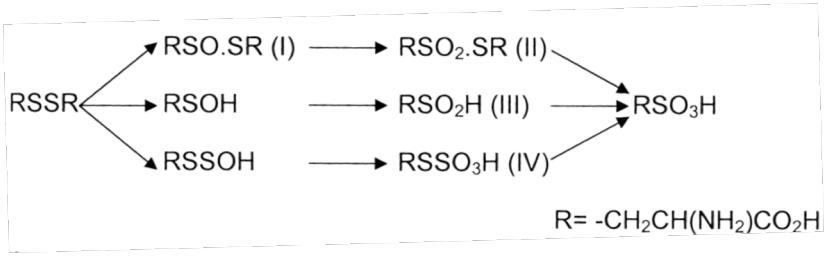

Figure 3.1.4 Oxidation of cystine di-sulphide to cysteic acid (Maclaren & Milligan, 1981)

The chemical state change of the sulphur can be observed using x-ray photoelectron spectroscopy (XPS) as the sulphur converts from its S^{2+} oxidation state in cystine to the S^{6+} oxidation state of the sulphate ion in cysteic acid (Carr *et al.,* 1985). This shift in the chemical state is detected as formation of a new S (2p) peak at a binding energy of 168 eV, shifted from the 164 eV binding energy of S^{2+}. The presence of a surface lipid layer is determined from the relative atomic percentages of carbon and nitrogen; a high C/N ratio indicates the presence of a carbon rich layer. The removal of surface lipids by photo-oxidation will result in a lower C/N value (Carr *et al.*, 1985).

3.1.2 Silk

Silk fibres are very smooth-surfaced filaments with a rounded triangular cross-section and a diameter of around 10 μm. The smooth surfaces reflect light, which gives silk its characteristic lustre. Silk is composed of 18 amino acids that form two sequences of polypeptide, a heavy H-chain and a light L-chain, examples of amino acid composition are given in Table 3.1.3. The first three amino acids, glycine, alanine and serine, constitute over 80% of the silk fibre in an approximate 3:2:1 ratio. The H-chain is 5253 residues long and is made up of mainly glycine, alanine, serine and some tyrosine, valine and threonine plus five cysteine residues, only one of which forms a disulphide bond with the L-chain. The L-chain consists of 262 amino acid residues and contains three cysteine residues of which two form a disulphide bridge and the other is available for disulphide linkage with the H-chain.

Table 3.1.2 Amino acid composition of silk fibroin

	Residue percentage				
Amino acid	**Fibre**	**Fibre**	**Fibre**	**H-chain**	**L-chain**
Glycine	43.7	43.7	44.6	49.4	9.2
Alanine	30.3	29.3	29.4	29.8	14.2
Serine	9.9	10.7	12.1	11.3	9.0
Tyrosine	5.2	5.5	5.2	4.6	2.8
Valine	1.8	2.4	2.2	2.0	6.4
Aspartic acid/Asn	1.5	1.8	1.3	0.7	14.8
Glutamic acid/Gln	1.2	1.2	1.0	0.7	9.2
Threoine	0.7	0.9	0.9	0.5	3.0
Phenylalanine	1.2	0.9	0.6	0.4	2.7
Isoleucine	0.8	0.7	0.7	0.1	7.8
Leucine	0.7	0.6	0.5	0.1	7.5
Arginine	0.9	0.5	0.5	0.2	4.5
Lysine	0.2	0.3	0.3	0.1	1.2
Proline	0.4	-	0.4	0.3	3.2
Histidine	0.4	-	0.1	0.1	2.3
Methionine	0.9	-	0.1	-	0.4
Tryptophan	-	-	0.1	-	-
Cysteine	-	-	0.2	-	1.4
Reference	Yanagi *et al.,* 2000	Becker & Tuross, 1993	Robson, 1998	Robson, 1998	Robson, 1998

Exposure to radiation causes photo-yellowing and photo-tendering of the silk fibre (Robson, 1986). Yellowing is attributed to photo-oxidation of tyrosine and tryptophan residues. UV exposure results in loss of tensile strength and other physical degradation, an effect that is stronger in wet fabric, due to the cleaving of hydrogen bonds between the crystalline regions of the fibre. Nitrogen gas is released by photo-degrading silk.

XPS analysis of silk fibres detected a high C/N ratio at the fibre surface, which is attributed to a higher concentration of the carbon-rich tyrosine residue. Sulphur was most prevalent in cysteic acid form, detected by its S^{6+} oxidation state, however,

this was not due to oxidation of the silk surface. Subsequent oxidative removal of the outer layer of the silk fibre led to a complete loss of sulphur, a decrease in carbon and relative increases in oxygen and nitrogen (Shao *et al.,* 2002).

3.1.3 Metallic thread

The characterisation of metallic threads in textiles has received much attention due to the extremely detrimental effect that physical and environmental degradation has on the originally beautiful, shimmering threads. Corrosion of the metallic filament often results in a blackened appearance that severely impairs the appearance of the textile. The conservation of historic metallic threads is problematic due to the risk of cleaning methods on the surrounding textile material and on the fibrous core of the thread (Johansen, 2009). Various mechanical and chemical methods are used to clean metallic threads, none of which are faultless, therefore proper assessment of the nature of the materials and the risks involved must be performed (Hacke *et al.,* 2003; Jaro, 2009).

A variety of analytical techniques are used to determine the nature and composition of the corrosion products that form on metallic threads in historic textiles, most notably scanning electron microscopy with energy dispersive x-ray spectrometry (SEM/EDS) (Indictor *et al.,* 1989; Járó *et al.,* 1999; Nord & Tronner, 2000; Tronner *et al.,* 2002; Rogerson & Garside, 2006; Cakir *et al.,* 2006; Abdel-Kareem & Al-Saad, 2007; Karatzani, 2008). Other methods include time of flight secondary ion mass spectrometry (ToF-SIMS) (Carr *et al.,* 2004*;* Howell *et al.,* 2007), atomic absorption spectroscopy (AAS) (Cakir *et al.,* 2006), Auger electron spectroscopy (AES) (Nord & Tonner, 2000), and microprobe analysis (Hoke & Petrascheck-Heim, 1977).

These studies of historic threads found that the metal filaments, which are wrapped around a fibrous core, commonly consist of silver and/or copper covered with a thin gold layer, with some traces of zinc and nickel alloys, tin, iron and aluminium. Silver corrosion products, such as silver sulphide and silver chloride, are often detected at the surface of metallic threads due to the gold layers being very thin, <1 μm (Tronner *et al.,* 2002). Similarly copper corrosion products are detected at the sample surface when the metal filament contains copper (Karatzani, 2008). Electron micrographs of the sample surface reveal variations in the corrosion product morphologies; sulphide crystals are distinguished into sharp or rounded

formations (Cakir *et al.,* 2006; Hacke, 2006), while Hacke also describes a delamination or flaking of the surface, which is attributed to a silver sulphide corrosion product growing over the underlying copper corrosion. The sharp crystals of silver sulphide are often referred to as whiskers (Sease et al., 1997) while the rounded crystals are called cauliflowers or flowers.

Potential corrosion products that may form in typical tapestry display conditions are comprised of silver and copper in the metal filament, sulphur from the environment and from volatilization of sulphur from the wool and silk fibres, chlorine from handling or from salts used in the dyeing process, carbon and oxygen. Silver will react with atmospheric sulphurous gases, primarily H_2S and OCS then CS_2 and SO_2, to form Ag_2S, Ag_2O and Ag_2SO_4 (Franey *et al.,* 1985). The principal component of silver tarnish is silver sulphide, the formation of which is accelerated by illumination and temperature (Yang *et al.,* 2007). Copper corrosion products that may form in this environment comprise Cu_2O, Cu_2S, $CuSO_4$ (Rice *et al.,* 1981). In addition AgCl and Cu_2Cl may form.

3.2 Determining the gamut of colours of natural dyes

3.2.1 Introduction

As part of the European wide project Monitoring of Damage in Historic Tapestries (MODHT), Hacke constructed model tapestries to assist in studies regarding ageing of the historic tapestry materials. Historic tapestry materials were researched and suitable representative yarns were found; the wool used was 3-ply, 158 Tex, English wool yarn, the silk was 2-ply, 66 Tex, Italian spun silk. There were two types of model tapestry fabric woven both having a warp density of 8 ends per centimetre; one fabric was woven with a wool warp and wool weft of 28 ends per cm, the other with a wool warp and silk weft of 35 ends per cm (Hacke, 2006).

The fabrics were separated into a total of 41 samples; 23 wool and 18 silk. These samples were dyed using the natural dyes and ingredients which would have been employed to colour historic tapestry yarns, using dyeing recipes formulated from medieval texts. Particular dyestuffs were utilised in several dyeings using differing recipes as noted in Table 3.2.1.

Table 3.2.1: Dyeings performed on model tapestry materials for MODHT project stating the dyestuff and mordant used for each sample

	Wool samples	**Dye**	**Mordant**
1	Undyed		
2	Blank Dyed		
3	Blank Dyed with lye		
4	Alum Mordanted		Alum
5	Alder Bark Tannin		Alder Bark
6	Oak Gall Tannin		Oak Gall
7	Black W1	Iron Sulphate	Oak Gall
8	Black W2	Iron Sulphate	Oak Gall
9	Black W2 no rinse	Iron Sulphate	Oak Gall
10	Black W3	Iron Sulphate	Alder Bark
11	Black W4	Copper & Iron Sulphate	Oak Gall
12	Red W1	Madder	Semelwater & Alum
13	Red W1_wl	Madder	Semelwater & Alum
14	Red W2	Madder	Oak Gall & Alum
15	Red W2_wl	Madder	Oak Gall & Alum
16	Red W3	Brazilwood	Alum
17	Red W4	Cochineal & Turmeric	Alum & Tartaric Acid & Sandalwood
18	Red W5	Cochineal	Alum & Tartaric Acid & Sandalwood
19	Yellow W1	Weld	Alum
20	Yellow W2	Dyer's Greenweed	Alum
21	Blue W1	Woad	
22	Green W1	Weld & Woad	
23	Green W2	Woad & Weld	Alum
	Silk samples	**Dye**	**Mordant**
1	Undyed		
2	Oak Gall		Oak Gall
3	Black S1a	Iron Sulphate	
4	Black S1b	Iron Sulphate	
5	Red S1a	Brazilwood	Alum
6	Red S1b	Brazilwood	Alum
7	Red S1c	Brazilwood	Alum
8	Red S1d	Brazilwood	Alum
9	Red S2a	Madder	Alum
10	Red S2b	Madder	Alum
11	Red S2c	Madder	Alum
12	Red S3	Cochineal	Alum & Copper Turnings
13	Yellow S1b	Weld	Alum
14	Yellow S3b	Dyer's Greenweed	Alum
15	Blue S1 pale	Woad	
16	Blue S1 dark	Woad	
17	Green S1b	Weld & Woad	Alum
18	Green S2b	Woad & Weld	Alum

Due to photo-fading which has occurred on the *Story of Abraham* tapestries, the colours which are visible at present do not represent the original appearance of the dyed materials. The colours of the model dyed samples are indicative of the shades producible in the 16th century when the *Abraham* tapestries were completed. Colour measurements of these samples provide a database of the range of colours which it was necessary to produce using the projection equipment for the recolouration project.

There are several limitations to the range of colours which we can produce, firstly the limit of all realisable colours as indicated by the spectrum locus in the CIE chromaticity diagram. Colours are limited in the lightness scale due to the upper threshold determined by the luminance of the illuminant and the lower threshold due to the fact that even the darkest of colours reflect some light from the surface. The gamut of colours is then limited by the constraints of the colourants and their mixing capabilities. If the choice of colourants are well spaced within the hue circle, a large number of colours are attainable (Hunt, 1995; Berns, 2000).

3.2.2 Experimental method

Colour measurement of the 23 wool and 18 silk dyed fabric samples was performed using the following method. Spectrophotometric measurements taken over a spectral interval of 400 to 700 nanometers (nm) with a spectral resolution of 10 nm were taken using D65 illuminant and 10 degree field of view on a Spectraflash 600 instrument with specular reflectance excluded and UV included. Calibration of the machine was performed using a white standard, black trap and green standard. The reflectance factor, the ratio of the flux reflected from the specimen to the flux reflected from the standard white, is recorded.

3.2.3 Results and discussion

The spectral reflectance data for the wool and silk samples is contained in Appendix B. The reflectance factor of a sample measured at each 10 nm wavelength over the visible spectrum is plotted as a Spectral Reflectance Curve. The spectral reflectance data is used to calculate tristimulus values by multiplying (at each wavelength interval) the reflectance factor, R, by the relative power of the CIE standard illuminant, S, and the CIE standard observer colour-matching functions, x_λ, y_λ and z_λ

(see Equations 1-4, Section 4.1.3). The sums of the multiplications for each of the functions are the tristimulus values X, Y, and Z.

The chromaticity coordinates *x*, *y*, and *z*, of a colour are found by taking the ratios of the tristimulus values to their sum, X + Y + Z (see Equations 5 & 6, Section 4.1.3). The chromaticity coordinates *x* and *y* are then plotted onto the chromaticity diagram for the 1964 standard observer. A script was written using MATLAB to calculate the chromaticities of the dyed samples with the aid of functions written by Westland and Ripamonti (2004). The chromaticities of the dyed wool and silk samples are shown plotted on the CIE chromaticity diagram in Figure 3.2.1, where the curved blue line represents the spectrum locus of all possible colours, calculated for the CIE 1964 10-degree standard observer.

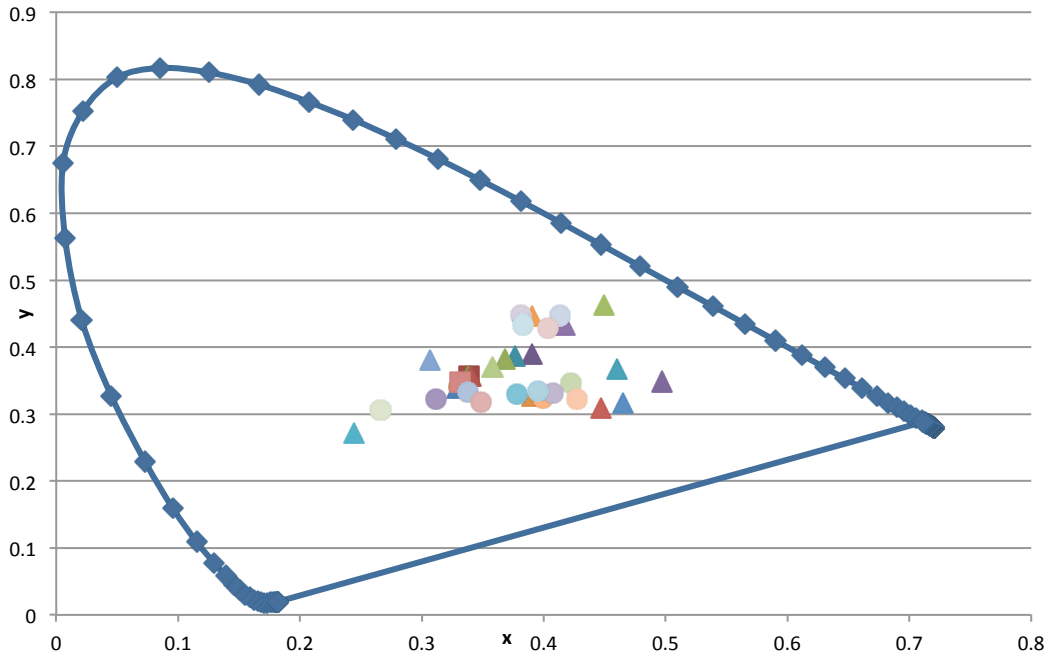

Figure 3.2.1 The CIE 1964 *x, y* chromaticity diagram with wool model tapestry samples (triangles) and silk model tapestry samples (circles)

The characterisation of the hyperspectral imaging system and the projection system is reported in Chapters 4 and 5 respectively. The gamut of producible colours has been calculated for the system. This information will be compared with the gamut of natural dyes specified from the model tapestry samples to determine whether the full range of shades can be digitally reproduced. The gamut of colours that can be projected is calculable for differing illuminants therefore it is possible to ascertain if

all the natural dye shades present in the model tapestry samples can be projected firstly onto a white screen and consequently onto the historic tapestry itself where it hangs in the Queen's Guard Chamber at Hampton Court Palace.

3.3 Physical characterisation of unaged and artificially aged model tapestry materials

This section outlines two experiments, which investigate environmental factors responsible for the degradation of wool, silk and metallic threads within 16th century tapestries.

Both studies use standard techniques from conservation science to assess how different environmental factors degrade the textile and metallic components of tapestry materials. Model tapestries were constructed from modern materials using traditional weaving techniques and were coloured using medieval dye recipes as described in Section 3.2.1. These model tapestries were constructed using techniques, which were as similar as possible to the original *Story of Abraham* tapestries. Wool and silk yarns were dyed using a range of medieval dye materials and recipes to create a collection of coloured yarns to be used as weft threads. These wefts were then woven with an undyed wool warp to produce an authentic tapestry structure.

The first study investigates the effects of light exposure on the tapestry materials. Section 3.3.4 of the study assesses the photo-fading characteristics of fabrics dyed with various natural dye and mordant combinations. Reproductions of gilt metallic threads were sewn with silk thread to the surface of the model tapestry fabric. The samples were placed in a Weatherometer and irradiated with light exposures equivalent to standard museum conditions of 100, 300 and 500 years. The samples were measured using colour measurement and surface analysis equipment. The samples were then analysed to determine whether the dye/mordant combination influenced the formation of corrosion products on the metallic threads.

The second study investigates the effect of thermal ageing on tapestry materials. Section 3.3.5 outlines how the corrosion of metallic threads can be influenced by environmental conditions such as heat and humidity. Thermal degeneration was

simulated using the well-known Oddy Test method (Bamberger *et al.,* 1999; Pretzel & Shibayama, 2003; Robinet & Thickett, 2003). The Oddy test is an accelerated ageing test used to assess the amount of corrosion caused by an interaction between metallic threads and certain dye/mordant combinations. The corrosion products present on metallic threads, copper coupons and silver coupons were measured using advanced surface analysis techniques; Scanning Electron Microscopy (SEM); Energy Dispersive X-ray analysis (EDX); and X-ray Photoelectron Spectroscopy (XPS). These methods have proven to be useful for the scientific analysis of modern and historic metallic threads in previous studies (see section 3.1.3).

The novel dataset of results from these experiments will be a useful resource for conservators in the future.

3.3.1 Experimental Materials

Table 3.3.1 outlines the selection of 22 different natural dye/mordant/fibre combinations that were used in this study that were taken from the set of model tapestry fabrics constructed by Hacke (see Section 3.2.1). This range of samples permits a full study of the degradative effect of the individual fibres, dyes and mordants that would have been used during the period when Henry VIII commissioned the Story of Abraham tapestries.

Table 3.3.1 Composition of dyed model tapestry samples used in the study

Sample name for this study	Sample name used by Hacke	Weft Fibre	Colour	Dyestuff	Mordant
Undyed Wool	Undyed Wool	Wool	-	-	-
W Alum	Alum Mordanted Wool	Wool	-	-	Alum
W Alder	Alder Bark Tannin Wool	Wool	-	-	Alder Bark
W Oak Gall	Oak Gall Wool	Wool	-	-	Oak Gall
W Iron	Black W2	Wool	Black	Iron Sulphate	Oak Gall
W Copper	Black W4	Wool	Black	Copper & Iron Sulphate	Oak Gall
W Madder	Red W1	Wool	Red	Madder	Semelwater & Alum
W Madder 2	Red W2	Wool	Red	Madder	Oak Gall & Alum
W Brazil	Red W3	Wool	Red	Brazilwood	Alum
W Coch	Red W5	Wool	Red	Cochineal	Alum & Tartaric Acid & Sandalwood
W Weld	Yellow W1	Wool	Yellow	Weld	Alum
W Gweed	Yellow W2	Wool	Yellow	Dyer's Greenweed	Alum
W Woad	Blue W1	Wool	Blue	Woad	-
Undyed Silk	Undyed Silk	Silk	-	-	-
S Oak Gall	Oak Gall Silk	Silk	-	-	Oak Gall
S Iron	Black S1b	Silk	Black	Iron Sulphate	-
S Brazil	Red S1d	Silk	Red	Brazilwood	Alum
S Madder	Red S2c	Silk	Red	Madder	Alum
S Coch	Red S3	Silk	Red	Cochineal	Alum & Copper Turnings
S Weld	Yellow S1b	Silk	Yellow	Weld	Alum
S Gweed	Yellow S3b	Silk	Yellow	Dyer's Greenweed	Alum
S Woad	Blue S1 dark	Silk	Blue	Woad	-

Mr Bill Barnes at Goldenthreads, UK, produced a model of the type of gold and silver metallic thread manufactured during the 16th century. A metal filament was manufactured using the 'cast, drawn and rolled' technique whereby an 85

micrometre (μm) diameter wire (copper electroplated with 1% silver and 0.5% gold) is flattened between steel rollers. The metallic thread was constructed by spinning the filament around a silk fibre core, dyed with young fustic (Hacke, 2006).

The metallic thread was cleaned using heptane then rinsed in acetone to remove any organic material remaining from the manufacturing process.

Coupons of copper and silver, >99.9% purity, were provided by the Textile Conservation Studio at Hampton Court Palace for use in the thermal ageing experiment reported in Section 3.3.5. The 10 x 35 x 0.25 mm coupons were polished using a glass bristle brush then degreased in acetone.

3.3.2 Common Methodology

3.3.2.1 Imaging

Images of the samples were taken using a compact camera Canon Digital IXUS 70.

3.3.2.2 Visual corrosion scale

Each of the photo- and thermal aged metallic threads and the copper and silver coupons were given a corrosion rating based on visual analysis of their colour appearance and corrosion coverage of the sample surface. Each set of samples was graded by comparison, on a scale of 1-5 with 1 being the lowest level of appearance degradation and 5 being the highest. Although this is not a fully quantitative method of assessing corrosion it still allows comparisons of the changes in visual appearance of the metallic threads and coupons. Conservators working in industry use similar methods to determine the worst affected samples in ageing tests. This allows them to make decisions on the materials that will be used in display cases with real artefacts (Daniels & Ward, 1982). Part of this study is to assess the impact of ageing on the visual appearance of the tapestry and which dyes may cause the most tarnishing of the metallic threads. Colour measurement has been investigated as a method of quantifying corrosion, using the b* value of the CIELAB system as an indication of the increased brown tint of tarnished silver; however, no correlation was found (Hallett *et al.,* 2003).

3.3.2.3 SEM/EDX

The Hitachi S-3000N variable pressure SEM instrument with a tungsten electron source and four quadrant backscattered electron detector was used for this study in high vacuum mode, at a 15 mm working distance for both imaging and EDX analysis. SEM images of the 500 hour photo-aged metallic thread samples and the thermal aged copper and silver coupons were obtained for the study of the corrosion on the surface of the samples. Images were taken of each of the metallic threads at 60x magnification, approximate 39 spot size and 25 kV accelerating voltage with smaller scale images of areas of heavy corrosion present on some samples taken at 150x magnification. EDX analysis was performed on up to 4 different points on each of the metallic thread samples. The copper and silver coupons were imaged and analysed at 1000x magnification, approximate 33 spot size and 20 kV accelerating voltage.

3.3.2.4 XPS

XPS analysis was performed on the thermal aged metallic threads and copper and silver coupons, 500 hour photo-aged metallic threads and some unexposed and photo-aged dyed wool and silk fibre samples. The analysis was performed using a Kratos Axis Ultra X-ray photoelectron spectrometer, which has an aluminium/magnesium dual anode and a monochromated aluminium X-ray source. Wide scan spectra in the range 1000 – 0 eV binding energy were collected for all samples and high resolution scans of C (1s), O (1s), N (1s), S (2p), Cl (2p), Cu (2p), Ag (3d) and Au (4f) energy bands were collected depending on which samples were being analysed.

3.3.2.4.1 Interpretation of the XPS spectra

This section describes the process of interpreting the peaks of XPS spectra, using results from the following experiments. This information precedes the results section due to its relevance to both photo-ageing and thermal ageing experiments.
XPS data analysis was performed using the CasaXPS software. Binding energies of elements were taken from experimental results listed in the NIST XPS Database.

The **C (1s)** XP peak typically has a binding energy of 285 eV. Various carbon species have different binding energies that determine the position and shape of the C (1s) peak.

- Binding energies (eV) of typical carbon residues
- @ 285.0 = C, -CH, CC
- @ 286.2 = CN, CS, CCl
- @ 286.6 = –COH
- @ 288.0 = carbonyls, C=O, O-C-O
- @ 289.0 = carboxyls, O-C=O

The carbon present on all of the artificially aged samples can be attributed to contamination in addition to the carbon associated with the corrosion products. The spectra shown in Figure 3.3.1 is the high-resolution spectra of the C (1s) peak of the thermal aged copper W Brazil sample. The peak has been fitted with 3 component peaks that indicated carbon in at least three different states. Some of the carbon is possibly attributable to copper carbonate corrosion at 289.0 eV.

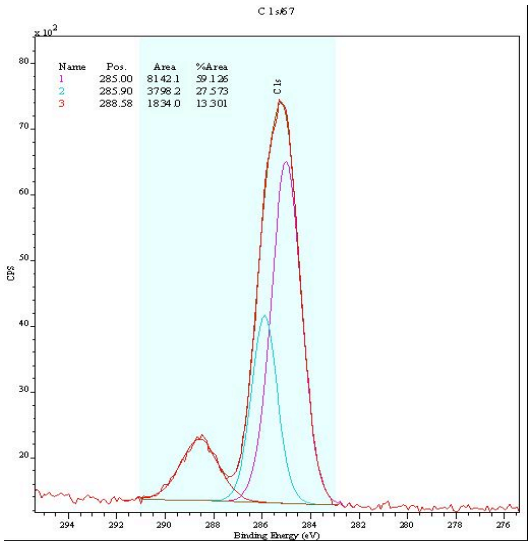

Figure 3.3.1. XPS high resolution spectrum of Thermal aged copper W Brazil sample, C (1s) peak

The **O (1s)** XP peak typically has a binding energy of 532 eV. The binding energies of the various oxygen species fall within a small spatial range and it is therefore difficult to identify the individual component peaks that make up the single O (1s) peak. The O (1s) peak of the thermal aged copper W Brazil spectrum is shown in Figure 3.3.2, the curve is typical of the oxygen signals detected on all samples.

- Binding energies (eV) of typical oxygen containing corrosion products
- @ 529 = AgO, Ag_2O
- @ 530-531 = CuO, Cu_2O, $Cu(OH)_2$
- @ 532 = $CuSO_4$

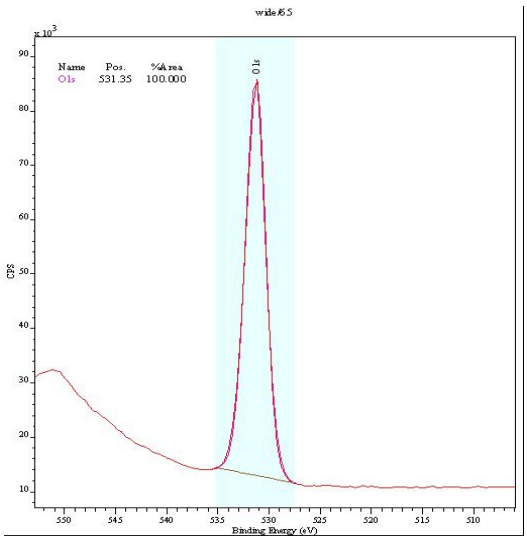

Figure 3.3.2 XPS high resolution spectrum of Thermal aged copper W Brazil sample, O (1s) peak

The **Cu (2p)** XP peak typically has a binding energy of 932 eV and exhibits spin orbit splitting into Cu ($2p_{3/2}$) and Cu ($2p_{1/2}$) signals. The peaks have an intensity ratio of 2:1 and a binding energy difference of 19.9 eV.

- Binding energies (eV) of typical copper containing residues
- @ 932.0 = Cu, CuS, Cu_2S, CuCl, Cu_2O
- @ 933.0 = CuO
- @ 934.5 = $CuCl_2$, $Cu(OH)_2$, $CuSO_4$
- @ 935.0 = $CuCO_3$

The two spectra shown in Figure 3.3.3 illustrate the Cu ($2p_{3/2}$) peaks comprising different copper containing residues. The first spectrum, Figure 3.3.3 (a) is of the thermal aged copper control sample, which has a well-defined peak that has been fitted with a single component peak. This suggests copper corrosion is made up of copper oxides, as there was no S present on this sample. The second spectrum, Figure 3.3.3 (b), is of the thermal aged copper W Brazil sample which exhibits a wider shouldered peak which has been fitted with 3 component peaks. These peaks suggest there are a variety of copper containing residues on this sample, possibly copper oxides, copper sulphides and copper sulphates.

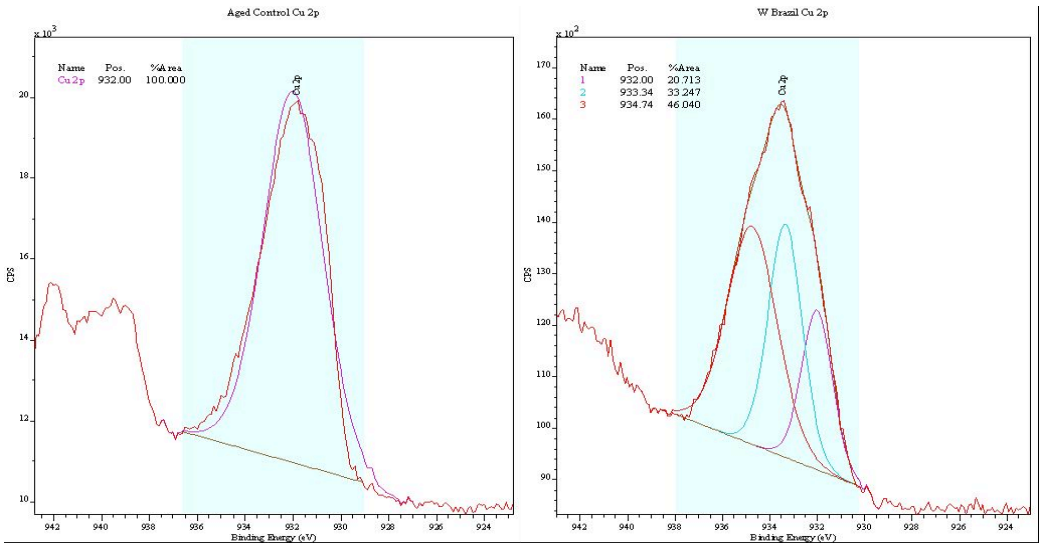

Figure 3.3.3 XPS high resolution spectra of (a) Thermal aged copper control sample, (b) Thermal aged copper W Brazil sample, Cu (2p) peaks.

The **Ag (3d)** XP peak typically has a binding energy of 368 eV and exhibits spin orbit splitting into Ag ($3d_{5/2}$) and Ag ($3d_{3/2}$) signals. The peaks have an intensity ratio of 3:2 and a binding energy difference of 6 eV.

- Binding energies (eV) of typical silver residues.
- @ 367.5 = AgO, Ag_2CO_3
- @ 368.0 = Ag, Ag_2O, Ag_2S, AgCl, Ag_2SO_4

The spectrum shown in Figure 3.3.4 is the high-resolution scan of the Ag (3d) peak of thermal aged silver W Brazil sample. It shows the two distinct peaks of the spin orbits. However, it is not possible to distinguish the different chemical states of silver by fitting component peaks as the binding energies of the silver residues are very similar and do not affect the shape of the peak.

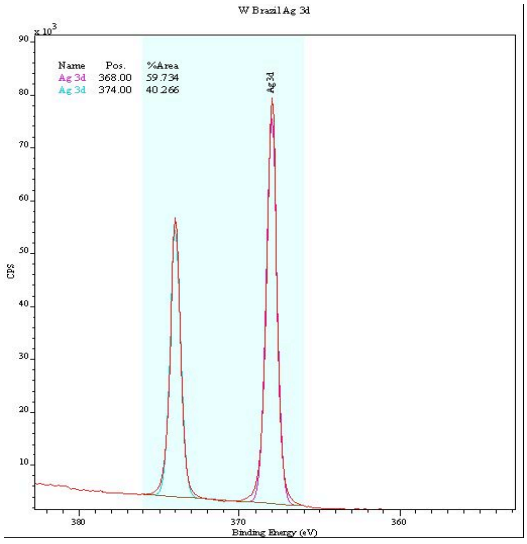

Figure 3.3.4 XPS high resolution spectrum of thermal aged silver W Brazil sample, Ag (3d) peak.

The **Au (4f)** XP peak typically has a binding energy of 84 eV and exhibits spin orbit splitting into Au ($4f_{7/2}$) and Au ($4f_{5/2}$) signals. The peaks have an intensity ratio of 4:3 and a binding energy difference of 3.7 eV. Gold is inert and does not form any corrosion products on the aged metallic threads. The spectrum in Figure 3.3.5 is the high-resolution scan of the Au (4f) peak of the unaged metallic thread. It shows the two distinct peaks of the spin orbits.

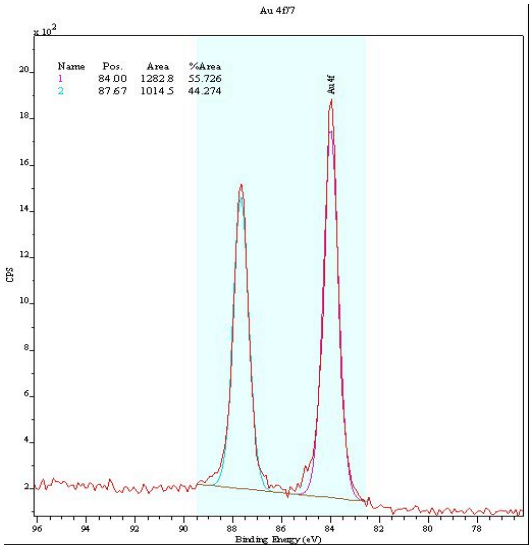

Figure 3.3.5 XPS high resolution spectrum of unaged metallic thread sample, Au (4f) peak.

The **S (2p)** XP peak typically has a binding energy of 164 eV and exhibits spin orbit splitting into S ($2p_{3/2}$) and S ($2p_{1/2}$) signals. The peaks have an intensity ratio of 2:1 and a binding energy difference of 1.2 eV. The binding energies of the various oxidation states of sulphur are distinct so that identification of the peaks corresponding to the chemical states is possible. Quantification of the relative % of the peak components was performed using peak fitting. This distinction enables identification of the corrosion products present on the samples.

- Binding energies (eV) of typical S (2p) chemical states and corrosion products
- @ 162 – 164 = sulphides (S^{2+}), Ag_2S, CuS, Cu_2S
- @ 166 = (S^{4+}), =S=O
- @ 168 = sulphates (S^{6+}), Ag_2SO_4, $CuSO_4$

The XPS high-resolution S (2p) spectra were peak fitted and quantification of the sulphur peaks was carried out. Most of the spectra had very distinct spin orbit splitting of either one or both of the chemical states. However, some spectra were too noisy to distinguish the $2p_{3/2}$ and $2p_{1/2}$ split peaks, in these cases a single curve

was fitted to the component peak. The areas of the peaks were quantified and ratios of the S^{2+} and S^{6+} chemical states were calculated.

The spectra in Figure 3.3.6 show the high-resolution scan of the S (2p) peaks of two thermal aged samples. The first, Figure 3.3.6 (a), is thermal aged silver W Brazil sample, which is distinct by the lack of a signal at the higher binding energy of the S^{6+} oxidation state, 168 eV. The spin orbit splitting of the peak @ 164 eV is very clear. These results indicate that the principal corrosion product present is Silver Sulphide and there are little or no sulphates on the silver coupon. The aged silver coupons all exhibited similar results whereby there was little or no sulphur found in its higher oxidation state. The average content of S^{6+} on thermal aged silver coupons was 5.4%.

The second spectrum, Figure 3.3.6 (b), is thermal aged copper S Gweed sample which has peaks at the 164 eV and 168 eV binding energies. This spectrum is more noisy than the first, however, the component peaks of the spin orbit splitting and the two oxidation states are clear. The presence of sulphur in its higher oxidation indicates that there are sulphates present on the copper coupon suggesting a combination of copper sulphides and copper sulphate corrosion. The aged copper coupons had an average value of S^{6+} content of 38%.

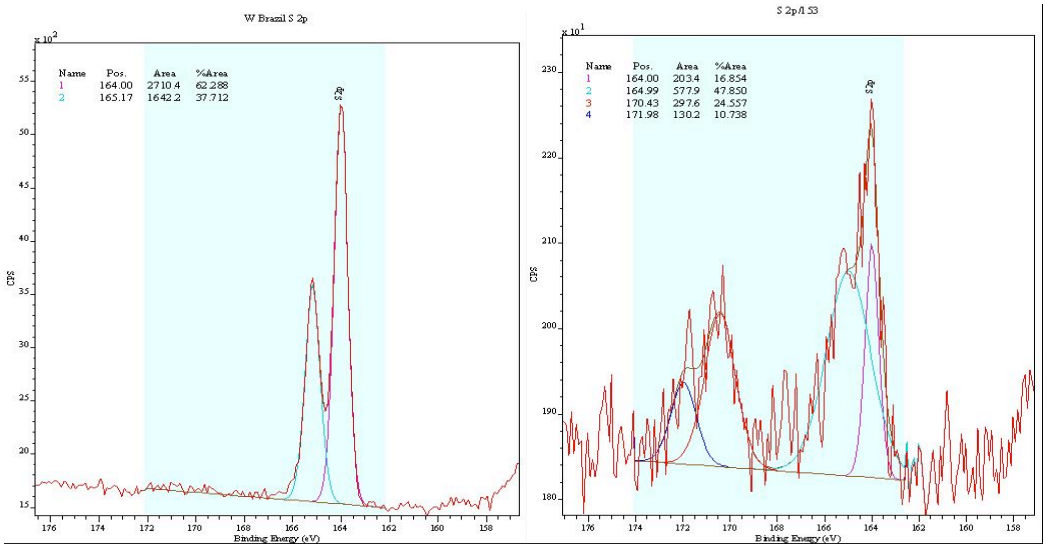

Figure 3.3.6 XPS high resolution spectra of (a) Thermal aged silver W Brazil sample, (b) Thermal aged copper S Gweed sample, S (2p) peaks.

The amount of sulphur in its different oxidation states varies on the metallic threads samples where silver and copper corrosion products are both present. The average S^{6+} content on photo-aged metallic threads, relative to the S^{2+} proportion, is 44%,

while the average on thermal aged metallic threads is 47%. There is some positive correlation between the amount of copper detected at the surface of the photo aged metallic thread samples and the amount of S^{6+} present. This indicates that the increased level of copper present is forming sulphates on the sample surface.

The identification of the various oxidation states of sulphur is important in the analysis of the ageing of the wool fibre samples. Sulphur is predominantly present in wool as a disulphide linkage in the amino acid cystine. Exposure to photo-radiation causes oxidation of the disulphide linkage to form cysteic acid. In this process the sulphur converts from its S^{2+} oxidation state to S^{6+}. XPS analysis of unaged - undyed wool fibres revealed a S^{6+} content of 17% which is attributed to the exposure of the sheep to photo-oxidation. After 500 hours of accelerated photo-ageing, the S^{6+} content increased to 35%.

The **Cl (2p)** XP peak typically has a binding energy of 198 eV and exhibits spin orbit splitting into Cl ($2p_{3/2}$) and Cl ($2p_{1/2}$) signals. The peaks have an intensity ratio of 2:1 and a binding energy difference of 1.6 eV.

- Binding energies (eV) of typical chlorine containing corrosion products
- @ 198 eV = AgCl
- @ 199 eV = CuCl, $CuCl_2$

There was chlorine present on all of the thermal aged silver coupons, which is attributed to AgCl corrosion. There was no chlorine found on the copper coupons, however, it was detected on some thermal aged metallic threads and most of the photo-aged metallic threads on which Copper Chloride corrosion products may be present. The presence of chlorine on the samples is likely due to handling of the samples or from salt used in dyeing. Most of the photo-aged samples contained chlorine with the exception of W Undyed and S Undyed, which suggests that chlorine is introduced during the dyeing process.

The high-resolution spectrum in Figure 3.3.7 is of the Cl (2p) peak of the thermal aged silver W Brazil sample shows the spin orbit splitting of the peak which has been fitted with the two component peaks.

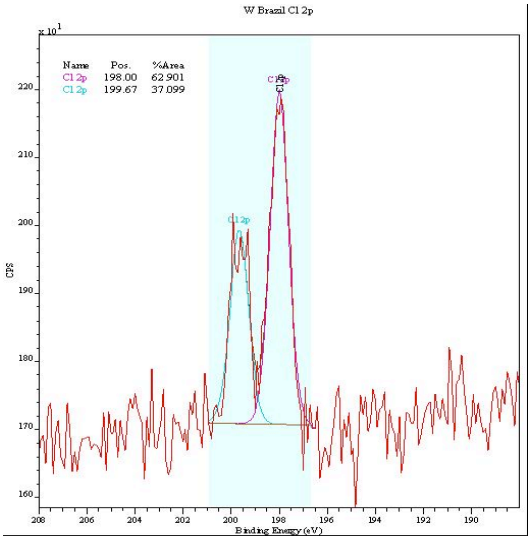

Figure 3.3.7 XPS high resolution spectrum of thermal aged silver W Brazil sample, Cl (2p) peak.

3.3.3 Experiment 1: Photo-ageing

3.3.3.1 Methodology

The samples were prepared for photo-ageing by sewing three 12 cm lengths of the model metallic thread onto each fabric sample of 13.5 x 4.5 cm using undyed silk thread, shown in Figure 3.3.8. The 22 separate fabric samples were exposed to photo-radiation in a Xenotest 150S instrument with Atlas Xenon lamp and window glass filter with UV cut-off at 320 nm. The relative humidity in the sample chamber was controlled at 50-60% and the temperature at 25°C. The spectral power distribution of the irradiation source closely matches that of sunlight in indoor conditions. The samples were irradiated for a total of 500 hours, which is approximately equivalent to 500 years of light exposure in a museum environment. The samples were divided during the experiment by cutting the fabric between the three metallic threads. One strip of the fabric was removed after ageing for 100 hours while another strip was removed after 300 hours of exposure leaving the final strip to be exposed for a total of 500 hours.

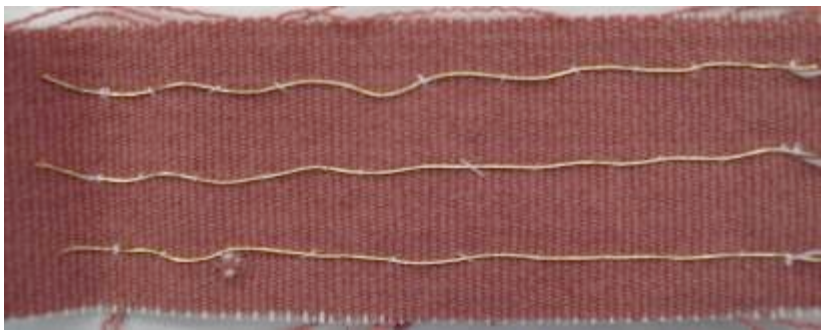

Figure 3.3.8 Photograph illustrating the construction of a model tapestry sample for photo-ageing

3.3.3.2 Results and Discussion

3.3.3.2.1 Visual analysis of metallic threads

Images of the photo-aged metallic threads were taken under a microscope spectrophotometer (MSP). Each dyed sample had been exposed separately for 100 hours, 300 hours and 500 hours giving 3 levels of ageing for each sample. As a result the images show the progressive degradation of the metallic threads in contact with each of the 22 varying dye/mordant combinations. Three images were taken along the length of the metallic threads. Examples of the W Alum (alum mordanted wool) samples are shown in Figure 3.3.9.

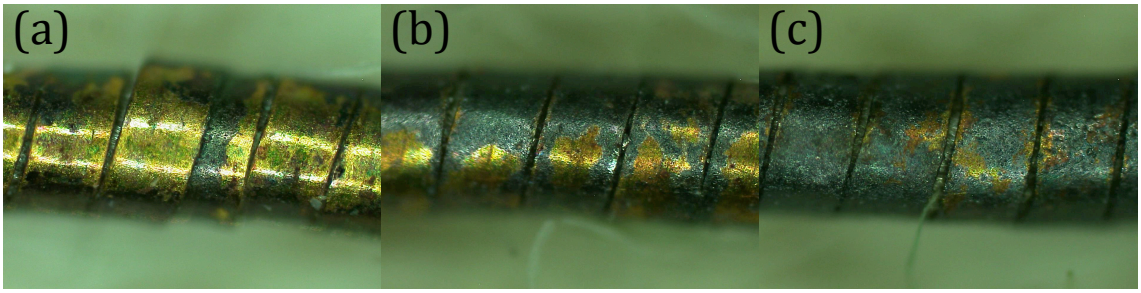

Figure 3.3.9 Samples of photo-aged metallic threads attatched to alum mordanted wool fabric: (a) 100 hour photo-aged, (b) 300 hour photo-aged, (c) 500 hour photo-aged.

An assessment of the visual corrosion of the photo-aged metallic threads was performed by analysing these images and assigning each of the dye/mordant combinations a corrosion grade based on the factors outlined in Table 3.3.2. The samples were scaled comparatively so that the range of values highlighted the least affected and the most affected samples. The levels assigned to each of the samples are given in Table 3.3.3.

Table 3.3.2 Factors used to assess the visual corrosion scale of photo-aged metallic threads

1	No tarnishing
2	Tarnishing of the thread/patches of corrosion
3	Larger patches of corrosion with grey/green corrosion products
4	A range of corrosion products and pitting of the surface
5	Complete corrosion of the surface

Table 3.3.3 Level of corrosion on photo-aged samples as assessed by the visual corrosion scale

Sample	Level of corrosion of photo-aged thread
W Undyed	3
W Alum	5
W Alder	2
W Oakgall	1
W Iron	4
W Copper	4
W Madder	3
W Madder2	2
W Brazil	2
W Coch	3
W Weld	3
W Gweed	2
W Woad	4
S Undyed	2
S Oakgall	3
S Iron	2
S Brazil	4
S Madder	2
S Coch	3
S Weld	3
S Gweed	2
S Woad	2

The W Alum metallic thread showed the highest level of corrosion as indicated by the value of 5 on the visual corrosion scale. On average the wool samples exhibited higher levels of corrosion (2.9) than the silk samples (2.6). The colour of corrosion products visible on the metallic threads ranged from green to red-brown to grey and black. The corrosion products appear to form initially at the edges of the metal

filament and at scratches on the surface of the filament. The growth of the corrosion then continues across the surface of the metal filament and covers it almost completely in the case of W Alum. The appearance of the metallic threads deteriorates progressively as the coverage of the corrosion increases and the colour changes from gold to grey and black.

SEM micrographs of the photo-aged metallic threads show more detailed images of the corrosion products, which form on the surface of the threads. The unaged control metallic thread is shown in Figure 3.3.10 (a) to have a smooth surface with no visible growths on the surface while the W Alum sample is covered with a corrosion residue signified by a darker shade, Figure 3.3.10 (b). The W Oakgall sample was identified by the visual corrosion scale as having the lowest level of corrosion, which is confirmed by the clear smooth appearance of the sample under SEM, Figure 3.3.10 (c). The S Oakgall sample shown in Figure 3.3.10 (d) highlights the growth of the corrosion products from the edges of the metal filament. It is at the edges of the filament where the gilding layer is thinner due to the cracks formed during the compression of flattening the gilt wire into a filament. In addition corrosion products with different morphologies can be seen on the various samples shown in Figure 3.3.11.

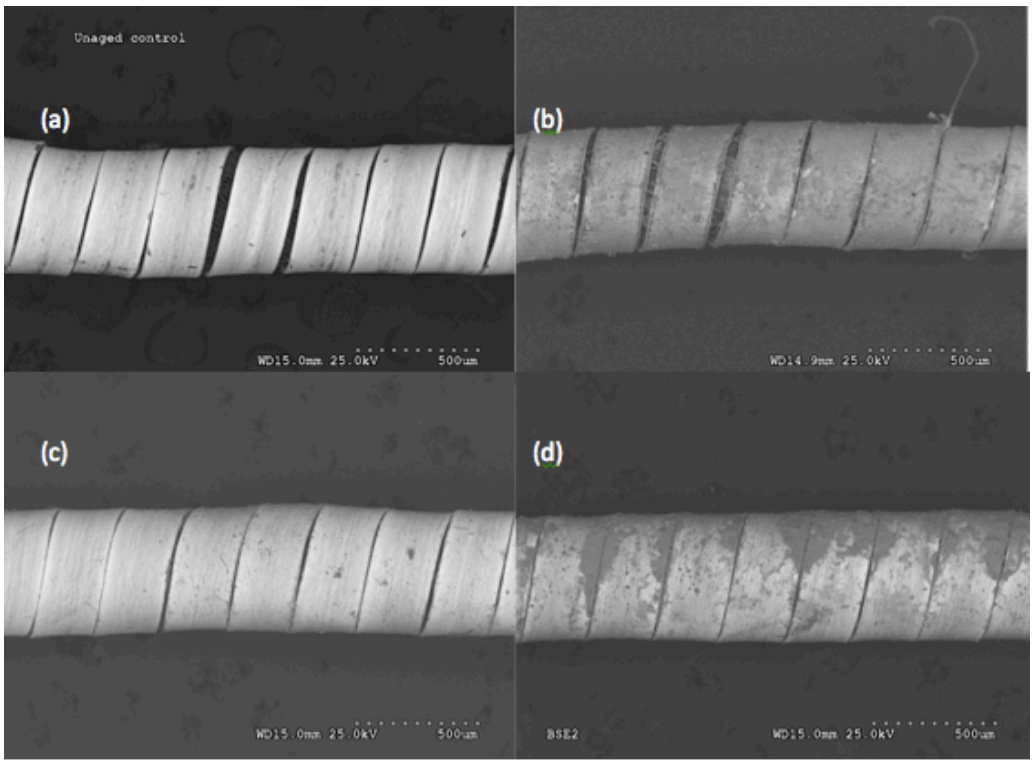

Figure 3.3.10 SEM micrographs of sections of the 500 hour photo-aged metallic thread sample: (a) unaged metallic thread, (b) W Alum, (c) W Oakgall, (d) S Oakgall

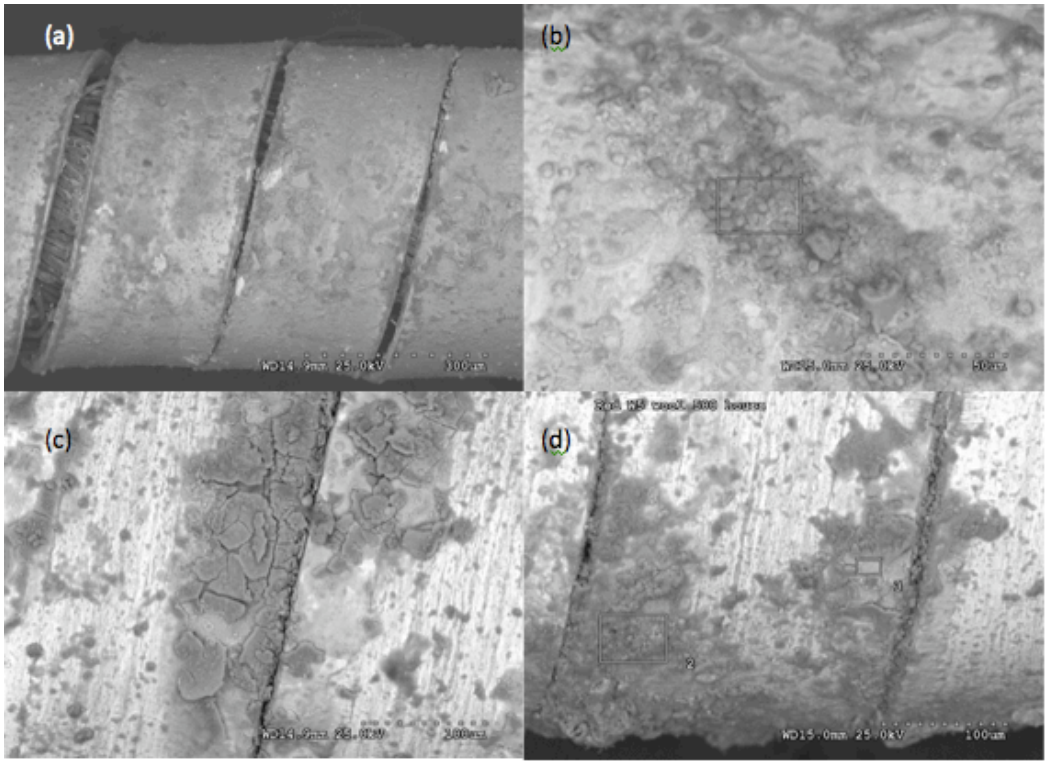

Figure 3.3.11 Detailed SEM micrographs of 500 hour photo-aged metallic thread samples: (a) W Alum, (b) W Brazil, (c) W Weld, (d) W Coch

Figure 3.3.11 (a) shows the W Alum sample, which is covered, in a continuous layer of corrosion with patches of thicker residues. The core silk fibres can be seen in this image through gaps in the metal filament wrapped around the 'Z' twisted core. Figure 3.3.11 (b) shows a growth of rounded corrosion product, which is visible over the total area but is more concentrated and forms larger residues in the central patch. The corrosion product formed in Figure 3.3.11 (c) has a different morphology and appears as flakes which have grown over the under layer of tarnishing and are paring away from the surface. The W Coch sample in Figure 3.3.11 (d) illustrates the presence of several different corrosion morphologies on a single sample; there is rounded corrosion and flakes and it can be seen clearly that the corrosion forms initially at the edges of the metal filament. It is clear that the lighter areas are where the gilding is still visible; the corrosion products grow over this layer obscuring the gold surface.

3.3.3.2.2 Surface analysis of metallic threads

EDX analysis was performed on up to 4 different areas on each of the photo-aged metallic thread samples in order to identify the elements that are present on the surface and in the corrosion products. The average percentage-by-weight values for each sample are given in the following discussion.

EDX analysis of the unaged metallic thread indicated the presence of 7% gold, 13% silver and 54% copper along with carbon (24%) and oxygen (1%). Carbon and oxygen values are attributed mostly to contamination of the surface; however, they may contribute to some corrosion residues - the presence of metal oxides is highly likely. XPS analysis of the unaged metallic thread detects average values of 10.3% gold and 8.2% silver as well as carbon (68.5%) and oxygen (13.1%) on the sample surface. The difference in the EDX and XPS values is due to the sampling depths of the techniques. The use of these two different techniques confirms the structure of the metal filament. EDX has a profiling depth of approximately 1-2 μm (1000-2000 nm) whereas XPS has a much smaller profiling depth of approximately 10 nm. The EDX instrument detects the surface gold and silver layers and also the underlying copper bulk of the filament while the more surface sensitive XPS instrument detects only the gold and silver layers at the surface (Nord & Tronner, 2000).

After 500 hours of photo-ageing the average EDX results of all of the irradiated metallic thread samples are 6.1% gold, 6.9% silver and 45.4% copper. The average XPS results are 0.4% gold, 0.8% silver and 6.3% copper. The difference in the XPS results after ageing indicates that during ageing the copper migrates to the surface of the samples through the gold and silver layers and is the main component in the top 10 nm of the surface. The EDX results are not as affected after ageing which is due to the depth of analysis, in that the copper and silver may migrate to the surface and form corrosion products while the EDX technique still detects the underlying gilt surface. The diagram in Figure 3.3.12 illustrates the changes in the surface composition of the metal filament during photo-ageing, note the movement of copper and silver ions to the sample surface and the growth of the corrosion layer over the gilt layer. The sampling depths of the two analytical techniques are approximated.

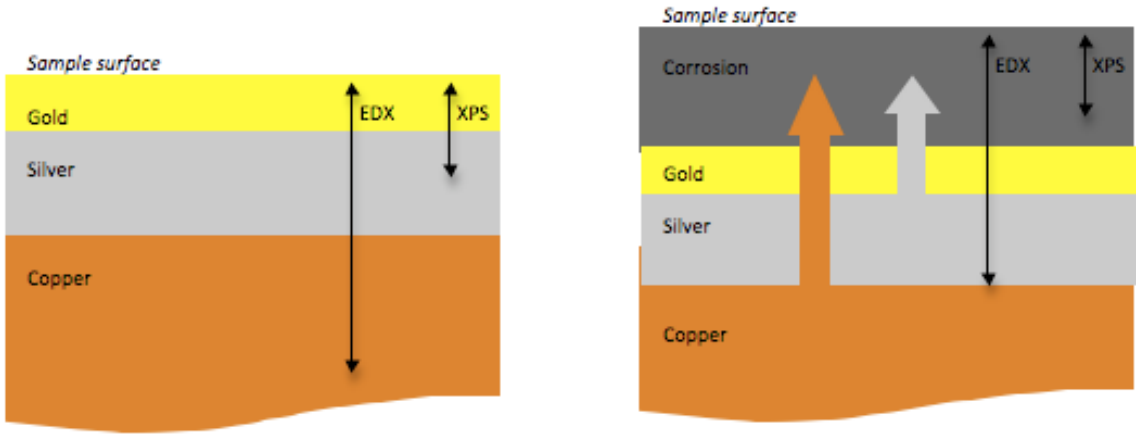

Figure 3.3.12 Diagram of the surface composition of the metal filament before and after photo-ageing

To evaluate the photo-ageing effects of the various dye/mordant combinations, ratios of the metallic elements of the surface analysis data have been calculated. This eliminates the contribution of the contamination products so that the values can be compared with each other. Figures 3.3.13 and 3.3.14 are graphs of the relative amounts of gold, silver and copper present on the wool and silk photo-aged metallic thread samples detected by EDX. As discussed, the Unaged Control sample contains a high proportion of copper at the surface 1-2 μm whilst the relative amounts do not change drastically after photo-ageing. The values for the wool and silk samples are comparable, with no dye/mordant combinations having a noticably different effect. Figures 3.3.15 and 3.3.16 display the data obtained from XPS analysis of the wool and silk photo-aged metallic thread samples.

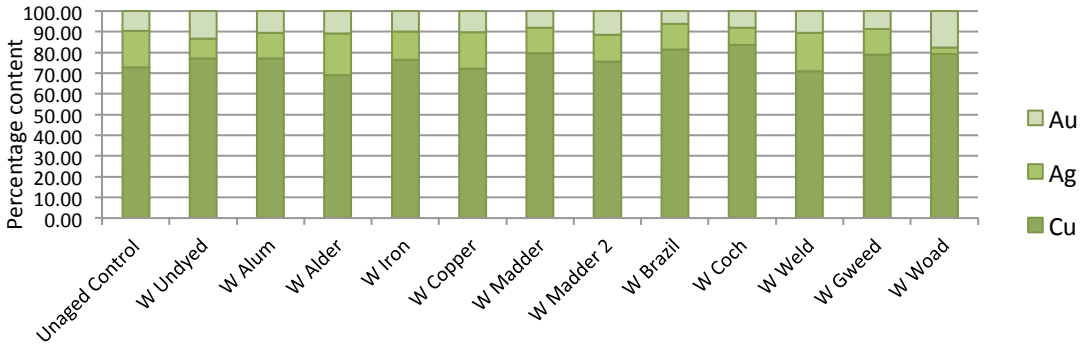

Figure 3.3.13 EDX data. Relative amounts of Au, Ag and Cu on wool photo-aged metallic thread samples

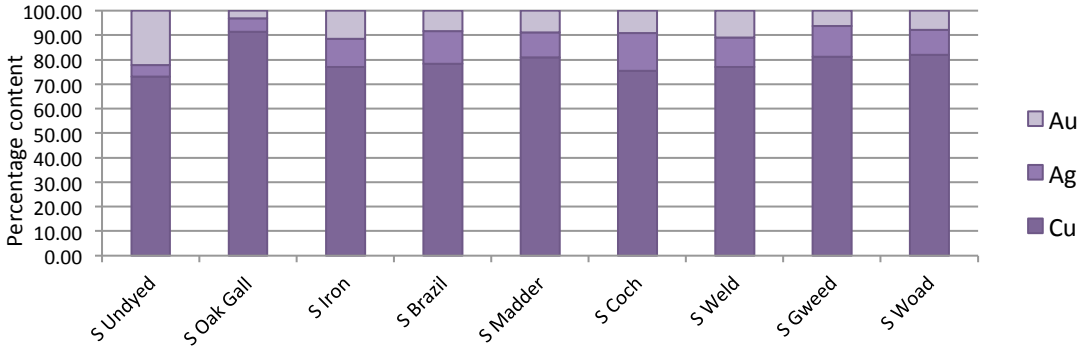

Figure 3.3.14 EDX data. Relative amounts of Au, Ag and Cu on silk photo-aged metallic thread samples

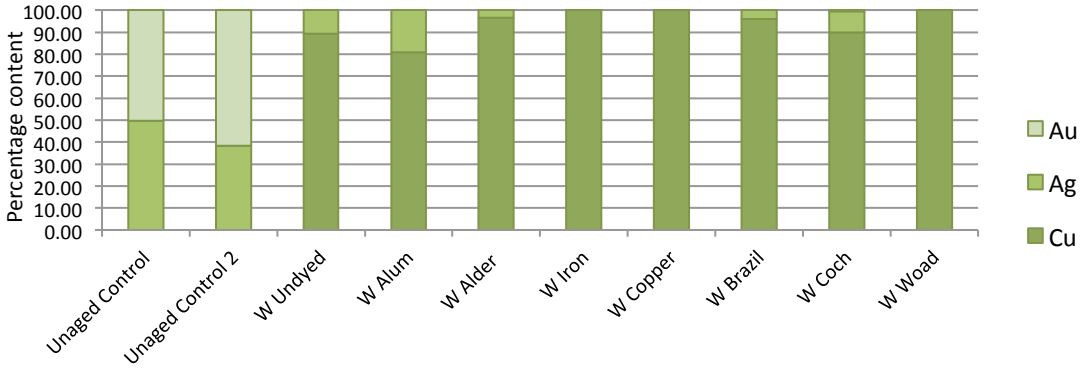

Figure 3.3.15 XPS data. Relative amounts of Au, Ag and Cu on wool photo-aged metallic thread samples

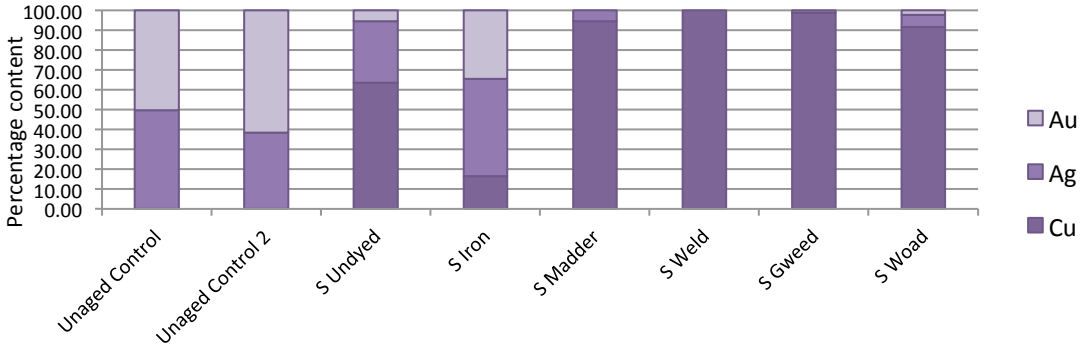

Figure 3.3.16 XPS data. Relative amounts of Au, Ag and Cu on silk photo-aged metallic thread samples

The XPS data graphs show clearly the difference between the unaged samples and the photo-aged samples. Only gold and silver has been detected on the two Unaged Control metallic threads while the other samples are dominated by the copper signal. Most of the samples have a small silver percentage and very little or no detectable gold. There is no noticeable trend as to which dye/mordant combinations have a specific metallic content, the exceptions being S Undyed, which exhibits a larger percentage of gold than most other samples, and S Iron which does not fit the trend. Visual assessment of these two samples gave both a 2/5 grading on the visual corrosion scale indicating a low level of corrosion coverage or small patches of corrosion. The anomalous results of the surface analysis of the S Iron sample is attributed to surveyed an area of low corrosion.

The lack of influence of the dye/mordant combinations is possibly due to the nature of the experiment. The radiation in the Xenotest instrument falls directly onto the metallic threads as well as the dyed fabric samples that they are mounted onto. The effect of the radiation on the metallic threads is equal for all samples. The heat caused by the radiation triggers the migration of the copper and silver through the gold layer. The temperature experienced by the samples during the photo-ageing experiment has been measured at up to 40°C. The effect of the radiation on the dyed fabrics is the volatilisation of sulphur compounds from the wool fibres and from compounds present in the dye and mordant residues. The samples are not isolated in the Xenotest Weatherometer, which means all samples are potentially exposed to any gases released during photo-ageing. However, the closer vicinity to the dyed fabrics has resulted in the observed variations in the level of corrosion, and the variety of corrosion products that have formed on the individual samples, as can be seen from visual analysis of the metallic threads.

The surface analysis of the metallic threads revealed the elements that are present at the surface. The range of photo-aged metallic threads contained C, O, Cu, Ag, Au, S, Cl, Si, N, Ca, K (EDX), Al (EDX), Na (EDX) and Mn (XPS). The EDX data had average values of 15% C and 19% O whereas the XPS data gave average values of 49% C and 30% O. These large values are attributed predominantly to contamination with possibly some carbon and oxygen contained within the corrosion products. The origin of the sulphur present on most of the samples is from the photo-oxidation of

the sulphur containing amino acids in wool fibres. No S was detected on the unaged control metallic thread sample. The origin of chlorine is possibly from salt used during the dyeing process and from handling. Cl was detected using XPS on most of the photo-aged samples with the exception of W Undyed and S Undyed indicating that Cl is introduced during dyeing. The presence of Al, Mn, K, Mg, Si, Na and Ca is attributed to contamination.

It was not possible to confidently use the sulphur weight % values (EDX) and atomic % values (XPS) quantitatively to characterise the corrosion behaviour due to the high level of C and O contamination on the surface of the metal filament. It was not possible to distinguish the amount of C and O that was contained in corrosion products and which was contamination. Therefore the amount of sulphur relative to the metal contribution at the sample surface i.e. S/(Cu+Ag+Au) was used for data comparison. There was no sulphur detected on the unaged control metallic thread samples whereas sulphur was detected on nearly all of the photo-aged metallic thread samples which indicates that the formation of sulphur containing residues on the samples occurs due to photo-ageing. The highest levels of S/(Cu+Ag+Au) were detected on W Undyed, W Alum and W Copper samples, the highest being W Alum (0.04) using EDX analysis, and W Undyed (0.88) using XPS. S/(Cu+Ag+Au) values are larger for XPS than for EDX due to the higher surface sensitivity of the XPS technique. XPS analyses less of the bulk metal than EDX, therefore the sulphur at the surface contributes more to the S/(Cu+Ag+Au) ratio. The XPS data showed that on average wool samples exhibited a larger ratio of S/(Cu+Ag+Au) at 0.61 than the silk samples at 0.22. The higher level of S present on the wool samples was due to photo-ageing causing oxidative cleavage of the disulphide bond in wool. Silk has a relatively low content of sulphur amino acids, which leads to a reduced amount of volatilised sulphur. However, the silk fabric samples do have a wool warp that will contribute to the sulphur content found on the silk samples. The S/(Cu+Ag+Au) values obtained using EDX, for wool and silk samples are shown in Figures 3.3.17 and 3.3.18. The XPS data is shown in Figures 3.3.21 and 3.3.22.

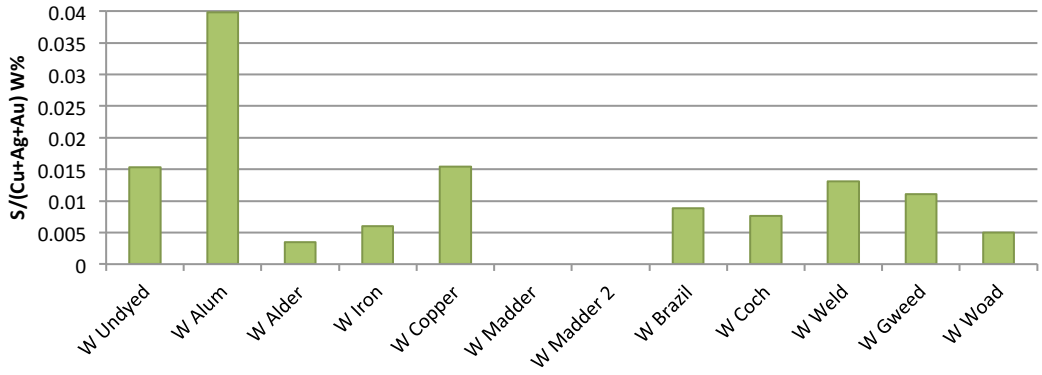

Figure 3.3.17 EDX data. S/(Cu+Ag+Au) of wool photo-aged metallic thread samples

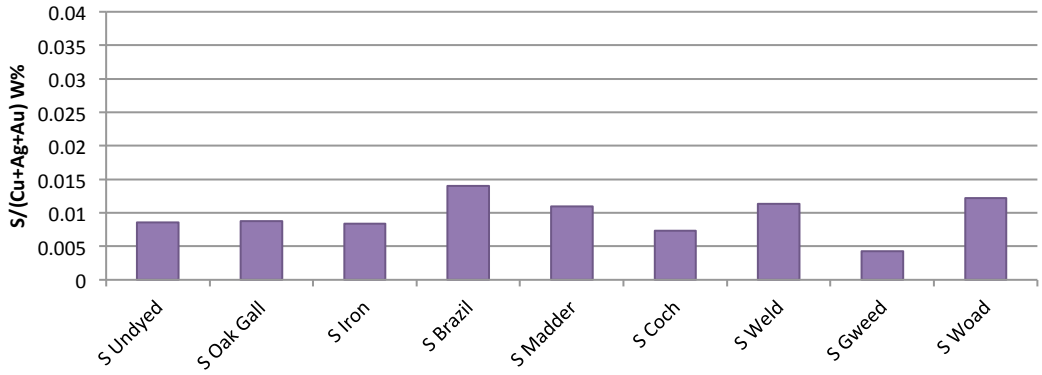

Figure 3.3.18 EDX data. S/(Cu+Ag+Au) of silk photo-aged metallic thread samples

To determine the influence of sulphur content on the perceived degradation of the metallic thread samples, S/(Cu+Ag+Au) has been plotted against the visual corrosion scale in Figures 3.3.19 and 3.3.20.

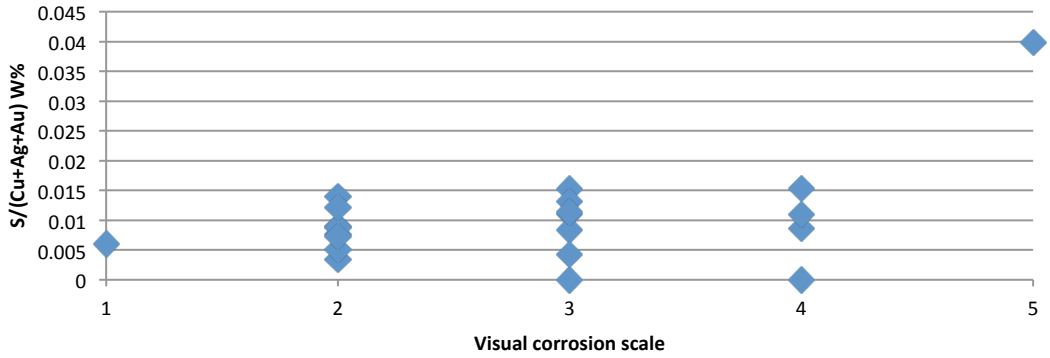

Figure 3.3.19 EDX data. S/(Cu+Ag+Au) against the visual corrosion scale of photo-aged metallic thread samples

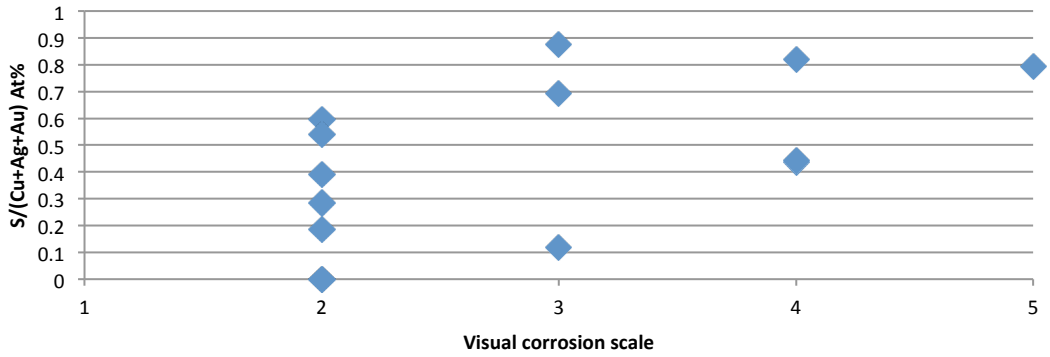

Figure 3.3.20 XPS data. S/(Cu+Ag+Au) against the visual corrosion scale of photo-aged metallic thread samples

There appears to be a broad correlation between the sulphur content detected by EDX and XPS and the visual level of corrosion of the photo-aged metallic thread samples. However, there are a range of S/(Cu+Ag+Au) values present on samples that have been judged to have similar levels of corrosion coverage, which indicates that the sulphur content may not be the sole factor in the degradation appearance of the metallic threads. The possible influence of chlorine content was investigated but was found to have no direct impact on the appearance of the metallic threads.

High resolution XP spectra of the S (2p) peak were curve fitted using the CASA XPS software to determine the relative percentages of the component peaks. The peaks found at different binding energies signify the presence of sulphur in at least two chemical states. The initial peak at 164 eV and secondary peak at 168 eV were attributed to sulphide (2^+) and sulphate (6^+) respectively. The average content of sulphur in its higher oxidation state (6^+) relative to its lower oxidation state (2^+) on the photo-aged samples is 44%. There is correlation on some samples between the higher levels of copper present at the sample surface and the increased level of S (6^+), which was attributed to the formation of copper sulphate corrosion, $CuSO_4$. The amount of sulphur in its different oxidation states relative to the metallic content at the sample surface is shown in Figures 3.3.21 and 3.3.22. Where it was not possible to distinguish the separate oxidation states, the overall amount of sulphur detected was plotted.

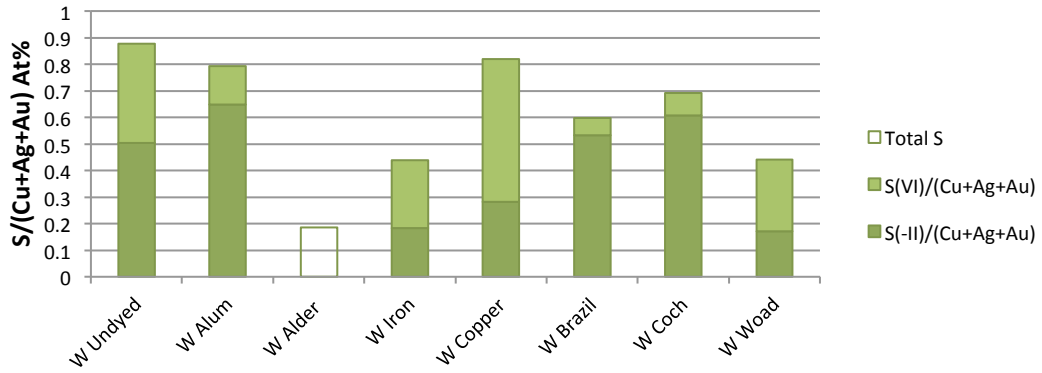

Figure 3.3.21 XPS data. S/(Cu+Ag+Au) of wool photo-aged metallic thread samples showing content of S 2p oxidation states

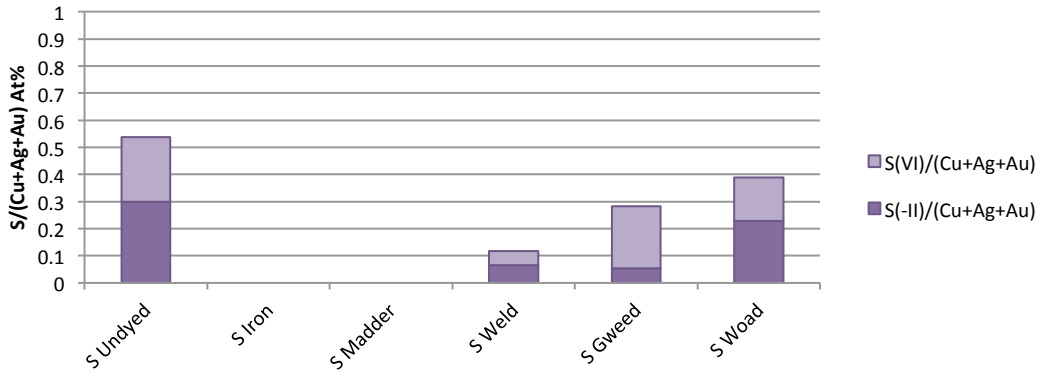

Figure 3.3.22 XPS data. S/(Cu+Ag+Au) of silk photo-aged metallic thread samples showing content of S 2p oxidation states

3.3.3.2.3 Colour measurement of dyed tapestry fabric

Images of the unaged fabric and the photo-aged fabric samples with metallic threads attached were taken with a Canon Digital IXUS 70 compact digital camera in a light booth under daylight, with the MiniColorChecker chart for reference. The images illustrate the progressive photo-fading of the dyed fabrics from the unaged sample to after 100, 300 and 500 hours of exposure to photo-radiation. Figure 3.3.23 shows two examples; the blue W Woad samples remain relatively unfaded after exposure to light whereas the red S Brazil fabric is extremely photo-faded.

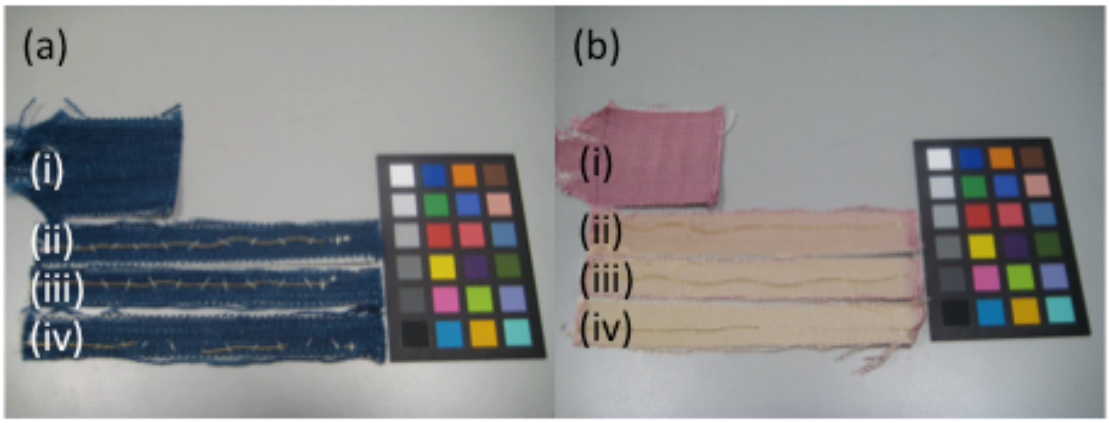

Figure 3.3.23 Samples of photo-aged fabric and metallic threads: (a) woad dyed wool sample *W Woad* (i) unexposed fabric, (ii) 100 hour photo-aged, (iii) 300 hour photo-aged, (iv) 500 hour photo-aged sample, (b) brazilwood dyed silk sample *S Brazil* (i) unexposed fabric, (ii) 100 hour photo-aged, (iii) 300 hour photo-aged, (iv) 500 hour photo-aged sample.

A Datacolor Spectraflash 600 spectrophotometer was used to measure the reflectance spectra of the dyed fabric samples before ageing and after 100 hours, 300 hours and 500 hours of photo-ageing. The samples were measured using a small aperture, UV and specular excluded using D65 illuminant and 10 degree field of view. Results shown in Table 3.3.4 are given as CIELAB values with ΔE^*_{ab} colour difference calculated using the dyed unaged fabric as the standard and the aged samples (after 100, 300 and 500 hours light exposure) as the batches. L* values give the lightness of the sample, as the samples are exposed to radiation, photo-fading of the dyes results in increased lightness values. The a* and b* values indicate the positions of the samples in colour space. A light fast dye such as woad exhibits relatively constant results for L*, a* and b* (W Woad sample). After 500 hours of photo-ageing the hue has remained constant (dH* = 0), the difference in chroma is negligible and the sample has lightened by a very small amount (dL*=1.55, dC*=0.66). In contrast, the brazilwood dyed wool sample (W Brazil) becomes lighter and more neutral when exposed to greater concentrations of light, dL* = 26.2, dC* = -2.51. Interestingly the hue of the W Brazil sample has changed dramatically, dH* = 21.7, which is attributed to the red dye being lost and the 500 hour sample having the colour of photo-yellowed wool. The highest ΔE^*_{ab} values, and therefore the most fugitive dyes are found for brazilwood and weld, ΔE^*_{ab} W Brazil = 34.1, S Brazil = 28.5, W Weld = 34.9, S Weld = 21.1.

Table 3.3.4 CIELAB values for model dyed fabric samples prior and post photo-ageing

	Unaged			100 hours				300 hours				500 hours						
Sample	**L***	**a***	**b***	**L***	**a***	**b***	**ΔE***	**L***	**a***	**b***	**ΔE***	**L***	**a***	**b***	**ΔE***	**ΔL***	**ΔC***	**ΔH***
W Undyed	77.9	-0.2	12.0	80.7	-0.6	12.7	2.9	81.1	-0.9	14.7	4.3	80.7	-0.7	14.6	3.8	2.7	2.63	0.47
W Alum	84.2	-0.2	12.7	86.4	-0.5	11.1	2.7	84.9	-1.3	15.1	2.8	84.9	-1.4	17.3	4.8	0.7	4.65	0.95
W Alder	54.8	5.7	23.4	60.7	5.6	24.1	5.9	64.2	4.6	23.4	9.5	67.2	3.7	22.1	12.6	12.4	-1.66	1.71
W Oakgall	63.8	2.9	23.5	62.8	5.0	30.2	7.1	64.3	4.5	27.9	4.7	66.5	4.0	25.9	3.8	2.7	2.52	0.72
W Iron	25.8	1.4	2.1	29.7	1.6	5.0	4.8	29.3	1.4	5.6	4.9	30.1	0.9	6.3	6.0	4.3	3.85	1.70
W Copper	32.2	1.1	12.6	36.8	1.2	15.3	5.2	37.8	0.9	17.0	7.1	40.9	0.6	17.9	10.2	8.7	5.22	0.75
W Madder	33.9	31.5	21.9	40.6	31.0	21.7	6.7	46.4	28.1	20.9	13.0	50.0	25.5	19.4	17.4	16.1	-6.30	1.51
W Madder2	39.6	23.6	22.9	46.1	21.4	22.9	6.9	52.5	15.9	20.9	15.1	55.2	13.8	20.5	18.6	15.6	-8.14	5.94
W Brazil	48.3	21.9	7.9	65.9	9.3	18.0	23.9	70.8	5.9	20.0	30.1	74.5	3.9	20.4	34.1	26.2	-2.51	21.7
W Coch	41.1	37.3	9.4	47.1	28.7	5.5	11.2	53.9	20.9	7.1	20.9	60.3	15.0	8.7	29.4	19.1	-21.2	7.18
W Weld	67.8	3.1	63.0	71.3	2.6	43.3	20.1	74.2	1.7	33.8	30.0	75.2	1.7	28.9	34.9	7.4	-34.1	0.45
W Gweed	58.3	1.8	40.1	63.1	2.1	32.0	9.4	66.2	1.7	27.6	14.8	68.6	1.5	23.2	19.8	10.3	-16.9	0.54
W Woad	28.0	-3.4	-13.8	31.4	-3.5	-13.4	3.4	29.3	-3.2	-14.4	1.4	29.5	-3.5	-14.5	1.6	1.5	0.66	0.00
S Undyed	84.7	0.8	8.4	84.0	0.6	11.9	3.6	83.2	0.8	16.3	8.1	82.9	1.2	18.3	10.1	-1.8	-9.98	0.42
S Oakgall	72.8	2.4	18.4	68.9	3.6	27.1	9.6	70.6	3.4	27.2	9.2	68.9	4.1	27.2	9.8	-4.0	-8.93	0.41
S Iron	20.9	1.1	-1.2	21.5	0.9	-0.9	0.7	21.3	1.0	-0.2	1.1	21.3	0.6	0.6	1.9	0.3	-0.82	1.68
S Brazil	56.2	15.5	0.9	68.2	5.9	14.9	20.8	73.4	3.8	16.5	26.0	76.1	2.6	16.7	28.5	19.9	1.30	20.39
S Madder	60.9	25.2	12.0	66.3	19.3	12.6	8.0	71.0	13.9	14.3	15.3	72.3	12.5	15.5	17.4	11.4	-8.03	10.44
S Coch	43.2	30.2	10.4	44.0	25.1	7.2	6.1	47.8	20.0	7.4	11.6	48.8	17.4	7.9	14.2	5.6	-12.8	2.27
S Weld	72.3	-3.0	51.5	71.2	1.1	42.3	10.1	73.0	1.0	33.9	18.0	74.2	1.1	30.8	21.1	1.9	-20.7	3.72
S Gweed	68.7	-0.8	41.8	69.7	1.8	32.7	9.5	71.9	1.9	27.2	15.1	72.5	2.1	24.3	18.1	3.8	-17.4	3.39
S Woad	41.7	-7.3	-9.1	44.2	-7.8	-8.7	2.5	48.0	-8.8	-6.0	7.2	49.7	-8.1	-4.7	9.1	8.0	-2.32	3.80

Figures 3.3.24 and 3.3.25 display the colour differences between the unaged dyed fabric and the wool and silk fabric samples respectively, after 100, 300 and 500 hours of accelerated photo-ageing. Note that the woad dyed wool sample W Woad demonstrates the smallest change in ΔE^*_{ab} values and thus has a high level of light fastness. Brazilwood and weld dyed wool and silk samples have poor light fastness. Woad has a lower light fastness on silk than on wool.

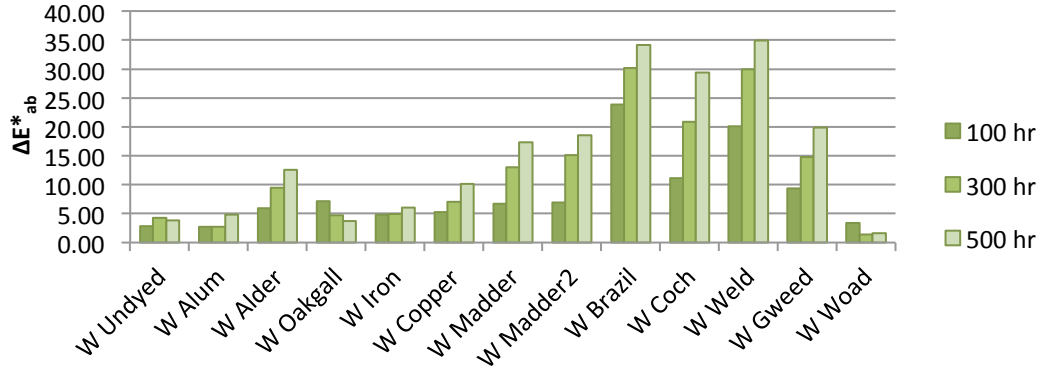

Figure 3.3.24 Colour difference of wool samples calculated after 100, 300 and 500 hours of photo-ageing

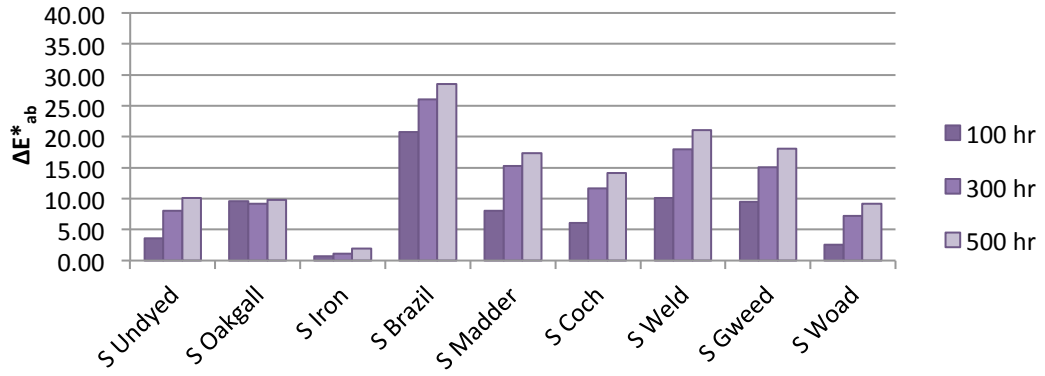

Figure 3.3.25 Colour difference of silk samples calculated after 100, 300 and 500 hours of photo-ageing

The brazilwood and cochineal dyed wool samples (W Brazil and W Coch) can be compared in terms of fading rates; W Brazil has a high ΔE^*_{ab} value after 100 hours and relatively small colour change after 300 and 500 hours whereas the colour differences in W Coch are more gradual over time. This effect is represented using CIELAB L* (lightness) plotted against C* (chroma) in Figure 3.3.26 for W Brazil and Figure 3.3.27 for W Coch. Underneath each plot is a representation of the colour fading profiles for each dye after 0, 100, 300 and 500 hours obtained by transforming CIELAB values to sRGB under illuminant D65, using the Colour Toolbox in MATLAB (Westland & Ripamonti, 2004). It can be seen that after 100 hours the brazilwood fabric has faded significantly and by 500 hours little of the original colour has remained. The fading of cochineal fabric is more gradual and some colour still remains after 500 hours.

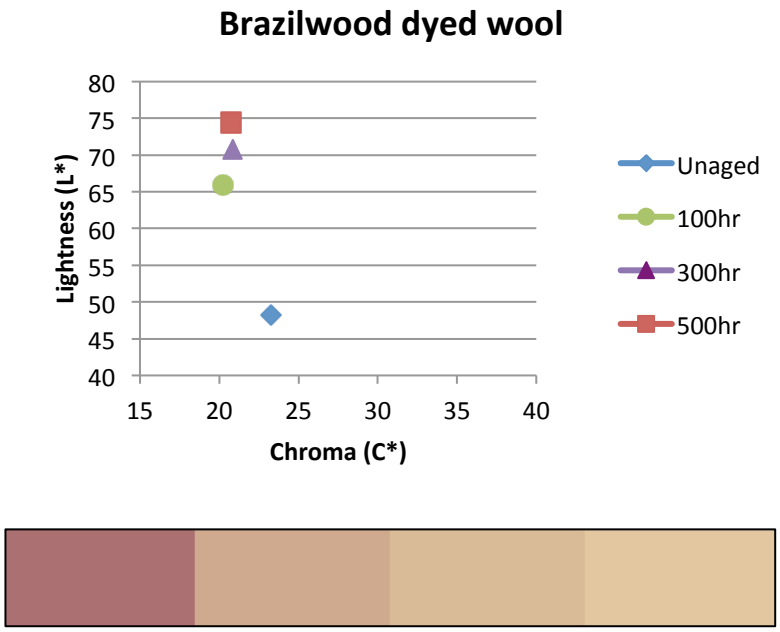

Figure 3.3.26. A plot of lightness (L*) against chroma (C*) for sample W Brazil after 100, 300 and 500 hours of photo-ageing

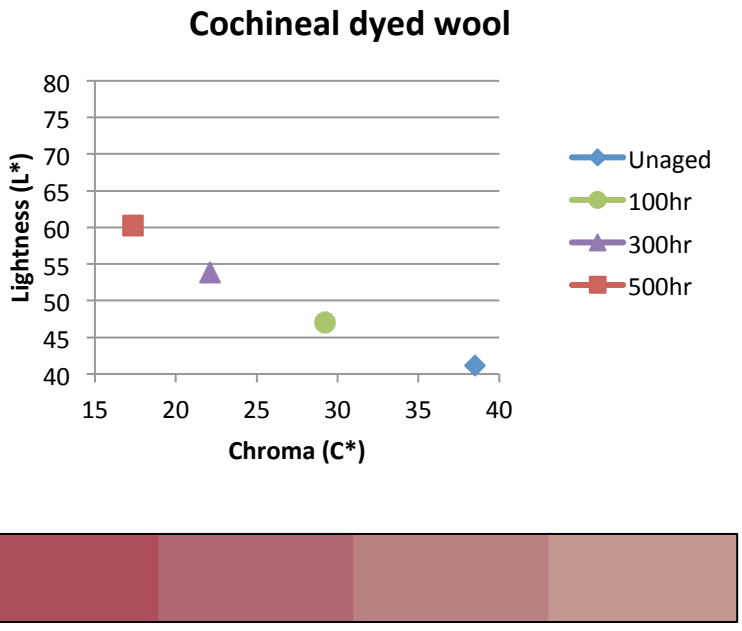

Figure 3.3.27. A plot of lightness (L*) against chroma (C*) for sample W Coch after 100, 300 and 500 hours of photo-ageing

Both undyed wool and silk samples experience an increase in chroma after 500 hours of photo ageing, which is attributed to photo-yellowing of the fibres.

3.3.3.2.4 Surface analysis of dyed wool fibres

To investigate the composition of the wool fibres and to evaluate the effects of photo-ageing at the fibre surface, XPS analysis was performed on undyed wool and several dyed wool samples, before and after photo-ageing. A selection of the wool samples were chosen for analysis to investigate the composition of a variety of dyed fibres; W Undyed was chosen as a standard, mordanted wool samples W Alum and W Oakgall were selected so that the two main mordants could be investigated and also due to the high level of corrosion found on the W Alum photo-aged metallic thread. In addition two dyed samples were selected; W Copper and W Madder2. The processing methods for the selected samples are shown in Table 3.3.5.

Table 3.3.5 Processing methods for wool fibre samples selected for surface analysis

	Mordanting process	Dyeing process	Total processing time
W Undyed	-	-	0 hours
W Alum	Alum 1.5 hours	-	1.5 hours
W Oakgall	Oakgall 2 hours	-	2 hours
W Copper	Oakgall 2 hours	Copper & Iron Sulphate 1.5 hours	3.5 hours
W Madder2	Oakgall 2 hours Alum 2 hours	Madder 3 hours	7 hours

XPS analysis of various undyed, mordanted and dyed wool fibres detected C, O, N, S, Si, Al, Cu, Fe and Ca species at the sample surface. The detection of C, O, N and S species at the fibre surface was due to wool proteins, Si detected on most samples was attributed to contamination. Al was present on the alum mordanted sample at 5.5 At%. This value increased to 6.8% after photo-ageing possibly due to migration initiated by heat or the breakdown of the surface layer that revealed the protein layer where the metal ions are located. Cu and Fe species were detected on the W Copper sample which has been dyed with both iron sulphate and copper sulphate. Cu content of 0.2%, increased to 0.3% after photo-ageing. Fe content of 0.1% increased to 0.3% after photo-ageing. Ca was detected on only one sample and was attributed to contamination.

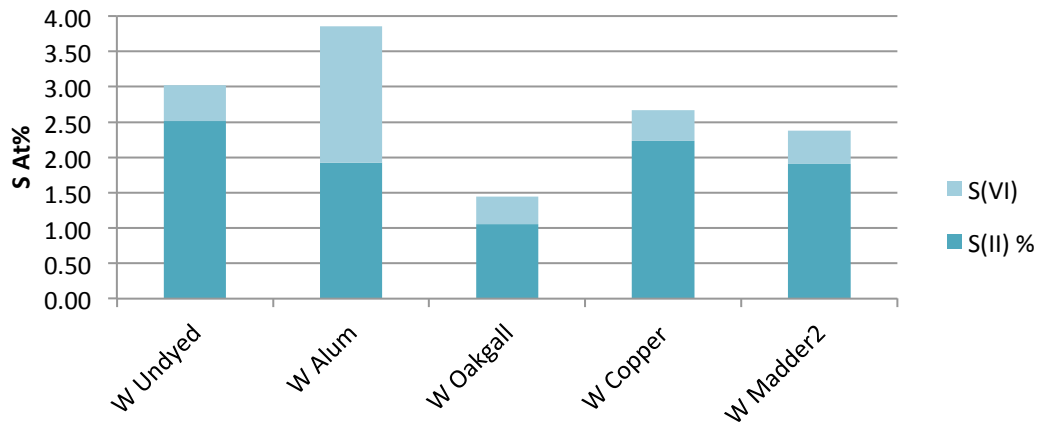

Figure 3.3.28 S2p peak components of mordanted and dyed wool fibres

Figure 3.3.28 shows the sulphur content of the 500 hour photo-aged wool fibres, indicating the relative content of the different S(2p) oxidation states. Photo-oxidation of wool causes the breakage of the disulphide crosslinks in cystine, and the formation of cysteic acid, which is indicated by the change in oxidation state from S^{2+} to S^{6+}. There is S^{6+} present in unaged wool because the sheep are exposed to light during their lifetime therefore photo-oxidation will occur on the sheep.

XPS of W Undyed detected 3.0% sulphur which consists of 83% S^{2+} and 17% S^{6+}. More cysteic acid is formed after 500 hours photo-ageing, 65% S^{2+} to 35% S^{6+} for 3.2% sulphur. The S^{6+} contribution for W Alum and W Copper fabrics increased after photo-ageing. W Alum has a particularly high concentration of S^{6+} before and after ageing, which is attributed to the alum mordanting process that involves boiling the wool with alum, $Al_2(SO_4)_3$, for 90 minutes during which time the $-SO_4^{2-}$ from alum must have an affinity for the wool fibre as the sulphate remains after the fibres are rinsed. This addition of sulphur containing residues to the wool accounts for the increase in sulphur from W Undyed (3.0%) to W Alum (3.9%).

W Oakgall has a lower S content than undyed wool. The removal of surface S containing residues probably occurs during the 2 hour boiling of the mordanting process. W Copper is mordanted with oakgall for 2 hours, and then dyed with iron sulphate and copper sulphate for 90 minutes, which accounts for the increase in S content. W Madder2 is mordanted with oakgall for 2 hours, then mordanted with alum for 2 hours, then dyed with madder for 3 hours. This is the longest processing time of all the dyed samples. The alum mordant doesn't seem to have the same

effect of increasing the S^{6+} content of the W Madder2 fibre sample. However, the fibres have been pre-treated with oakgall that must prevent the $-SO_4^{2-}$ from fixing to the wool in the same way, so that the sulphate is rinsed out during the subsequent dyeing process. The tannate in oak galls is anionic and this may indeed provide electrostatic repulsion.

XPS analysis of wool fibres shows that the dyeing and mordant processes with the longer processing times produce a lower surface Sulphur content in the wool fibre due to hydrothermal degradation of the cysteine, leading to lanthionine formation and loss of sulphide. This reduced sulphur could contribute to a lower level of corrosion products on the metallic threads adjacent to these fibres. The sulphur levels on the fibres decreased further after photo-ageing due to the possible greater susceptibility of lanthionine to photo-volatilisation.

3.3.4 Experiment 2: Thermal ageing

3.3.4.1 Methodology

Thermal degradation was simulated by performing an Oddy Test on the metallic and textile components of the model tapestry. The Oddy test is an accelerated ageing test used to assess the corrosiveness of each dye/mordant combination. Test tubes were prepared for each sample containing 2 grams of the dyed fabric and a vial of de-ionised water sufficient to maintain a relative humidity of 100%. Coupons of copper and silver and a 5 cm folded length of metallic thread were suspended from a silicone stopper by inserting them 5 mm into slits cut into the stopper. The tubes containing the dyed fabric and one control sample containing only the vial of de-ionised water were sealed with the stoppers. The 22 fabric samples and one control sample were incubated at 60°C for 28 days. The experimental setup is shown in Figure 3.3.29. The experiment was carried out in the Textile conservation Studio at Hampton Court Palace. The metallic samples were stored in acid-free tissue paper after removal from the test tubes.

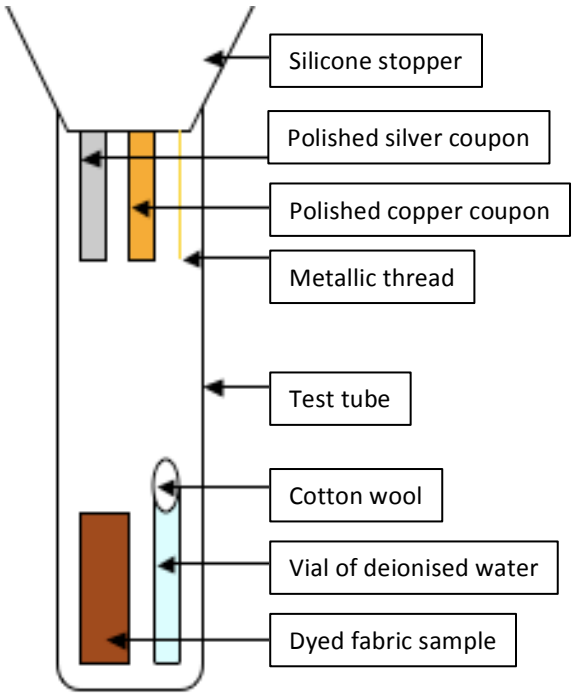

Figure 3.3.29 Oddy Test setup

3.3.4.2 Results and Discussion

3.3.4.2.1 Visual analysis of metal coupons and metallic threads

Images of the copper coupons, silver coupons and metallic threads from each sample tube were taken using a digital camera. These images were used to assess the level of corrosion seen on each of the sample sets. The coverage of corrosion, and the severity of the discolouration of the metallic surface were judged comparatively so that each sample set has its own visual corrosion scale. The factors that were used to grade the metal coupons and the metallic thread samples are outlined in Table 3.3.6. Examples of one sample from each of the 5 levels of the visual corrosion scale for the metal coupons and threads are shown in Figures 3.3.30 – 3.3.34. The values assigned for each of the dye/mordant combinations are given in Table 3.3.7.

Table 3.3.6 Factors used to assess the visual corrosion scales of thermal aged copper coupons, silver coupons and metallic threads

Copper coupons	
1	Slight discolouration of metal giving a red tinge
2	Tarnishing at the tip of the sample
3	Tarnishing of the bottom third of the sample with corrosion at the tip
4	Tarnishing of at least half of the sample with corrosion at the tip
5	Tarnishing of the whole sample with pronounced corrosion
Silver coupons	
1	No discolouration of the sample
2	Slight tarnishing at the tip
3	Grey tarnishing on the bottom quarter of the sample
4	Dark grey tarnishing of the sample with corrosion at the tip
5	Significant corrosion on the sample
Thermal aged metallic threads	
1	No discolouration of the sample
2	Discolouration of the sample
3	Tarnishing of the complete sample
4	Significant corrosion of sample
5	Complete corrosion of sample

Figure 3.3.30 Thermal aged copper coupons. One sample from each of the 5 levels of the visual corrosion scale; (a) Control sample (1), (b) S Oakgall (2), (c) W Iron (1), (d) W Coch (4), (e) W Alum (5)

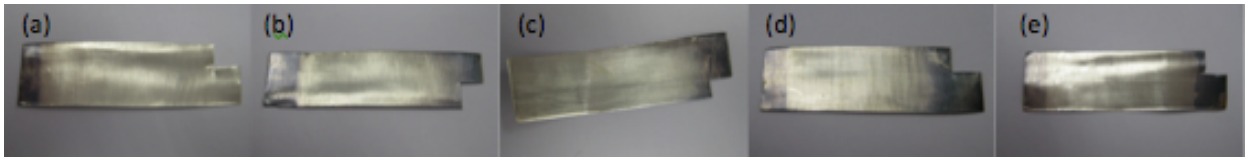

Figure 3.3.31 Thermal aged silver coupons. One sample from each of the 5 levels of the visual corrosion scale; (a) W Copper (1), (b) W Woad (2), (c) W Oakgall (3), (d) W Coch (4), (e) W Madder2 (5)

Figure 3.3.32 Thermal aged metallic threads. One sample from each of the 5 levels of the visual corrosion scale; (a) S Brazil (1), (b) W Undyed (2), (c) W Copper (3), (d) W Weld (4), (e) W Iron (5)

Table 3.3.7 Level of corrosion on thermal aged samples as assessed by the visual corrosion scales

Sample	Copper coupon	Silver coupon	Thermal aged thread
Aged Control	1	1	1
W Undyed	5	3	2
W Alum	5	4	2
W Alder	4	4	2
W Oakgall	3	3	2
W Iron	3	2	5
W Copper	1	1	3
W Madder	4	4	4
W Madder2	3	5	5
W Brazil	5	3	2
W Coch	4	4	5
W Weld	3	4	4
W Gweed	4	3	5
W Woad	3	2	5
S Undyed	5	3	2
S Oakgall	2	2	2
S Iron	3	4	3
S Brazil	1	3	1
S Madder	3	5	4
S Coch	4	3	2
S Weld	5	2	2
S Gweed	2	2	4
S Woad	3	3	5

The effect of thermal ageing on the copper coupons is initial tarnishing of the surface, which is of a reddish brown colour. The variation in the colour of this film is due to the interference of light due to its thickness rather than differing corrosion products. The next stage of ageing is the formation of grey corrosion at the tip of the coupon closest to the fabric sample which then spreads to cover more of the sample surface, in some cases the whole coupon. In the most severe cases the corrosion at the sample tip is black. There are significant differences in the level of corrosion found on the various dye/mordant combinations. The wool samples were on average more corroded than the silk samples with W Undyed and W Alum being amongst the worst affected wool samples and S Undyed and S Weld being the worst affected silk samples. The least corroded samples were W Copper, S Oakgall and S

Gweed. The Control sample suffered the least effect with the reddish brown tarnish forming on the sample surface. The growth of the corrosion from the tip of the coupon closest to the fabric confirms that it is the degradation of the fabric that causes the metal to corrode. The ends of the metal coupons, which were inserted into a slit in the silicone stopper have suffered some tarnishing which is common in the Oddy Test experiment. This factor does not interfere with the analysis of corrosion on the coupons as the tarnishing is localised and does not spread down the sample.

The discolouration of the silver coupons is less severe than the copper coupons. The initial silver tarnish is light grey which forms on the bottom third of most samples, a dark grey corrosion product forms at the tip of the more corroded samples. As seen on the copper coupons, the growth of the silver tarnish is from the tip of the sample, spreading upwards; however, the discolouration covers a smaller area of the silver coupons than the copper on average. The wool samples were slightly more corroded than the silk samples on average with W Madder2 and S Madder being the worst affected. The least corroded samples were W Copper, W Woad, S Oakgall and S Weld. The Control sample suffered the least effect with no discolouration of the sample surface.

The metallic thread samples have a wider range of corrosion levels than the silver coupons. The samples which are least affected show some reddish brown discoloration of the surface which is followed by the formation of some green corrosion product at the edges of the metal filament. The next stage is the change from brown discolouration to grey corrosion, which covers the entire surface of some samples, and then the formation of a black corrosion product on the surface of some samples. The wool samples were more corroded on average than the silk samples with W Iron, W Madder2 and S Woad being the worst affected. The least corroded samples were W Oakgall and S Brazil. The Control sample showed some slight discolouration of the surface.

The three metallic test samples were all incubated in a single test tube with each of the fabric samples and a water source. The copper coupons showed more tarnishing and corrosion than the silver coupons, which is attributed to the higher

reactivity of copper and the preferential reaction of the gases present in the tube with the copper rather than the silver. The metallic threads contain copper and silver that are covered with a thin layer of gold. The protective effect of the gold layer can be seen in the samples that have less corrosion on the surface; however, the action of heat on the metals causes the copper and silver to migrate through the gold layer to the surface where they then react. The metallic threads appeared to withstand corrosion up to a point, after which they became heavily corroded and significantly visually degraded.

SEM images of the thermal aged copper coupons, shown in Figure 3.3.33, display a more detailed image of the corrosion products that have formed at the tip of the samples. The aged Control sample (a) shows small patches of corrosion formed over the entire surface, the W Undyed sample (b) displays a rod-like corrosion product whereas the W Gweed coupon (c) has rounded or *cauliflower* corrosion covering the surface. The control sample was given a visual corrosion scale grading of 1, the W Undyed a grading of 5 and W Gweed a grading of 4.

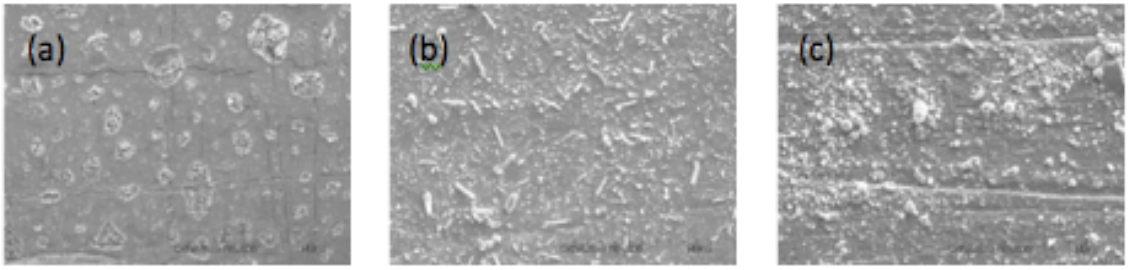

3.3.33 SEM micrographs of thermal aged copper coupons; (a) Control sample, (b) W Undyed, (c) W Gweed

The SEM images of the silver coupons show a much smaller range of corrosion morphologies than seen on the copper coupons. The corrosion products on each of the samples shown in Figure 3.3.34 are flake-like, growing over the surface in separate layer. The control sample (a) was given a visual corrosion scale grading of 1 while the W Alder (b) and S Iron (c) samples were given a grading of 4 indicating worse affected samples although there is little difference visible from the SEM micrographs.

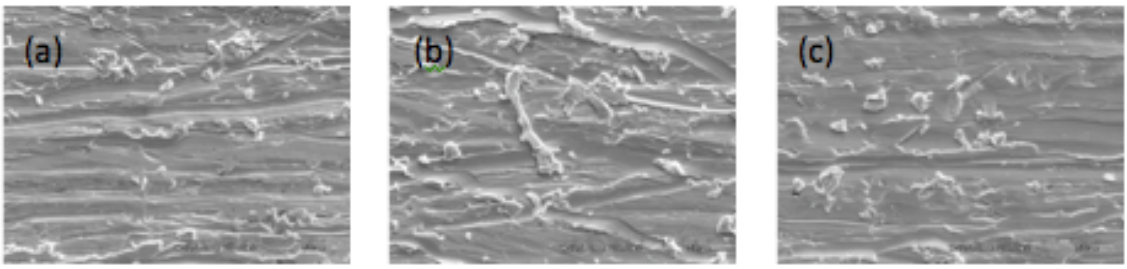

Figure 3.3.34 SEM micrographs of thermal aged silver coupons; (a) Control sample, (b) W Alder, (c) S Iron

3.3.4.2.2 Surface analysis of copper coupons, silver coupons and metallic threads

Surface analysis of the copper coupons, silver coupons and metallic threads was performed on an area from the tip of the sample that was closest to the fabric. This is where the corrosion initially forms on the metal samples in the test tube. EDX analysis of the thermal aged copper coupons was carried out on up to 2 areas of the sample with the average results given here. The aged control sample was found to contain 34% carbon, 7% oxygen and 59% copper. The carbon and oxygen values are attributed to contamination of the sample surface, however, some of this content may be contained within corrosion products. After thermal ageing the average values for all of the dye/mordant combinations is 20% carbon, 11% oxygen, 68% copper and 1% sulphur. The presence of sulphur on the samples incubated with the fabric and not on the control sample indicates that sulphur is introduced due to the degradation of the wool and silk fabric. The corrosion products on the surface are copper and sulphur based while the increase in oxygen content may be attributed to formation of copper oxides on the sample surface.

XPS analysis of the thermal aged copper coupons detected 54% carbon, 28% oxygen and 12% copper at the surface of the Control sample, with traces of Si and Mn. The XPS values of C and O are much higher than the EDX values due to the higher surface sensitivity of the XPS instrument. EDX has a sampling depth of approximately 1-2 μm whereas XPS samples to a depth of only approximately 10 nm. The contamination of the sample surface swamps the XPS signal while the EDX method analyses more of the bulk metal below the sample surface, leading to higher values for the copper content. The average values for the thermal aged samples which were incubated with the various dye/mordant combination fabrics were 60% carbon, 23% oxygen, 9% copper and 2% sulphur with traces of Si and Mn on all

samples and N on some of the samples. The Si, Mn and N values are attributed to contamination.

EDX analysis of the thermal aged silver coupon Control sample detected 6% carbon, 93% silver and traces of Mg. No oxygen was detected on any of the silver coupons using EDX. The average values of the silver coupons aged with fabric were 5% carbon, 92% silver, 1% sulphur and 0.6% chlorine with traces of Mg contamination on some samples. The presence of sulphur and chlorine on most coupons must be attributed to the degradation of the wool and silk fabric. XPS analysis of the silver control sample found 58% carbon, 16% oxygen, 18% silver, 0.5% sulphur, 1.4% chlorine and traces of copper. As before, the high levels of C and O are due to contamination of the sample surface with the presence of Cu on the silver coupons also due to contamination during the Oddy Test. The average values of the thermal aged silver coupons incubated with fabric are 38% carbon, 15% oxygen, 29% silver, 8% sulphur, 2% chlorine and traces of Cu and Si contamination on all samples. The corrosion products on the silver coupons may be sulphur and chlorine based with some silver oxides likely.

XPS analysis of the thermal aged metallic threads Control sample found values of 71% carbon, 18% oxygen, 6% copper, 0.3% silver, 0.1% gold and traces of Si. The average values of the samples aged with fabric were 66% carbon, 20% oxygen, 4% copper, 0.3% silver, 0.03% gold and 1.8% sulphur with traces of Si on all samples and N, Cl and Ca on some samples. Gold and silver were detected on around half of the samples which corresponds with the visual analysis that many of the metallic threads resisted corrosion. The rest of the samples displayed almost complete coverage of corrosion over the sample surface which masked the underlying gold layer. Figures 3.3.35 and 3.3.36 show the relative amounts of Au, Ag and Cu at the surface of the thermal aged metallic threads in comparision with the XPS data from the unaged metallic thread. The thermal aged samples are dominated by copper, including the aged control sample which indicates that the copper has migrated to the surface solely due to exposure to heat. The increased level of copper at the surface of the samples which were incubated with fabric suggests that on the highly corroded samples, the copper is forming corrosion procucts on the surface which have grown over the underlying gold layer, reducing its contribution to the signal.

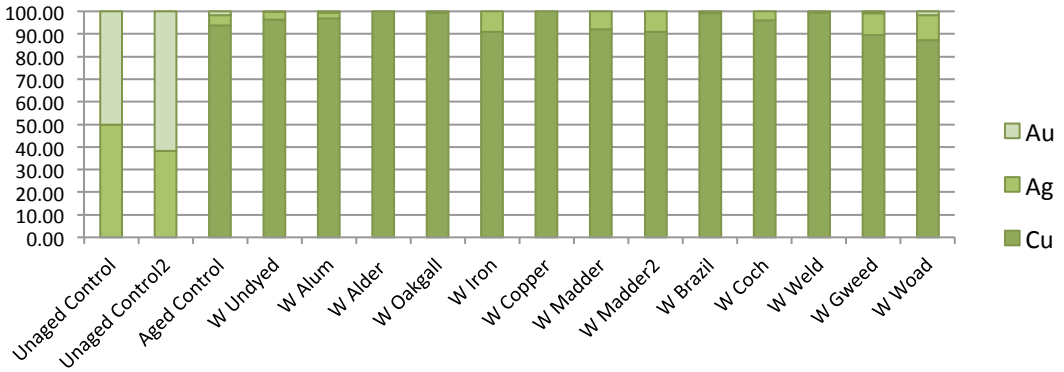

Figure 3.3.35 Relative amounts of Au, Ag and Cu on wool thermal aged metallic thread samples from XPS analysis

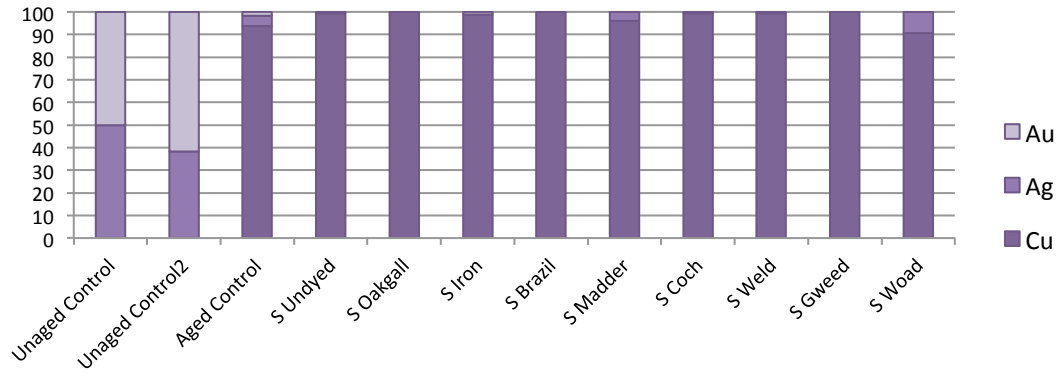

Figure 3.3.36 Relative amounts of Au, Ag and Cu on silk thermal aged metallic thread samples from XPS analysis

Most of the thermal aged coupons and metallic threads contained sulphur at the sample surface. In order to assess the influence of the sulphur content on the visual degradation and the amount and type of corrosion products formed on the samples it was necessary to compare the S values of the various dye/mordant combinations. However, it is not possible to use the S% values quantitatively because of the high level of C and O contamination on the samples. Therefore the amount of S present has been related to the metal content on the samples i.e. S/Cu is used for the copper coupons, S/Ag for the silver coupons and S/(Cu+Ag+Au) for the metallic threads.

No S was detected by XPS on the copper coupon and metallic thread that were in the control sample tube, which contained no fabric, however, some S was detected on the silver coupon. Although it was only a small amount this indicates that the atmospheric sulphur that was present in the test tube before it was sealed has reacted preferably with the silver coupon. The S present on all of the copper

coupons and metallic threads that were in the test tubes containing fabric has appeared during the ageing process and is present as corrosion residue on the sample surfaces. Sulphur is produced during the exposure of the wool and silk fabric to heat. The Oddy Tests prove that the release of sulphur and other gases during thermal ageing of the tapestry materials is detrimental to the appearance of the metallic threads that are woven into the tapestry fabric. The average S/Cu value on the copper coupons detected using EDX was 0.02 with the wool samples having a slightly higher average than silk samples. The highest value was for the W Gweed sample at 0.1, much higher than the average value. The graphs of the EDX data for wool and silk thermal aged copper coupons are shown in Figures 3.3.37 and 3.3.38 while the XPS data is shown in Figures 3.3.39 and 3.3.40. The average S/Cu value found using XPS was 0.24 for both wool and silk samples with the highest value recorded on W Gweed at 0.50. Visual assessment of the W Gweed copper coupon confirmed that this sample was particularly badly corroded. Corrosion products that may be present on the copper coupons include CuS, Cu_2S and CuO, which are black, Cu_2O which is red, $Cu(OH)_2$ and $CuSO_4$ which is blue/green. To determine the effect of sulphur content on the visual degradation of copper, S/Cu values have been plotted against the visual corrosion scale of the copper coupons in Figures 3.3.41 and 3.3.42. There seems to be slight correlation between the S/Cu content and the visual corrosion scale of copper coupons.

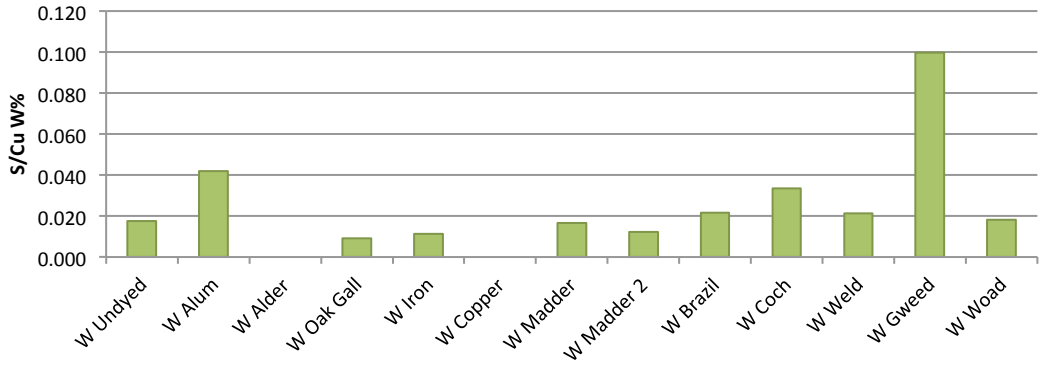

Figure 3.3.37 EDX data. S/Cu of wool thermal aged copper coupon samples

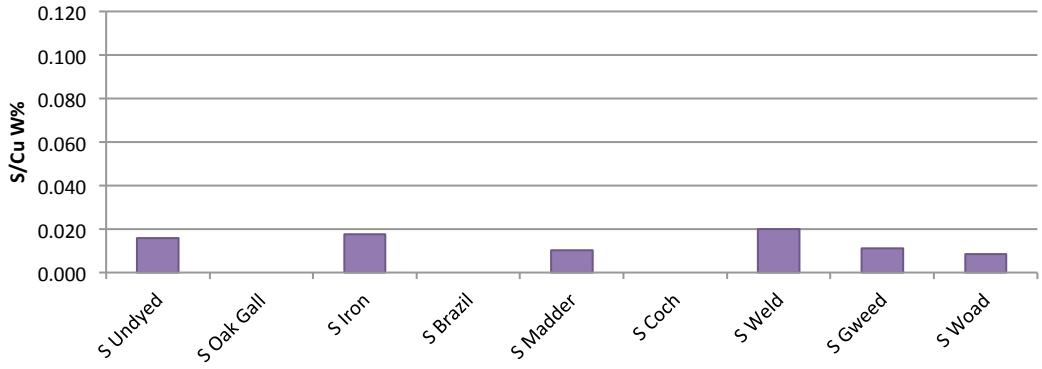

Figure 3.3.38 EDX data. S/Cu of silk thermal aged copper coupon samples

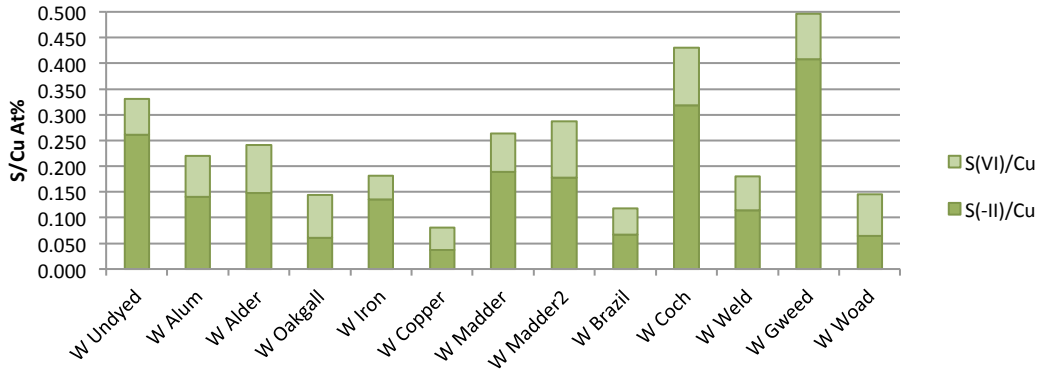

Figure 3.3.39 XPS data. S/Cu of wool thermal aged copper coupon samples

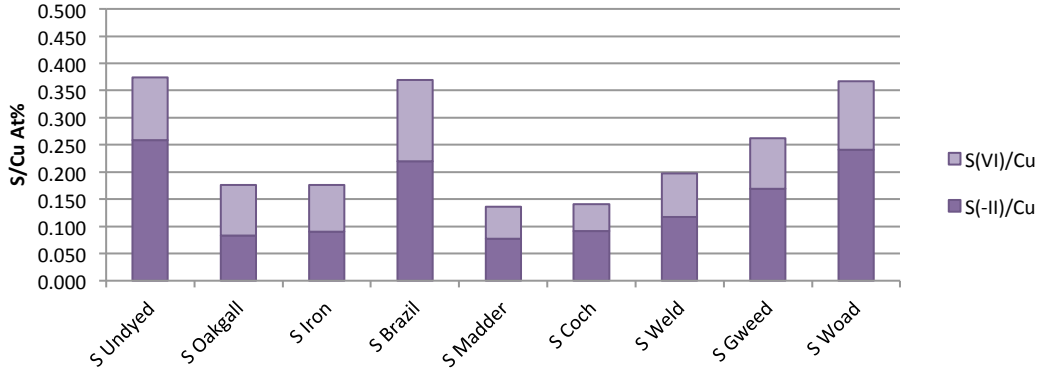

Figure 3.3.40 XPS data. S/Cu of silk thermal aged copper coupon samples

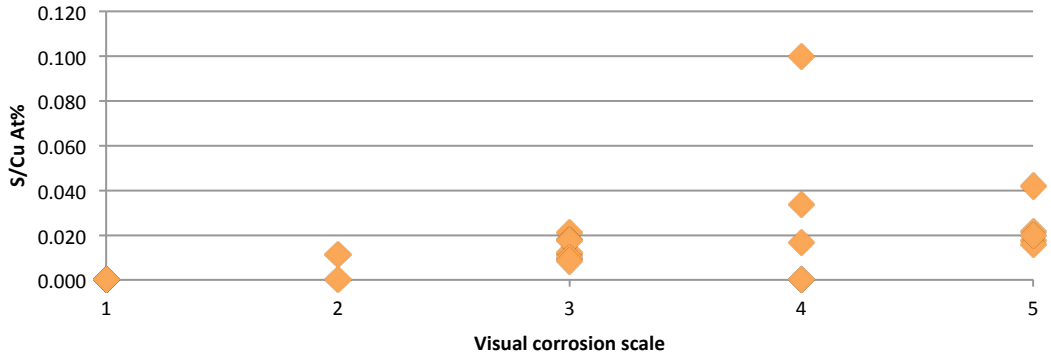

Figure 3.3.41 EDX data. S/Cu against the visual corrosion scale of thermal aged copper coupons

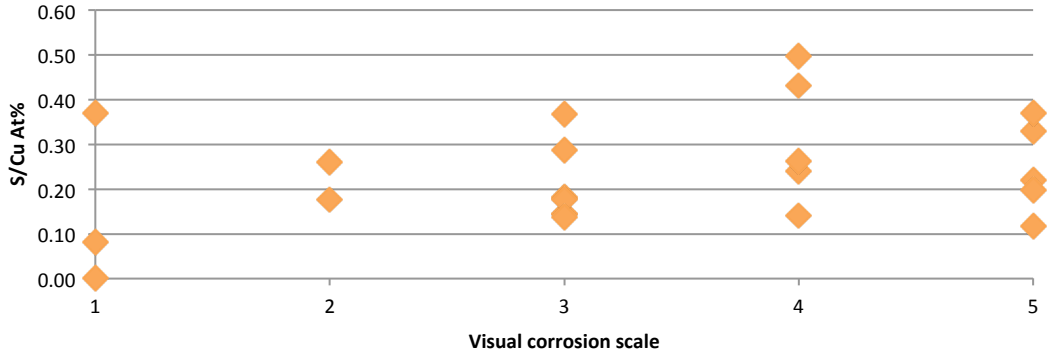

Figure 3.3.42 XPS data. S/Cu against the visual corrosion scale of thermal aged copper coupons

The average S/Ag value for the thermal aged silver coupons detected using EDX was 0.013 with an average wool value of 0.015 and silk value of 0.009. The S/Ag graphs of the EDX data for wool and silk are shown in Figures 3.3.43 and 3.3.44 while the XPS data are shown in Figures 3.3.45 and 3.3.46. The average S/Ag value from XPS data is 0.33 with an average wool value of 0.35 and silk value of 0.31. The highest S/Ag value was found on W Alum using both EDX and XPS analysis. The lowest values were found on W Copper and S Oakgall using XPS while EDX did not detect any S on these samples.

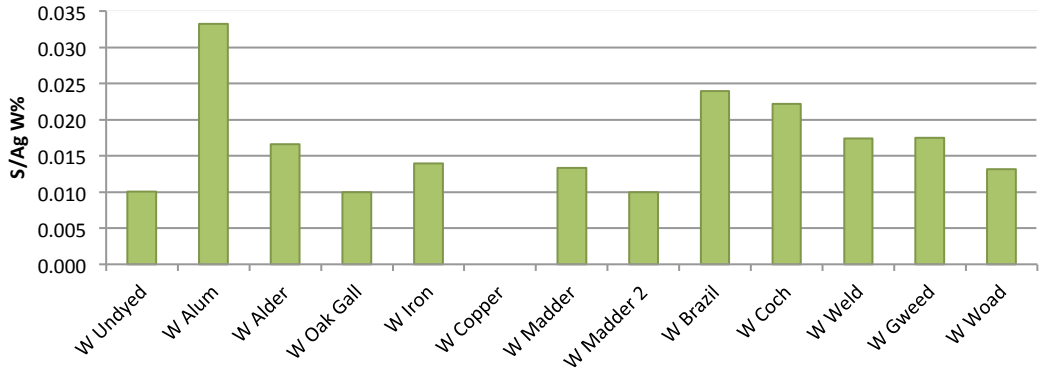

Figure 3.3.43 EDX data. S/Ag of wool thermal aged silver coupon samples

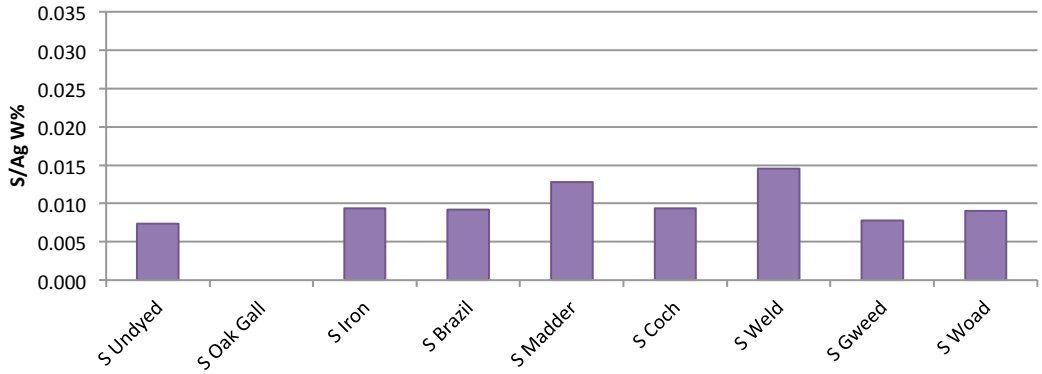

Figure 3.3.44 EDX data. S/Ag of wool thermal aged silver coupon samples

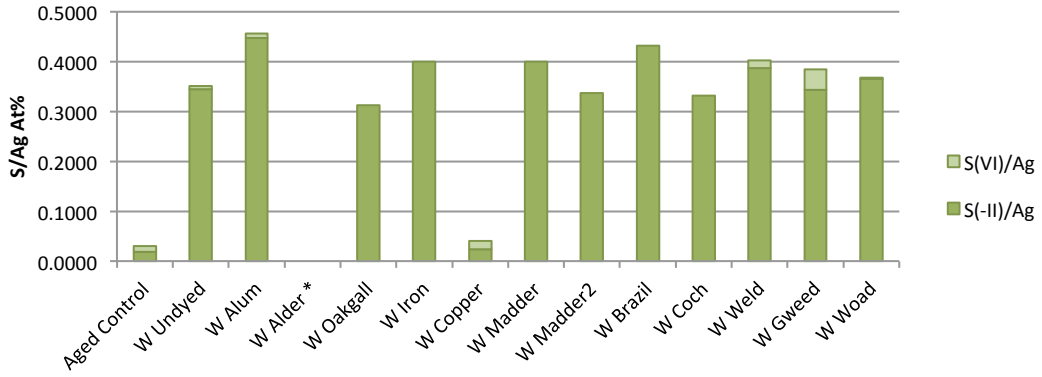

Figure 3.3.45 XPS data. S/Ag of wool thermal aged silver coupon samples

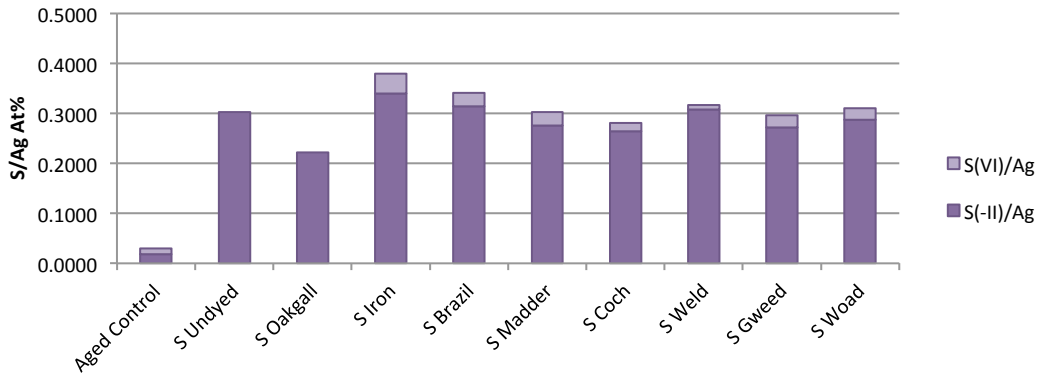

Figure 3.3.46 XPS data. S/Ag of silk thermal aged silver coupon samples

Visual analysis of the silver samples indicates that the higher the amount of S on a sample, the more tarnished the sample appears as W Alum has a high visual corrosion scale grading and the low S/Ag value samples have a low visual grading. To establish if there is a correlation between S level and amount of tarnish, S/Ag was plotted against the visual corrosion scale of thermal aged silver coupons for both EDX and XPS data, these graphs are shown in Figures 3.3.47 and 3.3.48. There is a positive correlation between the data indicating that the amount of sulphur on a sample has an increasingly degradative effect on silver coupons. However, as there is dispersion of the data points it is clear that S% isn't the only factor in the corrosion of silver coupons. The amount of chlorine present on the samples was tested for its effect on the visual degradation of silver samples; however, no correlation was found.

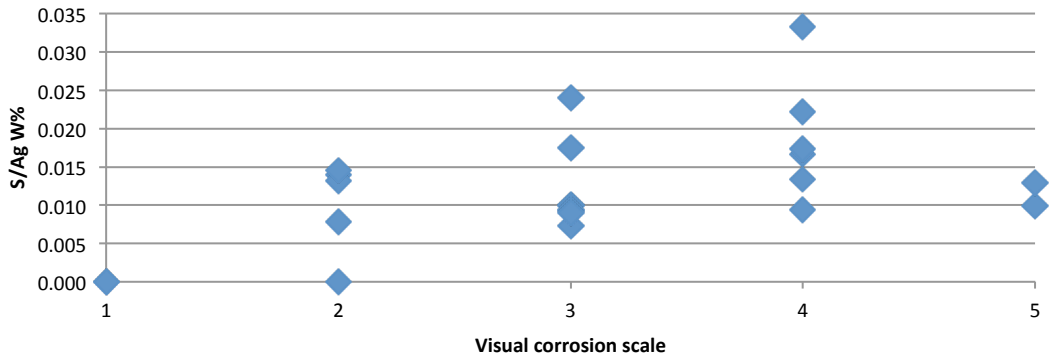

Figure 3.3.47 EDX data. S/Ag against the visual corrosion scale of thermal aged silver coupons

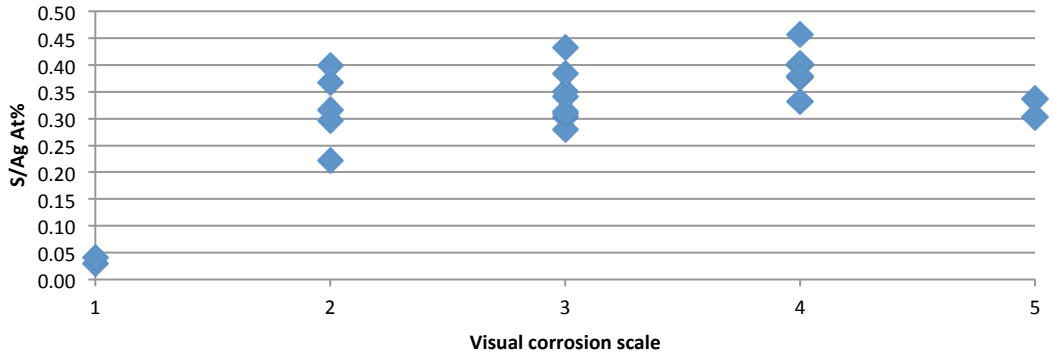

Figure 3.3.48 XPS data. S/Ag against the visual corrosion scale of thermal aged silver coupons

The graphs of the XPS data for wool and silk thermal aged metallic threads are shown in Figures 3.3.49 and 3.3.50. XPS analysis of thermal aged metallic threads detected no S on the control sample, which was incubated without fabric, therefore all sulphur residues that are detected on the other metallic thread samples are

present due to the heat causing release of sulphurous compounds from the wool and silk fibres. Some thermal aged metallic thread samples did not contain any sulphur on the surface, whereas the copper and silver coupons incubated with these fabrics had sometimes significantly high levels. This is attributed to the protective effect of the gold layer that covers the silver and copper bulk of the metal filament. The highest sulphur content of 1.1% was recorded for W Gweed whereas the highest level on the silk samples was also S Gweed. The average value of S/(Cu+Ag+Au) on wool samples was higher (0.43%) than on silk samples (0.21%).

The dyes that exhibited the highest levels of S/(Cu+Ag+Au) on the thermal aged metallic threads did not correlate with the photo-aged metallic threads.

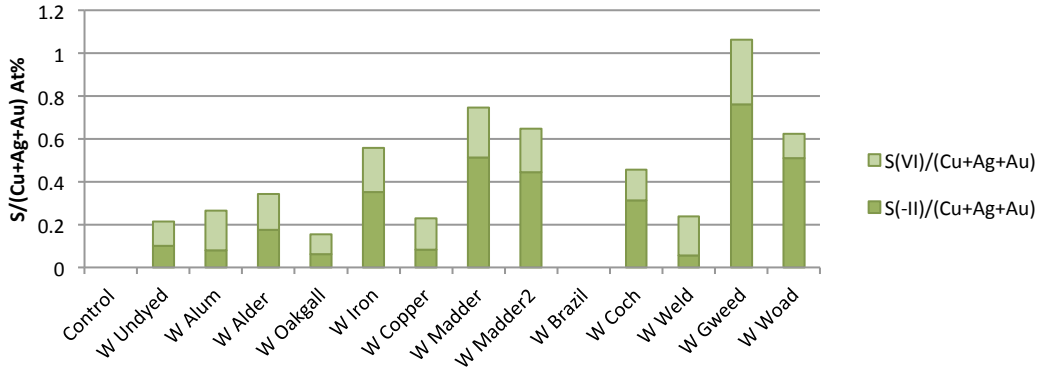

Figure 3.3.49 XPS data. S/(Cu + Ag +Au) of wool thermal aged silver coupon samples

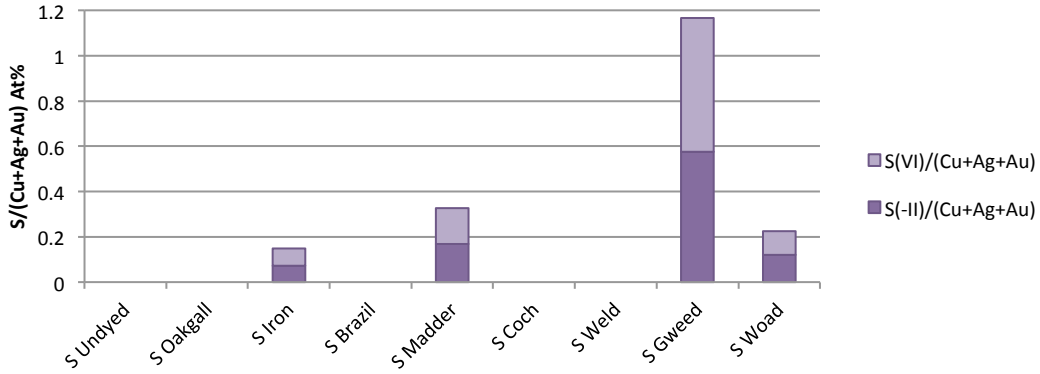

Figure 3.3.50 XPS data. S/(Cu + Ag +Au) of silk thermal aged silver coupon samples

3.3.5 Conclusions

The ageing characteristics of tapestry materials have been investigated using standard conservation science test methods with the purpose of more accurately determining the original appearance of a historic tapestry. The photo-ageing experiment emphasised the detrimental effect that exposure to light has on the appearance of tapestry materials; the dyed wool and silk fibres tend to lighten in colour whereas the metallic threads become darker due to formation of corrosion products at the metallic surface. The increased contrast between the materials damages the subtle colour balance of the tapestry design and the highlighting effect of the metallic threads is lost. Investigations as to the origins of the observed changes were undertaken. Colour measurements of the dyed wool and silk fibres before and after 100, 300 and 500 hours of accelerated photo-ageing provided fading profiles for each of the natural dyes on wool and silk substrates. These fading profiles allowed the identification of areas of specific natural dyes on the historic tapestry *The Oath and Departure of Eliezer* that led to the original appearance of the tapestry being recreated. It was found that natural dyes exhibited a range of fading rates; the most fugitive dyes were found to be Brazilwood and Weld while Woad was the most light-fast natural dye in use at the time of *The Oath and Departure of Eliezer*. Fading of the various coloured areas therefore did not occur simultaneously in time. The acquisition of the various fading profiles for the dyes was essential to the recreation of the appearance of the tapestry at various periods in time.

EDX and XPS analyses provided evidence for copper ion migration from the bulk of the metallic filament to the surface, a mechanism that has been previously detected in historic metallic threads (Hacke, 2006). XPS analysis detected 10% Au and 8% Ag at the outer 10 nm of the surface of the metal filament before ageing and 0.1% Au, 0.3% Ag and 6% Cu after thermal ageing for 28 days. The copper ions that migrate to the surface react to form part of the corrosion layers observed on the aged samples that impair the original gold appearance of the metallic thread. The average metallic composition at the surface of the 500 hour photo-aged samples was detected as 0.4% Au, 0.8% Ag and 6.3% Cu.

SEM images of the photo-aged metallic threads showed the presence of various corrosion morphologies at the surfaces of the metal filaments. Cauliflower corrosion products were observed on most of the samples while flakes of corrosion product growing over the surface were also observed, which is consistent with previous investigations into metallic threads taken from historic tapestries (Hacke, 2006). EDX spectra of the samples identified variations in the surface composition between the cauliflower type corrosion showing high copper content and the flakes of corrosion product and the smooth tarnished layer showing high silver content. Examination of images of the 100 hour, 300 hour and 500 hour photo-aged samples established that the corrosion products formed initially at the edges of the metal filament where the gold over-layer is thinner and at cracks or imperfections in the gold surface, then corrosion products spread over the surface completely obscuring the gold layer of some samples. However, no clear trends could be identified as to which corrosion products first appear.

XPS analysis of corrosion products on photo- and thermal aged metallic threads detected various amounts of gold, silver and copper as well as oxygen, carbon, sulphur and chlorine. High resolution scans confirmed the presence of sulphides and sulphates and at least two chemical states for copper. XPS analysis was hampered by high levels of carbon contamination that impaired the signals of the components of the corrosion products; nevertheless the various corrosion products identified during visual analysis of the aged metallic threads were attributed to AgO, Ag_2O, Ag2S, CuS, Cu_2S, CuO (gray/black), Cu_2O (red) and $CuSO_4$ (blue/green).

The influence of the dyed materials on the corrosion of the metallic threads was investigated by incubating silver and copper coupons and metallic thread with dyed wool and silk tapestry fabric. An adapted Oddy Test method was used, which is a standard test in conservation science to determine the corrosiveness of materials. The thermal degradation of the fabric samples led to various levels of corrosion on the metallic coupons and threads, however, no clear trends in the corrosiveness of natural dyes within the fibres were identified. The degradation products of the wool samples were more corrosive than the silk samples with more surface sulphur detected using EDX and XPS analysis on those samples incubated with dyed wool fabric. Thermal degradation of wool is known to release CO_2, CO, COS, H_2S, and CS_2

(Launer, 1971). It is suggested that the sulphurous gases adsorb onto the metal surface and react with the silver and copper ions that have migrated to the surface forming sulphur-containing corrosion products Ag_2S, Cu_2S, $CuSO_4$. XPS high resolution scans of the sulphur peak detected two oxidation states, S^{2+} and S^{6+} present on the thermal aged samples: Thermal aged silver coupons mostly contained sulphur in its lower oxidation state with an average value of 95% S^{2+} attributed to silver sulphide. Thermal aged copper coupons contained on average 62/38% S^{2+}/S^{6+} attributable to copper sulphide and copper sulphate formation while thermal aged metallic threads contained on average 53/47% S^{2+}/S^{6+} that can be attributed to the presence of copper sulphide, copper sulphate and silver sulphide.

XPS analysis of wool fibres identified the change in oxidation state of sulphur from S^{2+} to S^{6+}; the unaged undyed wool contained 17% S^{6+} which increased to 32% after 500 hours of photo-ageing attributed to the cystine di-sulphide bond being broken, forming cysteic acid. This confirms the findings of previous research into photo-oxidation of sulphur-containing amino acids in wool. For all metallic samples, greater levels of corrosion were observed on the samples incubated with wool rather than silk. There was a broad correlation between the amount of sulphur detected on the metal surfaces after ageing and the visual level of corrosion. The high levels of sulphur present on the highly corroded samples strongly suggests that the photo-oxidation of sulphur containing amino acids in wool is detrimental to the appearance of metallic threads in tapestries, in particular the formation of dark grey or black silver sulphide corrosion product.

4 Digital Conservation

4.1 Colour specification

4.1.1 What is colour?

Light is that part of the Electromagnetic Spectrum to which the human visual system is sensitive, ranging over the approximate wavelength region 380 to 780 nanometres (nm). A representation of the perceived colours of the wavelengths in the visible range is shown in Figure 4.1.1. Sources of light emit radiation over this range of wavelengths. The amount of light emitted at each wavelength across the spectrum is used to describe a light source and is plotted as a Spectral Power Distribution (SPD) curve. An even distribution of radiation over all the wavelengths in this range will produce a white light.

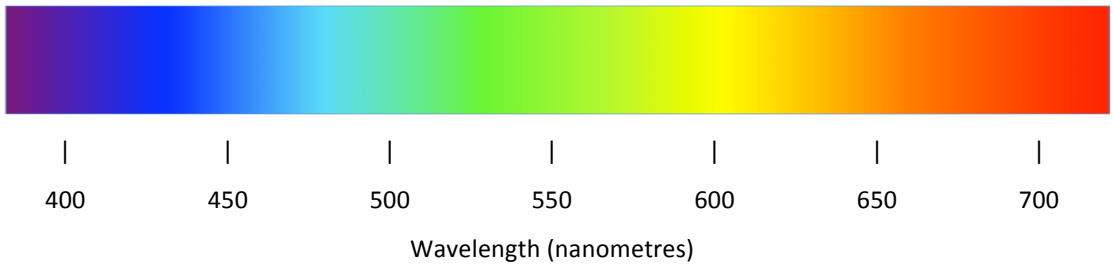

Figure 4.1.1 The visible spectrum

Coloured light is perceived when the spectral composition of the observed radiation varies over the visible range of wavelengths. Monochromatic light sources emit radiation over a very short range of wavelengths resulting in a coloured output, for example street lighting employs sodium which emits light at approximately 589 nm giving off a distinctive yellow-orange colour (Hunt, 1995).

The incident light illuminating an object can be transmitted, absorbed, reflected or scattered by the object. Colour is the result of these physical modifications as detected by the eye and interpreted in the brain (Berns, 2000). The colour of a surface depends on how much light is absorbed by the material and how much is scattered, transmitted and reflected at each of the wavelengths in the visible spectrum. The fraction of light reflected at each wavelength from a material is plotted as the *surface spectral reflectance (SSR) curve.* Figure 4.1.2 shows a typical

SSR curve of a blue colour, taken from spectrophotometric measurements carried out on a painting by Berns (2004). The SSR curve of a surface does not change when the light source is changed. If two samples have identical SSR curves then they will be a visual match under different light sources (Wyszecki & Stiles, 1982).

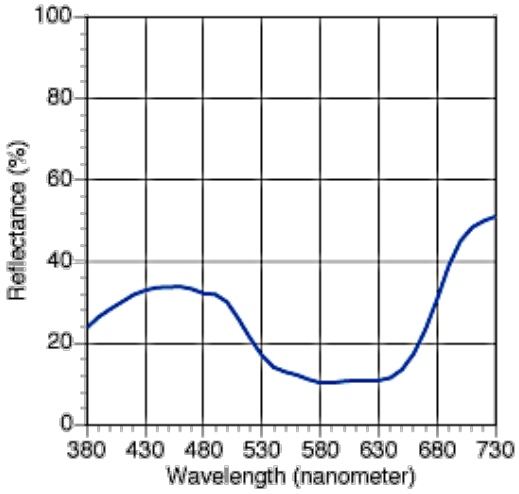

Figure 4.1.2: Surface spectral reflectance curve for an area of a painting, Georges Seurat's *La Grande Jatte*, 1884, indicating cobalt blue pigment, from work carried out by Berns (2004)

4.1.2 Colour mixing

Additive mixtures of light result in a brighter and less saturated colour. The luminance of the mixture is the sum of the combined luminances of the primaries. The primaries used for additive mixing are red, green and blue. Additive mixing of stimuli results in a radiant power distribution whereby for any wavelength interval in any part of the spectrum, the power is equal to the sum of the powers of the constituents of the mixture. The effect of this is that mixing blue and yellow lights produces white light due to the almost complete coverage of the spectrum by the constituent blue plus yellow power distributions.

Subtractive mixing is so called due to the removal of light coming from a source by an object so when colourants are mixed the results are always duller and darker. Subtractive primaries are chosen for their absorption of red, green and blue portions of white light therefore cyan, magenta and yellow are used. Dyes and pigments act by absorbing certain parts of the spectrum of white light more than others, for example a yellow pigment absorbs blue light.

4.1.3 CIE system of colour specification

Colour specification systems aim to numerically define a stimulus so that when viewed by an observer with normal colour vision, under the same observing conditions such as area, light and direction, two stimuli with equal colour specification will look identical. Similarly two stimuli which look the same will have the same numerical colour specification. Colours are defined by referencing them to standards in colour order systems which have been arranged in scales of lightness, hue and chroma.

The matching of samples using these colour order systems is undertaken under one set of viewing and lighting conditions; however, the appearance and perhaps the specification of the sample would likely change under a different set of conditions. Likewise if the match was performed by two or more different people, the results would probably not be the same. Metamerism is where two coloured surfaces match under one set of conditions but fail to match under another. Metamerism can be due to changes in illuminant, observer, field size or viewing angle. A perfect non-metameric match can only be achieved when the SSR curve of the batch is identical to the standard.

The CIE (Commision Internationale de l'Éclairage) developed a standardised system of colour specification by measuring the colour under designated lighting and viewing conditions and using a 'standard observer'.

Colour can be independently specified by matching stimuli to a combination of three monochromatic light sources whose radiant powers are adjusted so that the mixture of the light sources appears identical to the adjacent coloured sample. The colour matching experiment is illustrated in Figure 4.1.3. Every colour can be matched using three adjustable primary light sources, many by an additive mixture, however, some colours may require a negative value of one primary. The three primary light stimuli should be chosen so that none of the primaries can be colour matched by mixing the two other primaries.

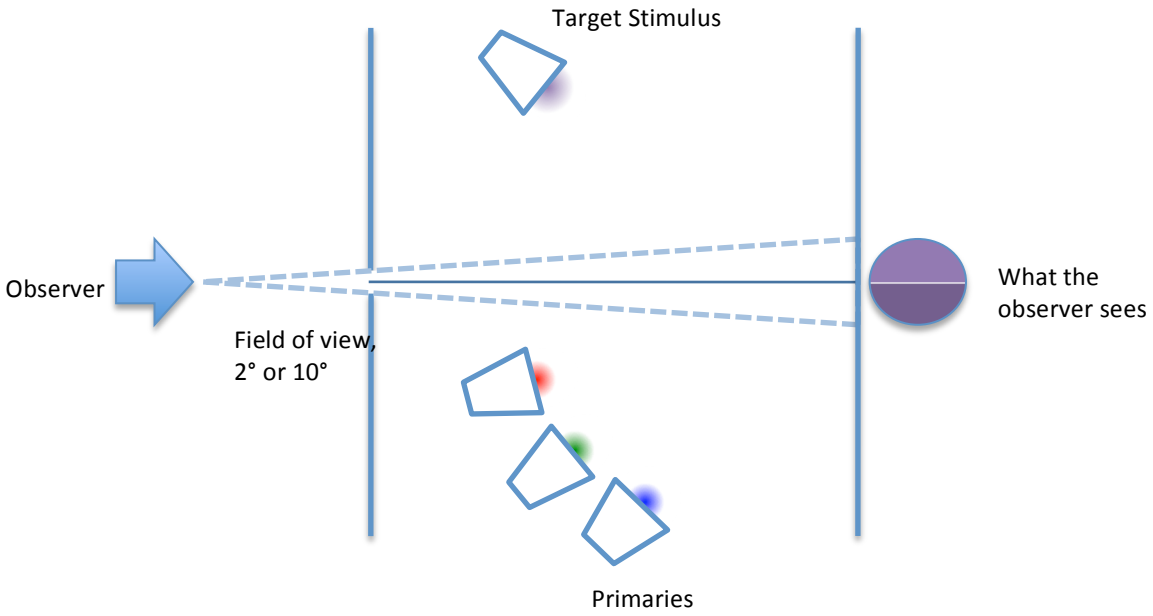

The observer adjusts the intensities of the three primaries so that the mixture of lights matches the target stimulus in the split screen

Figure 4.1.3 A schematic of the CIE colour matching experiment

The results of colour matching stimuli at wavelengths over the visible spectrum can be displayed in a curve where the amounts of each primary are functions of wavelength. These curves are called colour-matching functions and the quantities of each primary used to match a colour are called tristimulus values. The vision of an average human has been defined by the CIE from these colour matching experiments wherein a group of observers matched a monochromatic light source to a mixture of red, green and blue lights under a specified set of conditions. This resulted in a set of colour-matching functions, $\bar{r}_\lambda, \bar{g}_\lambda, \bar{b}_\lambda$, where each of the tristimulus values had positive and negative values. Another set of primaries was later defined that resulted in all-positive colour-matching functions, $\bar{x}_\lambda, \bar{y}_\lambda, \bar{z}_\lambda$. In 1931 this system was defined with a 2° field of view and is known as the X, Y, Z system or the 1931 standard observer and represents the colour vision of an average member of the human population. In 1964 the CIE adapted the standard observer to more accurately describe the vision of a human when colour matching in a larger field of view. The 1964 supplementary standard observer uses a set of colour matching functions, $\bar{x}_{10\lambda}, \bar{y}_{10\lambda}, \bar{z}_{10\lambda}$, obtained using a 10° field of view. Figure 4.1.4 shows the 1931 and 1964 standard observer colour-matching functions.

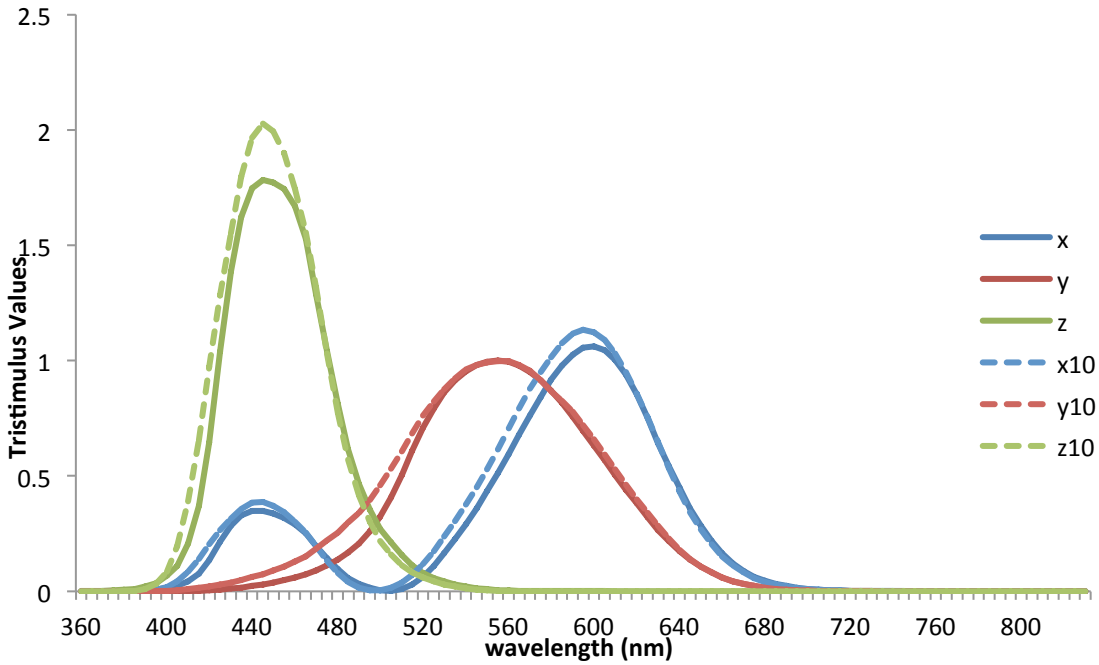

Figure 4.1.4: Colour-matching functions $\bar{x}_\lambda, \bar{y}_\lambda, \bar{z}_\lambda$ (solid lines) of the CIE 1931 standard observer and $\bar{x}_{10\lambda}, \bar{y}_{10\lambda}, \bar{z}_{10\lambda}$ (dashed lines) of the 1964 CIE standard observer (data from www.cvrl.org)

In 1931 the CIE defined three light sources by their spectral power distributions; illuminant A represents incandescent light of a tungsten filament lamp, equivalent to a black body radiator with a colour temperature of 2856 kelvin. Blackbodies are light sources that when heated will glow firstly a dull red then increasingly whiter and brighter, with the colour depending only on their temperature. The temperature of a blackbody is called its *colour temperature*, usually expressed in kelvins (K).

The CIE also defined illuminant B; tungsten with a yellow filter which simulates sunlight, and illuminant C; tungsten with a blue filter which simulates daylight, however, these two illuminants are no longer widely used.

In 1964 a set of illuminants based on natural daylight were defined, the spectral power distributions of daylight were measured and correlated to the colour temperatures of blackbody radiators. D65 is the CIE standard illuminant with a correlated colour temperature of 6500 K and has been adopted by many industries, such as paints and textiles, to simulate daylight whereas D50 is used in the graphic arts and computer industries (Berns, 2000). The spectral power distribution of the CIE illuminant D65 is shown in Figure 4.1.5.

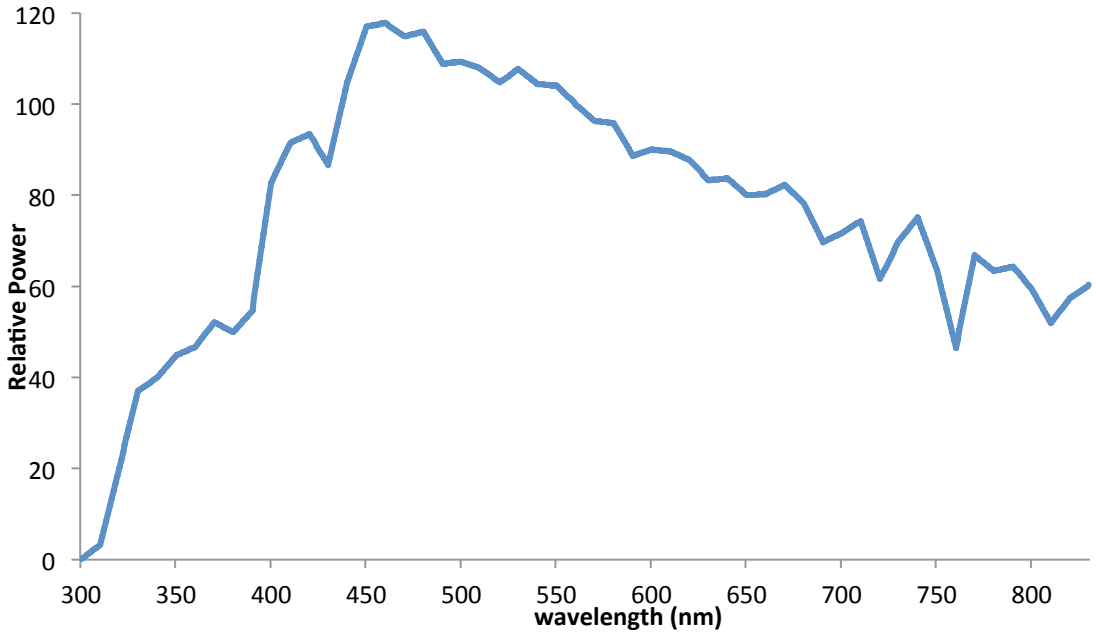

Figure 4.1.5: Spectral power distribution of the CIE illuminant D65

The CIE standard observers are used in conjunction with a CIE standard illuminant to calculate tristimulus values for a particular object. The spectral reflectance data, R, of the object is multiplied wavelength by wavelength with the standard illuminant data, S, and each of the colour-matching functions, $\bar{x}_\lambda, \bar{y}_\lambda, \bar{z}_\lambda$, of a standard observer. The results are summed for each colour-matching function and normalized to give the tristimulus values X, Y, and Z, as shown in Equations 1-4.

$$X = k\sum_{\lambda} S_\lambda R_\lambda \bar{x}_\lambda \qquad \textbf{Equation 1}$$

$$Y = k\sum_{\lambda} S_\lambda R_\lambda \bar{y}_\lambda \qquad \textbf{Equation 2}$$

$$Z = k\sum_{\lambda} S_\lambda R_\lambda \bar{z}_\lambda \qquad \textbf{Equation 3}$$

$$\boldsymbol{k = \frac{100}{\sum S_\lambda \bar{y}_\lambda}} \qquad \textbf{Equation 4}$$

where k is a normalising function to ensure that Y=100 for a perfect reflecting diffuser of any illuminant.

Chromaticity coordinates are calculated from the tristimulus values using Equations 5-7. This information is usually displayed on the 2-dimensional *x, y* chromaticity diagram in which the colour is indicated but the lightness information is not

represented. This is rectified by quoting the normalised Y tristimulus value along with the *x, y* chromaticity coordinates. The CIE *x, y* chromaticity diagram calculated using the 1931 standard observer, shown in Figure 4.1.6, has been artificially coloured to illustrate the locations of different colours on the diagram. The spectrum locus identifies the full gamut of visible colours.

$$x = \frac{X}{X + Y + Z}$$ **Equation 5**

$$y = \frac{Y}{X + Y + Z}$$ **Equation 6**

$$z = \frac{Z}{X + Y + Z}$$ **Equation 7**

$$x + y + z = 1$$ **Equation 8**

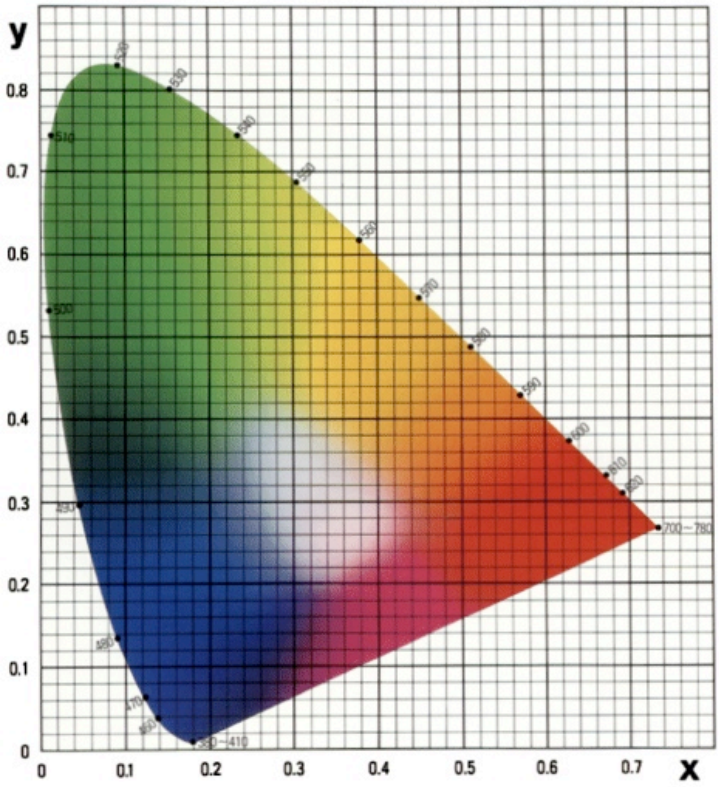

Figure 4.1.6: CIE 1931 *x, y* chromaticity diagram (MIT 2001)

4.1.4 Colour measurement

Colour measurement is performed by either measuring the tristimulus values of a sample or by calculating the colorimetric information from spectral measurements.

A colorimeter measures the tristimulus values of a light source or sample by using a set of tristimulus filters. A spectrophotometer measures reflectance or transmittance of a stimulus as a function of wavelength. From the spectral data, the colour information of the sample can be calculated for any illuminant. A telespectroradiometer is a spectrometer which uses a telescope to measure spectral radiance or irradiance. This instrument can be used to measure sources or stimuli.

4.1.5 CIELAB

CIE L*a*b* Color space is a system in which color differences are quantified relative to the perceived color change. The dimensions of the cylindrical color space relate to Hue, Chroma and Lightness and are perceptually uniform whereby equal shifts in the colour space are perceived as equal shifts by an observer. CIE L*a*b* coordinates of a sample are calculated by a series of non-linear equations from CIE XYZ.

$$L^* = 116\left(\frac{Y}{Y_n}\right)^{1/3} - 16 \qquad \textbf{Equation 9}$$

$$a^* = 500\left[\left(\frac{X}{X_n}\right)^{1/3} - \left(\frac{Y}{Y_n}\right)^{1/3}\right] \qquad \textbf{Equation 10}$$

$$b^* = 200\left[\left(\frac{Y}{Y_n}\right)^{1/3} - \left(\frac{Z}{Z_n}\right)^{1/3}\right] \qquad \textbf{Equation 11}$$

The colour difference between a sample and standard is calculated from

$$\Delta E = \left(\Delta L^{*2} + \Delta a^{*2} + \Delta b^{*2}\right)^{1/2} \qquad \textbf{Equation 12}$$

Furthermore the Lightness, Hue and Chroma differences are also calculated from L*a*b* differences:

ΔL^* is the same

$$\Delta C = \left(a_1{}^2 + b_1{}^2\right)^{1/2} - \left(a_2{}^2 + b_2{}^2\right)^{1/2} \qquad \textbf{Equation 13}$$

$$\Delta H = \left(\Delta E^2 - \Delta C^2 - \Delta L^{*2}\right)^{1/2} \qquad \textbf{Equation 14}$$

4.2 Digital imaging of cultural heritage

The digital conservation of cultural heritage is an active area of research that has received significant attention in recent years due to technological advances in the area of imaging science. Imaging is a non-invasive method of investigation of culturally significant items and is of central importance to the work of museums and galleries. Images serve as a record of the condition of the artifact and are used to monitor changes in the item's appearance in particular colour, therefore colour accuracy of the images is vital.

Traditional imaging techniques use trichromatic systems that filter the reflected light into three RGB channels. Multi- and hyperspectral imaging systems use a larger number of filters and the spectral information is captured at every pixel, which increases the colour accuracy of the image. Until now spectral imaging has mainly been used to digitally conserve culturally significant paintings. This study uses spectral imaging technology on tapestries for the first time.

4.2.1 Spectral imaging systems

An overview of the components used in spectral capture systems by Taplin and Berns (2005) describes the advantages and disadvantages of the available technology for assembling a spectral imaging system in a museum environment. These components include a camera and lens, a sensor and a set of filters and lighting. Many different image processing techniques are used to calibrate the system and reconstruct the spectal reflectance data from the multi-channel images (Zhao *et al.,* 2005a) (Zhao *et al.,* 2005b), (Rosen *et al.,* 2001).

A variety of imaging systems used to capture cultural heritage have been described below with their average performance stated as colour difference.

- Berns *et al.* (2005) imaged the GretagMacbeth ColorChecker DC target using a Jenoptik Eyelike Precision M11 digital camera and four Hensel Xenon strobes. The average performance of the camera was 1.9 ΔE_{00}.
- Imai *et al.* (2001) used a trichromatic IBM Pro 3000 digital camera system that consists of a scanning back and a RGB filter wheel to obtain multi-channel images of a custom target made up of 106 pigments. The average colorimetric accuracy of the spectral reconstruction of the target was 1.7

ΔE_{94}*.

- Zhao *et al.,* (2005b) imaged the GretagMacbeth ColorChecker DC target using a modified Sinarback 54H camera producing six-channel images. Spectral reconstrunction was performed using the matrix R method with an average performance of 0.9 ΔE_{00}.
- Martinez *et al.* (2002) reported the performance of the imaging systems used at the National Gallery. The VASARI system uses a monochromatic Kontron ProgRes digital camera with seven broadband Gaussian filters. Spectral reconstruction of the Macbeth ColorChecker Chart had an average colour error of 1 ΔE_{ab}*. The MARC system uses a CCD camera with RGB colour sensor, with a combination of macro- and micro- positioning. The colour error of spectral reconstruction is around 2 ΔE_{ab}*.
- Haneishi *et al.* (2000) measured the reflectance spectra of a set of 145 oil paints using a Kodak DCS420 CCD camera with Fuji Photo film triacetyl cellulose–based dye filters. The mean colorimetric colour difference, ΔE_{uv}*, was calculated for increasing numbers of filters. 3 filters = 3.42, 4 = 2.17, 5 = 1.24 and optimised at 6 filters giving a mean ΔE_{uv}* of 0.99.
- Foster *et al.* (2006) developed a hyperspectral imaging system based on a low-noise Peltier-cooled digital camera with a fast tunable liquid-crystal filter mounted in front of the lens, together with an infrared blocking filter. Images were acquired at 10-nm steps over 400–720 nm of test scenes comprising arrays of acrylic paint samples on a white background. Reflectance spectra estimated by hyperspectral imaging and by telespectroradiometry had a root-mean-square error of 0.011. This system has been used to image the 14th Century Haggadah held at John Rylands Library, Deansgate, Manchester (The Rylands Cairo Genizah Collection, 2010).

4.2.2 Applications of spectral imaging in conservation

The purposes of spectral imaging of cultural heritage can be divided into three main categories:

- Documentation: Creating a digital archive of the artefact to act as a permanent record of the condition and appearance of the item. This is

particularly relevant as a conservation practice as many museum artefacts change irreversibly with time (Imai *et al.,* 2001; Saunders, 1998).

- Commercial uses: Electronic resources of heritage collections are a modern and safe way of displaying items to the public that would otherwise not be available, without risk of damage. Innovative methods of presenting artefacts that are fragile, degraded or generally misunderstood aim to generate renewed interest such as the digital restoration of a tapestry as part of this project that both increases interest in tapestries and conservation practices. Also a projector has been used to fill in areas of the beautiful renaissance murals at the Broemserhof in Ruedesheim, Germany that had been damaged during the second world war (Live Production, 2010). An objective of the MARC project at the National Gallery is to make available high-resolution colorimetric images of all the paintings in the collection on the Gallery's server (Martinez *et al.,* 2002). Detailed images of some of the Special Collections Division of The John Rylands University Library, The University of Manchester can be viewed on-line (The Rylands Collection, 2011).
- Research: Spectral imaging has a wide scope for non-invasive analysis of the materials and properties of an artifact. Some of the areas of interest and the technical studies of items of cultural heritage, and materials used in their construction, are:
    - Examination of the artists' methods i.e. visualisation of sketches underneath the paint, retouched/repainted areas, identification of pigments in an artist's palette (Fischer & Kakoulli, 2006)
    - Pigment mapping uses the spectral information to split a coloured painted area into its constituent pigments. Mapping the pigments onto the image can be performed using segmentation algorithms (Zhao *et al.,* 2008)
    - Rejuvenating the appearance of a painting by replacing original pigment colour (Zhao *et al.,* 2008) and removal of varnish (Cotte & Dupraz,) (Martinez *et al.,* 2002)
    - Investigation into previous conservation and restoration treatments

- Rediscovering lost information in palimpsests, for example, analysis of the Dead Sea Scroll to reveal the unreadable script (Bearman & Spiro, 1996)

This study utilises a hyperspectral imaging system comparable to the one developed by Foster *et al.* (2006) that performed at a high level of colorimetric accuracy. The aims of spectral imaging of a photo-faded tapestry were to digitally conserve a colour-calibrated image to serve as an archive of its current condition and appearance, permitting comparisons between the state of the tapestry now and in the future to be made.

4.3 Hyperspectral Imaging of The Oath and Departure of Eliezer

The digital conservation of *The Oath and Departure* involved taking high resolution, colour-calibrated images of sections of the front of the tapestry that provided a digital archive of the current colour appearance and condition of the tapestry. The development of an imaging system that captures the spectral information of the tapestry at each pixel involved characterising each element of the imaging system and the determining the performance of the system. The results were then calibrated to ensure a high level of colorimetric accuracy.

4.3.1 Materials and instruments

4.3.1.1 Materials

The following materials were used during the spectral imaging of The Oath and Departure of Eliezer, the instrumental characterisation and in pilot studies for the development of this methodology.

1. X-Rite White Balance Card is a reference target used for characterising the light sources, the instruments and the hyperspectral imaging system. This target is a scientifically engineered white reference that provides a uniform surface that is spectrally neutral in any lighting condition for use in white balance procedures and spatial calibrations.

Figure 4.3.1 X-Rite White Balance Card

2. X-Rite Colorchecker Chart is a target consisting of 18 coloured patches and 6 grey-scale patches that was used to calibrate the various colour measurement techniques used. Some of the squares are primary colours and some are representative of natural objects, such as human skin, foliage and blue sky. The target provides a wide range of colours for analysing the colour rendition and gamut of different instruments used during this project.

Figure 4.3.2 X-Rite ColourChecker Chart

3. X-Rite Digital ColorChecker SG is a coloured target consisting of 140 patches that provides a larger colour gamut than the standard ColorChecker target for characterisation of instruments. The occurrence of coloured patches in multiple locations can be used to test if the sensor is spatially consistent.

Figure 4.3.3 X-Rite Digital ColorChecker SG

4. X-Rite Mini ColorChecker Chart is a smaller version of the standard ColorChecker target that was placed in the periphery of every hyperspectral image taken and used for calibration of the images.

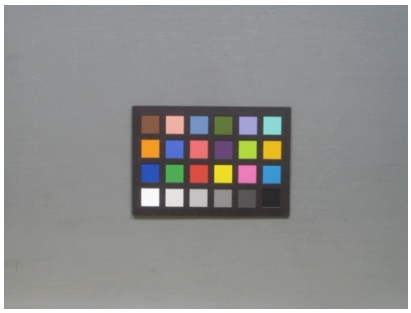

Figure 4.3.4 X-Rite Mini ColorChecker Chart

5. A light diffusing surround made of polystyrene was placed around the imaging area to provide a brighter and more light-controlled environment. Internal dimensions of the surround: 116 cm x 116 cm. Depth of the surround: 45 cm.
6. A light reflecting umbrella was placed above the imaging equipment to both reflect the lamp light onto the imaging area and to block out the ambient light.
7. Black-out material was used as a curtain above and around the imaging area to block out the ambient light thus creating a light controlled environment for the imaging.

8. A gantry was used as the mobile base for the imaging equipment so that the entire area of the tapestry could be imaged from a consistent position of about 1 metre. The gantry can be seen in the top left of the image in Figure 4.3.5.

Figure 4.3.5 Photo of the gantry above the tapestry

9. A Melinex polyester film barrier was placed between the tapestry and the light diffusing surround to protect the historic materials from damage and a Tyvek sheet covered the tapestry when it was not being imaged.

4.3.1.2 Instruments

1. Two studio lamps. Bowens UNI-LITE BW 3370 continuous light fluorescent lamps with removable diffusing material in front of the bulb were both used to illuminate the imaging area (Bowens 2011). The lamps are cool-running which was necessary when imaging the tapestry to eliminate any possible damage caused by heat. Subsequent usage of the terms 'Lamp 1' and 'Lamp 2' will refer to one of these studio lamps.
2. Macbeth SpectraLight II Light Booth was used for measuring the X-Rite ColorChecker Chart under Artificial Daylight.
3. Datacolor Spectraflash 600 Spectrophotometer was used to measure the X-Rite ColorChecker Chart. Reflectance data was recorded at 10 nm intervals from 400 nm to 700 nm.

4. Photoresearch PR-655 Spectrascan Spectroradiometer with fast scanning 128 element photodiode array is a portable spectroradiometer that was used throughout the project as a non-contact method of colour measurement. Its output is traceable to a calibration NIST standard (NIST Test Report No. 844/273080-06). It has a digital resolution of 16 bits. Dark frame subtraction is performed automatically and readings are given for Luminance, CIE XYZ and x, y values, dominant wavelength, correlated colour temperature (CCT) of the signal and CIE L*a*b* values. Radiance data at 4 nm intervals from 380 nm to 780 nm can be downloaded from the instrument using MATLAB (Photo Research, Inc 2011).

Figure 4.3.6 Photoresearch PR-655 Spectrascan Spectroradiometer

5. Retiga 4000R 12-bit, monochromatic CCD camera, with peltier thermoelectric cooling and a 4.19 million pixel sensor. The 12-bit camera will differentiate 4096 levels of grey allowing a greater dynamic range of pixel values than the standard 8-bits, with a cooling system to minimise thermal noise during low light, long exposure imaging. The high resolution sensor gives fine detailing and allows sharp images of larger size to be taken. The exposure time for the camera is controlled by the QCapture software on the PC and can be automatically calculated for each image. The camera is connected to the PC via a firewire cable (QImaging 2011).

Figure 4.3.7 Retiga 4000R 12-bit monochromatic camera

6. A Nikon DX AF-S Nikkor 18-55 mm lens (1:3.5 – 5.6, G II ED) was fitted to the camera.
7. VariSpec liquid crystal tunable filter is a high quality interference filter which is attached in front of the camera and lens. The wavelength band that it transmits is selected electronically using the VariSpec software loaded onto the PC. Since the filter has no moving parts, there will be no vibrations caused by changing the filter which is essential for reconstruction of the hyperspectral images. Hyperspectral imaging was carried out by imaging through 31 adjacent wavelength bands of 10 nm width from 400 nm to 700 nm. Filter transmission is spatially non-uniform when it is cold therefore the filter must be warmed up to around 20°C by cycling through the wavelengths for around 30 minutes. The filter is connected to the PC with a USB cable (CRi 2011).

Figure 4.3.8 VariSpec liquid crystal tunable filter

8. PC with 114 GB storage capacity was used to control the instruments and record the data and images.
9. DVD writer was used for data storage back-up

10. Canon Digital IXUS 70 compact camera was used to take images of sections of the tapestry on both the front and reverse sides.
11. MATLAB is a matrix calculation software tool that was used for performing colour science calculations and image analysis and image processing.
12. Adobe Photoshop is image analysis software, which was used for some image manipulation.

4.3.2 Experimental set-up

4.3.2.1 Pilot studies

Two pilot studies were carried out in order to test and optimise the hyperspectral imaging system. They utilised a different light source that was found to be too unstable to give reproducible results. The Micro NIKKOR 55 mm Nikon lens that was used was also found to be unsuitable as it limited the field of view and the image size to 35 cm squared. The new 18 – 55 mm NIKKOR lens gave a larger field of view to allow an image size of 50 cm squared.

Hyperspectral imaging of tapestry fragments and calibration standards was carried out and the reconstruction of spectral reflectance curves for each pixel was implemented using MATLAB software. Various algorithms were used and the most effective method of image processing was developed.

4.3.2.2 Imaging set-up

The Oath and Departure of Eliezer tapestry was imaged in the wash building of Hampton Court Palace. The wash building is a converted greenhouse in the grounds of the palace that is used by the conservators to inspect and clean tapestries. The wash table provided a flat surface of sufficient size to lay out the large tapestry while the movable gantry, which is positioned over the wash table, provided a base for the hyperspectral imaging equipment (see Figure 4.3.5).

Using the movable gantry platform situated above the wash table as a base for the imaging system, a boom was attached across the top rails of the platform using 2 x 2 studio clamps. A cross member was clamped to the boom which supported the camera and filter, 2 lamps and the light control equipment which comprised a light reflecting umbrella and a blackout curtain. The imaging equipment protruded a fixed distance of 29 cm from the gantry in order to obtain an uninterrupted view of

the tapestry. The camera was centred on the boom between the two lamps at a distance of 44 cm from each lamp. The lens was fitted to the front of the camera and the filter was attached to the front of the lens. The vertical distance from the front of the lens to the tapestry was 132 cm. The vertical distance from the diffusing material of the lamps to the tapestry was 103 cm. A schematic of the imaging set-up is shown in Figure 4.3.9.

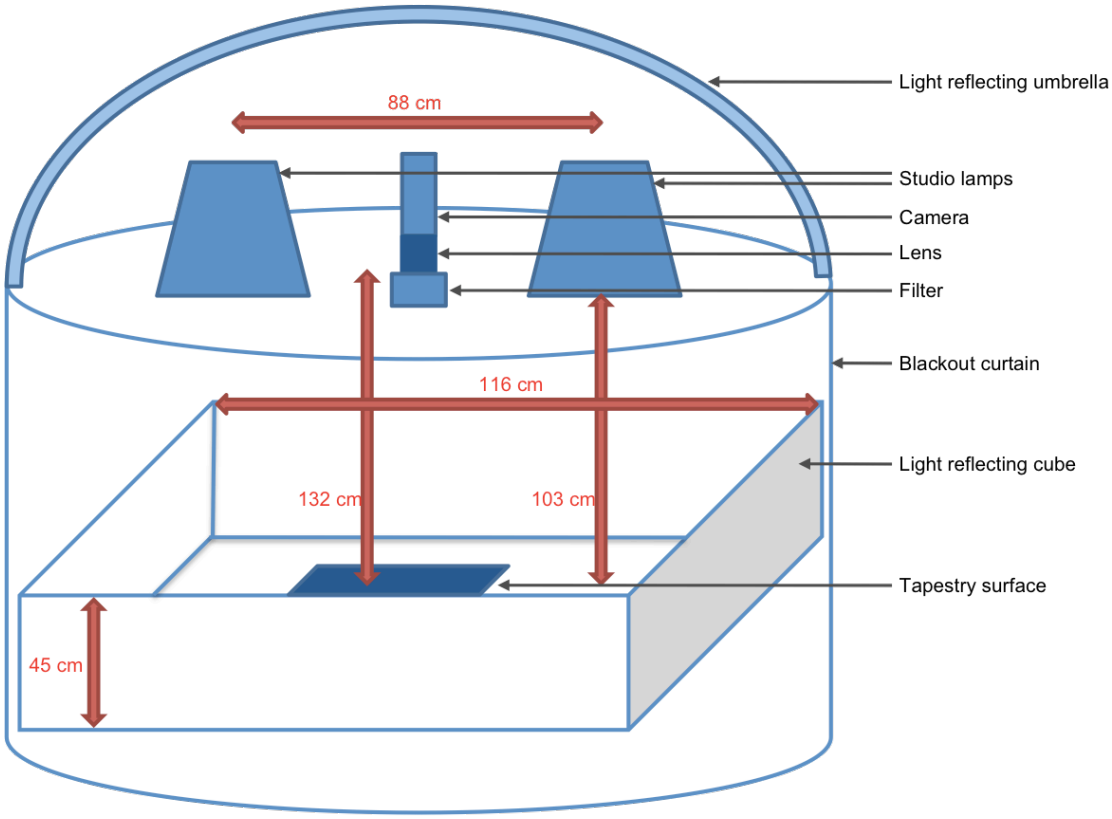

Figure 4.3.9 Schematic of the hyperspectral imaging set-up as used in the wash building of Hampton Court Palace

The image size obtained using this experimental set-up was 50 cm x 50 cm. The tapestry was divided into a total of 170 sections using a grid of threads at 50 cm intervals, which was used as a guide for aligning the images. The grey-scale image of tapestry section 'D7', taken by the 12-bit monochromatic camera, with the imaging section marked by a white template is shown in Figure 4.3.10. One of the hyperspectral images (540 nm) of the same section is shown in Figure 4.3.11. The periphery of the image provides an overlap with all adjacent sections that aided registration of the images during processing, while the Mini ColorChecker chart was used to calibrate each image as it was placed in the same location for every image taken.

Figure 4.3.10 12 bit camera image showing the 50 cm x 50 cm imaging section in the centre of the field, marked by a white template. Note the Mini ColorChecker chart above the centre section

Figure 4.3.11 540 nm wavelength band hyperspectral image showing the circular area produced by the filter. Note the Mini ColorChecker chart in the periphery

The light reflecting umbrella and black-out curtain were attached to the gantry and moved into position with the imaging system. A light diffusing surround was placed around the imaging area in the experimental set-up in order to create a diffuse light environment for imaging. The ceiling of the wash building was translucent which meant that light controlling equipment was necessary.

The working distance of the imaging system was restricted by the low ceiling height of the wash building, which restricted the overall image size obtainable. In addition, the filter restricted the imaging area to a circle as it was located in front of the lens so each image taken had a 50 cm x 50 cm area in the centre that would be cropped out as the final section of the image.

4.3.3 Instrument characterisation methodology

The experimental set-up for the hyperspectral imaging system as shown in Figure 4.3.9, including viewing distances, was used for measurements during instrument characterisation as stated. The darkened room, which was used during measurements, was located in the cellar of the Centre for Collection Care at Hampton Court Palace. This provided an environment in which no ambient light was present in order to accurately measure the performance of the components of the imaging system.

4.3.3.1 Analysis of temporal stability of light sources

The temporal properties of the two studio lamps were determined by measuring the output of the lamps using the following method:

1. Measurements were taken in the darkened room to eliminate errors due to ambient light
2. Spectral data was collected by the PR-655 spectroradiometer which was pointed directly at the lamps' diffusing material, at the centre of the lamp at a distance of 1 metre
3. Irradiance was measured as a function of time from when the lamps were switched on until a stable output was achieved
4. Readings were taken every 30 seconds for 1 hour
5. Readings were taken for luminance ($cd.m^{-2}$), CIE x and y values and CCT from the PR-655 display

Results are recorded and discussed in section 4.3.4.1.

4.3.3.2 Spectral power distribution of light sources

The spectral data of the irradiance of the light sources was collected by the PR-655 during the experiment described in 4.5.3.1. The results used to illustrate the Spectral Power Distributions (SPDs) of the light sources were taken at 30 minutes, 45 minutes and 60 minutes after switch on, when the lamps had stable outputs. The SPDs of the lamps were compared to the CIE standard illuminants to determine which illuminant described the light most accurately, for performing colour measurement calculations.

Results are recorded and discussed in section 4.3.4.2.

4.3.3.3 Analysis of spatial uniformity of light sources

The spatial uniformity of the output from the lamps was measured by taking readings across the surface of the diffusers using the following method:

1. Measurements were taken in the darkened room
2. Spectral data was collected by the PR-655 which was pointed directly at the diffusing material at a distance of 1 metre
3. The lamps had been switched on for at least 30 minutes prior to measuring
4. Readings were taken for luminance (cd.m^{-2}), CIE x and y values and CCT from the PR-655 display
5. Readings were taken from the nine different points on the diffuser surface shown in Figure 4.3.12

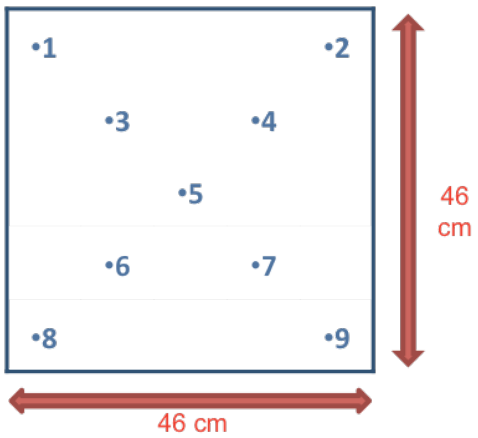

Figure 4.3.12 Positions on the lamp diffuser of the light source spatial uniformity measurements

The uniformity of the light that falls on the target imaging area was analysed by measuring the reflectance of the white target under each lamp and both lamps in the imaging area.

1. Measurements were taken in the darkened room
2. Spectral data was collected by the PR-655 which was pointed directly at the X-Rite White Balance Card, illuminated by each of the lamps and then both lamps at a distance of 1 metre
3. Readings were taken from the nine positions on the white target as shown in Figure 4.3.13
4. The lamps had been switched on for at least 1 hour prior to measuring

5. Luminance readings were taken in $cd.m^{-2}$ from the PR-655 display

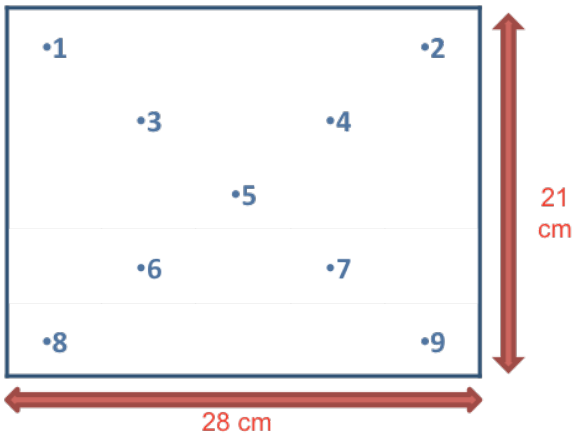

Figure 4.3.13 Positions on the White Balance Card of the reflected light spatial uniformity measurements

Results are recorded and discussed in section 4.3.4.3.

4.3.3.4 Analysis of spatial uniformity of the camera and light sources

The spatial uniformity of the camera and light sources was analysed by imaging the white target and coloured target using the 12-bit monochromatic camera in the experimental set-up using the following method:

1. The imaging system was set up on the gantry, above the tapestry in the wash building with the tapestry protected by the Tyvek sheet and the light control equipment in place around the imaging area
2. The imaging area was illuminated by both lamps
3. The lamps had been switched on for at least 30 minutes prior to imaging
4. The X-Rite White Balance Card and the X-Rite ColorChecker Chart were imaged in five different positions within the imaging area using the 12-bit monochromatic camera fitted with the lens
5. The images captured by the camera are shown in Figures 4.3.14 and 4.3.15
6. The images were analysed to determine the spatial uniformity of the light sources and camera

Results are recorded and discussed in section 4.3.4.4.

Figure 4.3.14 12-bit camera images of X-Rite White Balance Card

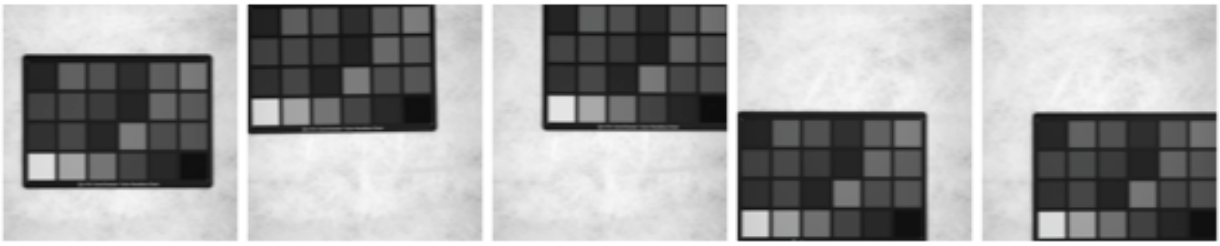

Figure 4.3.15 12-bit camera images of X-Rite ColorChecker Chart

4.3.3.5 Filter Transmission Analysis

The performance of the filter was analysed by measuring the amount of light that was transmitted by the filter at wavelength bands across the entire visible spectrum. The PR-655 was used to measure the light from Lamp 2 using the following method:

1. Measurements were taken in the darkened room
2. Lamp 2 was switched on for at least 40 minutes prior to measuring
3. The filter was placed in front of the PR-655 which was pointed directly at the centre of Lamp 2
4. The VariSpec computer software was used to select the desired wavelength band of the filter
5. Spectral data was collected at 10 nm intervals from 400 nm to 720 nm
6. Readings were taken for luminance ($cd.m^{-2}$), CIE x and y values and CCT from the PR-655 display
7. The experiment was repeated 3 times and the average values and standard deviations have been calculated
8. The chromaticity diagram for the transmission of the filter has been compared to the CIE 1964 chromaticity diagram under D65 illuminant
9. Spectral data was downloaded from the PR-655 to construct a complete transmission curve for the filter

Results are recorded and discussed in section 4.3.4.5.

4.3.3.6 Analysis of temporal stability of filter

Using the method described in section 4.3.3.5, the temporal stability of the filter was analysed by measuring the transmission as a function of time.

1. Measurements were taken at single wavelengths at 10 second intervals for 5 minutes
2. Five sets of data were recorded at five different wavelengths across the visible spectrum at points of highest intensity for the light source; 435 nm, 490 nm, 544 nm, 585 nm and 612 nm
3. Luminance ($cd.m^{-2}$) was recorded and the standard deviations were calculated to determine the stability of the filter readings

Results are recorded and discussed in section 4.3.4.6.

4.3.3.7 Analysis of spatial uniformity of filter

The hyperspectral imaging experimental set-up, described in 4.3.2.2 and illustrated in Figure 4.3.9, was used to determine the spatial uniformity of the filter. Hyperspectral images were taken of a white field, of the X-Rite Digital ColorChecker SG and the X-Rite Mini ColorChecker Chart in a white field. The hyperspectral images of the white field provided a spatial homogeneity analysis of the complete imaging system as the lights, camera and filter were tested simultaneously. The pixel values of the measured white field provide the normalising factor for the hyperspectral images. The exposure times for each wavelength band were determined from test imaging the white field at automatic exposure times calculated by the camera software. The exposure times were variable due to the non-uniform transmission of the filter whereby the bands at the very short and very long wavelengths had low levels of transmission and therefore longer exposure times than bands of higher transmission. The reported exposure time for each wavelength band was utilised for the hyperspectral imaging of the tapestry.

The reconstructed hyperspectral image of the X-Rite Digital ColorChecker SG was used to calibrate the performance of the imaging system by SF600 measurements of the chart and standard colour values provided by the manufacturer.

4.3.3.8 Analysis of performance of hyperspectral imaging system

The X-Rite Digital ColorChecker SG chart was imaged using the hyperspectral imaging system to determine the colorimetric accuracy of the reconstructed surface spectral reflectance curves by comparing the data to the known standard colour target.

The method and results are described in section 4.3.5.2.

4.3.3.9 Analysis of the colorimetric performance of the PR655

The PR655 spectroradiometer has been used to characterise the components of the hyperspectral imaging system. To ensure the readings being taken are accurate, the PR655 will be characterised and calibrated by the SF600 spectrophotometer.

Measurements of the X-Rite ColorChecker SG Chart were taken using the benchtop SF600 and the portable PR655 in the lightbooth under daylight. The tristimulus values XYZ were calculated from the reflectance values on the SF600, and were calculated from the luminance (Y) and chromaticity coordinates (x, y) given by the PR655. The chromaticity coordinates of the ColorChecker SG tiles measured by the two instruments are compared in Figure 4.3.16 while the average colour difference value was calculated at 2.26 ΔE^*_{ab}. The first operation was to normalise the PR655 data using the ColorChecker white tile as the white point. This improved the measurements by shifting them closer to the SF600 coordinates, reducing the ΔE^*_{ab} value to 1.66. A polynomial mapping function was then applied to the PR655 data that improved the performance and reduced the ΔE^*_{ab} value to 1.17, which was determined to be an acceptable match.

This 3rd order polynomial mapping function was found to minimise the overall ΔE^*_{ab}. This was utilised on the PR655 data to convert it to calibrated XYZ values, which would then be converted into a device independent colour space, CIELAB. This allowed a more accurate comparison between measurements from the different instruments.

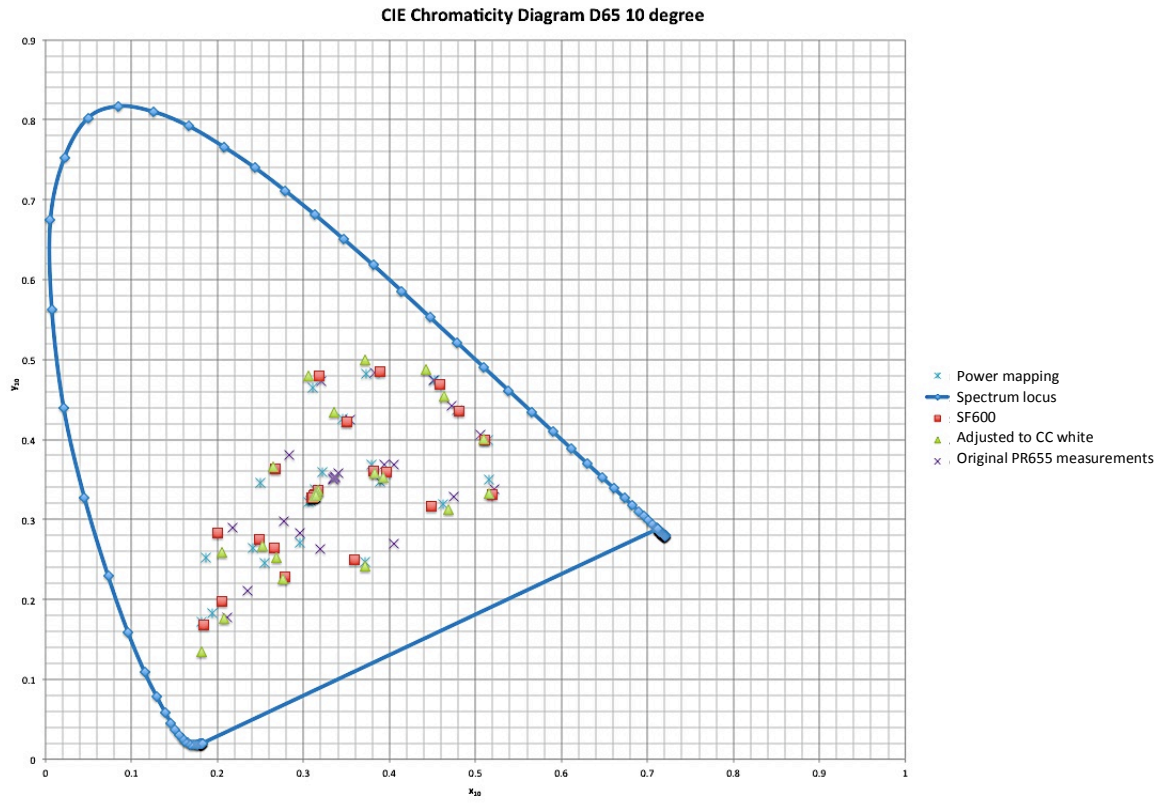

Figure 4.3.16 CIE chromaticity diagram of the SF600 and PR-655 instruments with PR-655 values converted by several methods

Figure 4.3.16 shows a CIE Chromaticity Diagram containing the chromaticity coordinates of the XRite ColorChecker SG chart. The chromaticity coordinates of three mapping techniques are also shown. These techniques include linear transform, 3rd order polynomial fit to XYZ and using a power function to fit the XYZ values.

4.3.4 Instrument characterisation results and discussions

4.3.4.1 Temporal stability of light sources

A graph of luminance as a function of time for both light sources is given in Figure 4.3.17. The average luminance, CCT and CIE x and y values were calculated after 10 minutes to eliminate errors from the initial warm up period.

Lamp 1: luminance	4730 cd.m^{-2}	Standard deviation:	19
CCT	5767 K		10
x	0.327		
y	0.346		
Lamp 2: luminance	6395 cd.m^{-2}	Standard deviation:	50
CCT	6020 K		11
x	0.320		
y	0.349		

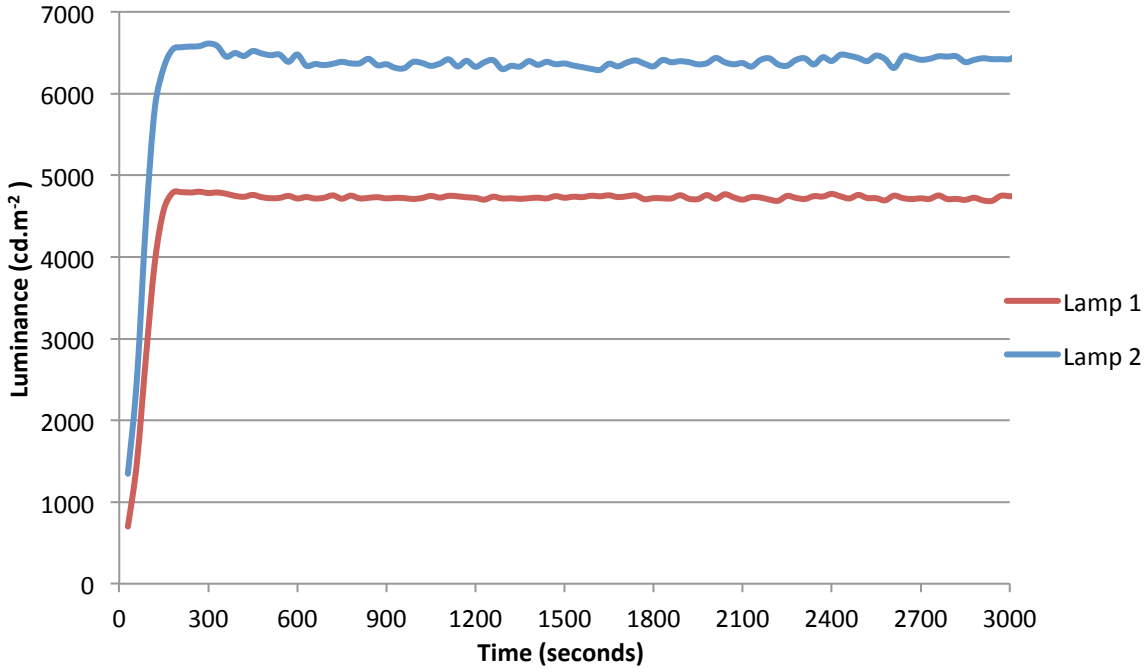

Figure 4.3.17 Graph of the temporal stability of the two studio lamps

As seen from Figure 4.3.17, the luminance of the lamps varies with time, which reduces the accuracy of colour measurements made using these light sources. However, the luminance becomes relatively constant after 15 minutes therefore any measurements must be taken after the lamps have been switched on for at least this

amount of time and the output has stabilised. In practice, the lamps were switched on for at least 30 minutes prior to any images being taken.

The average luminance of Lamp 2 is higher than that of Lamp 1, which must be due to a variation in the bulbs supplied. The two lamps were used together at fixed positions for all of the imaging work therefore any spatial variation in the light source due to the difference in luminances was constant and could be accounted for in image processing.

4.3.4.2 Spectral power distribution of light sources

Graphs of the spectral power distributions of three measurements of both light sources are shown in Figure 4.3.18. The peak wavelength of each set of data is 544 nm. The results for both lamps were found to be consistent as can be seen from Figure 4.3.18 where the three data sets overlap for each lamp. Therefore the '60 minute' data set has been selected as an example result for each lamp, to be used in further calculations and discussions.

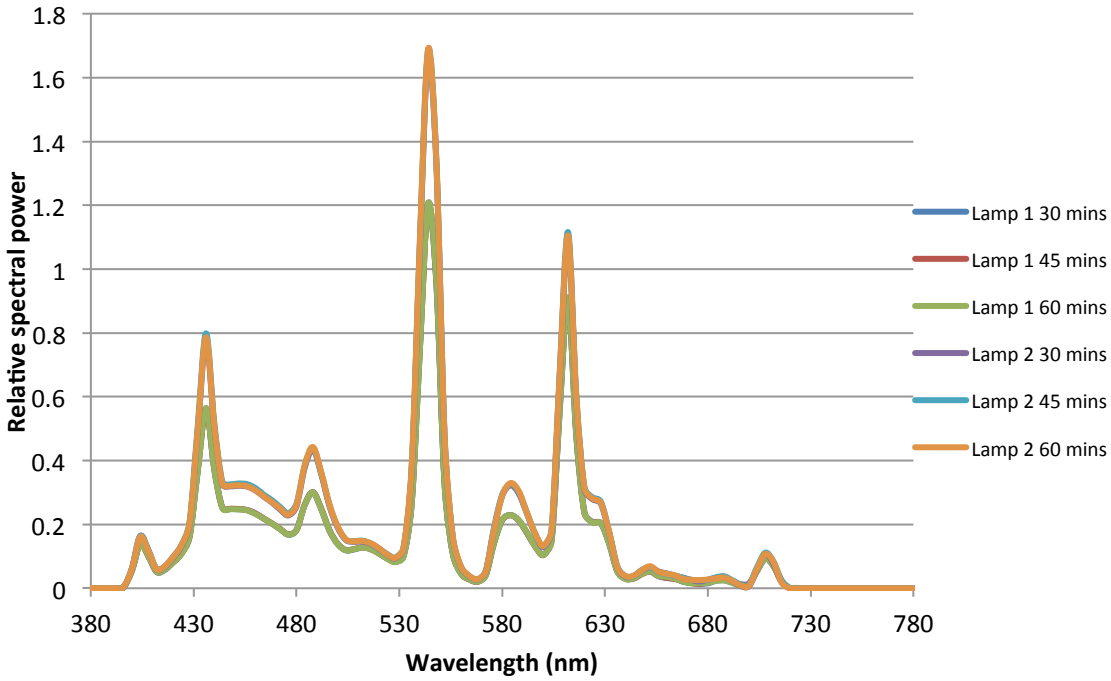

Figure 4.3.18 Spectral power distributions of light sources

The SPD of the lamps can be seen to have three major peaks, one in each of the blue, green and red wavelength regions at 436 nm, 544 nm and 612 nm respectively. The three peaks are caused by emissions of the three phosphors in the fluorescent

lamps. The CIE XYZ and x and y values, the CCT and the CIE1960 deviation from Planck's Blackbody Radiator Locus of the example data set of Lamp 1 and Lamp 2 are shown in Table 4.3.1.

Table 4.3.1 Raw colorimetric data of light sources taken from PR-655 spectral measurements

	Lamp 1	Lamp 2
X	4453	5869
Y	4720	6411
Z	4476	6017
x	0.3260	0.3208
y	0.3456	0.3504
CCT (K)	5766	5999
CIE1960 deviation from Planck's Blackbody Radiator Locus	0.0052	0.01

The outputs of the lamps have been compared to the SPDs of the CIE illuminant series F, as shown in Figure 4.3.19, and the curves were found to closely match the three-band group of illuminants F10, F11 and F12. The distribution F11 is used in preference to the others however, the CCTs of the lamps are closer to that of distribution F10 (5000 K).

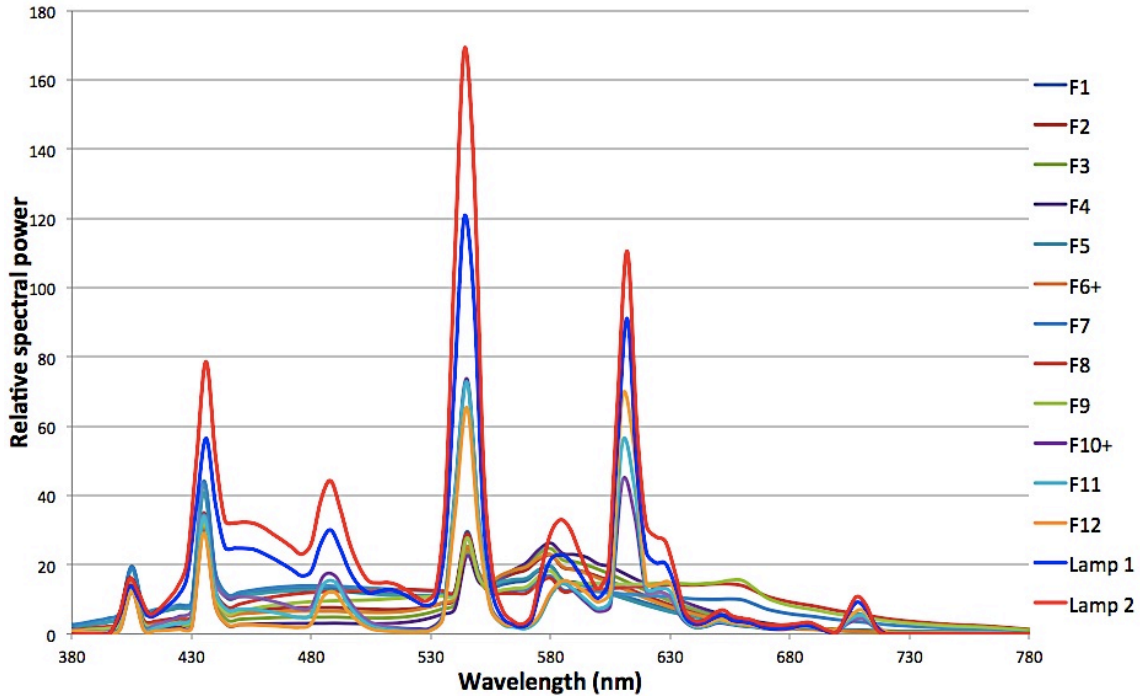

Figure 4.3.19 Spectral power distributions of the light sources and CIE illuminant series F

4.3.4.3 Spatial uniformity of light sources

The spatial uniformity of the lamp output was measured using the PR-655 pointed at different positions across the surface of the lamps' diffusers. The luminance, x and y values and CCT of the readings for both lamps are given in Table 4.3.2. The luminance values are shown at the positions at which they were measured on the lamp diffusers in Figure 4.3.20.

Table 4.3.2 Spatial uniformity measurements of Lamp 1 and Lamp 2 with diffusers taken using the PR655

	Lamp 1				Lamp 2			
Position	Luminance cd.m^{-2}	x	y	CCT (K)	Luminance cd.m^{-2}	x	y	CCT (K)
1	2414	0.325	0.346	5846	3117	0.319	0.349	6076
2	1949	0.326	0.347	5797	2986	0.319	0.349	6064
3	2828	0.325	0.346	5839	4063	0.319	0.348	6093
4	2743	0.325	0.346	5838	4045	0.319	0.349	6078
5	5284	0.326	0.345	5762	6314	0.32	0.35	5993
6	3249	0.325	0.346	5834	4117	0.319	0.348	6087
7	3396	0.325	0.345	5833	3908	0.319	0.349	6092
8	2155	0.324	0.346	5857	2876	0.32	0.35	6049
9	2207	0.324	0.346	5850	2868	0.319	0.349	6076

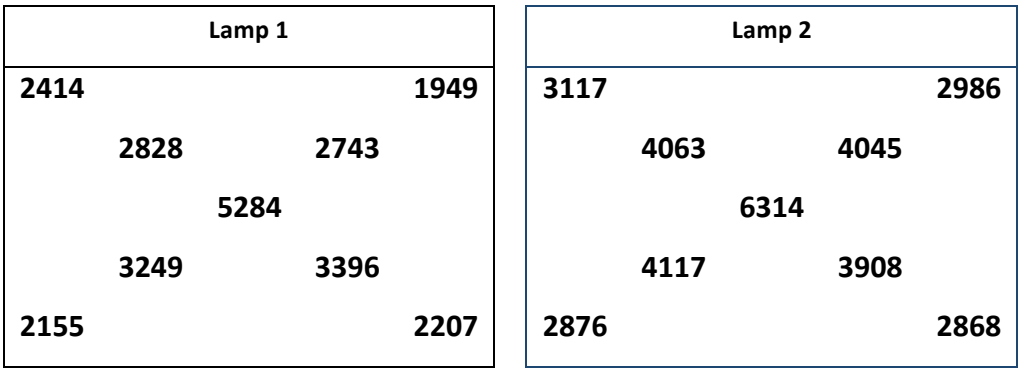

Figure 4.3.20 Schematic of spatial uniformity of Lamp 1 and Lamp 2; luminance measurements across the diffuser material (cd.m^{-2})

The output of both the lamps can be seen to approximately halve at the corners of the lamp diffusers compared to the measurements at the centre. The high value at the centre is due to the PR-655 pointing directly at the bulb whereas the diffusing material works to spread the light over a larger area. The spatial effect on the light which is received and reflected by a white target illuminated by the studio lamps

has been measured and the results can be found in Table 4.3.3 and Figures 4.3.21-22. As expected from the higher luminance values of the Lamp 2 output, the luminance of the light reflected from the white target illuminated by Lamp 2 are higher than those for Lamp 1. The light does not fall evenly across the surface of the white target, when illuminated by Lamp 1 the right hand side values are higher. For Lamp 2 the centre and lower half of the target have higher luminance values and when illuminated by both lamps the target has higher luminance values in the lower right hand section. The combined CCT of the lamps is 5831 K.

The results show that the light emitted from both of the studio lamps is not perfectly diffused by the diffusing material in front of the bulbs and that there is spatial variation in the light reflected from the white target. The spatial variation in reflected light could be due to the positioning of the lamps relative to the white target in the experimental set-up.

The spatial variations in the light source will cause an inaccuracy in the colorimetric data obtained from the hyperspectral imaging system. To improve the accuracy of the system, a spatial correction algorithm was performed for each hyperspectral image taken.

Table 4.3.3 Spatial uniformity measurements of X-Rite White Balance Card illuminated by studio lamps, taken using the PR-655

Illuminated by:	Lamp 1	Lamp 2	Lamp 1 and 2
Position	Luminance ($cd.m^{-2}$)	Luminance ($cd.m^{-2}$)	Luminance ($cd.m^{-2}$)
1	130.9	172.7	287.8
2	139.8	175	301.5
3	135.2	177.3	292
4	141	180.4	305.7
5	139.3	183.6	305.8
6	135	182.7	300.4
7	140.4	182.8	309.7
8	131.6	180.1	296.4
9	139.9	180.4	308.6

Target illuminated by Lamp 1					Target illuminated by Lamp 2				
131				140	173				175
	135		141			177		180	
		139					184		
	135		140			183		183	
132				140	180				180

Figure 4.3.21 Schematic of spatial uniformity of X-Rite White Balance Card illuminated by Lamp 1 and Lamp 2; luminance measurements across the white target (cd.m^{-2})

Target illuminated by both lamps				
288				302
	292		306	
		306		
	300		310	
296				309

Figure 4.3.22 Schematic of spatial uniformity of X-Rite White Balance Card illuminated by both Lamp 1 and Lamp 2; luminance measurements across the white target (cd.m^{-2})

4.3.4.4 Analysis of spatial uniformity of the camera and light sources

As discussed in 4.3.4.3 the spatial variability of the light source will affect the accuracy of the hyperspectral imaging system. The spatial uniformity of the camera must also be assessed to determine if this will affect the colorimetric performance of the imaging system. As described in section 4.3.3.4, images were taken, using the 12-bit monochromatic camera, of the X-Rite White Balance Card and ColorChecker Chart that were placed within the imaging area using the proper experimental set-up. These are grayscale images that can be used to assess the spatial uniformity of the camera in addition to the light sources by comparing the pixel values of points across the surface of the targets. There was found to be a variability of 3 L* units in the lightness of the white target at different positions, from L* = 88 at the right hand side to L* = 91 at the centre line.

4.3.4.5 Filter transmission analysis

The amount of light that is transmitted by the filter, at each of the wavelength bands across the visible spectrum, which will be selected for hyperspectral imaging, has been measured using the PR-655. The light source was one of the studio lamps.

The luminance values of the light, at each selected wavelength band, taken from the PR-655 are plotted in Figure 4.3.23. The luminance varies greatly across the visible spectrum with peaks at 540 nm, 580 nm and 610 nm, which correspond to peaks in the SPD of the light source. The filter transmission at both the short wavelength (≤450 nm) and the long wavelength (≥670 nm) ends of the spectrum is less than 2 $cd.m^{-2}$. The peak seen in the SPD of Lamp 2 at 436 nm for example is not detected on the filter transmission curve.

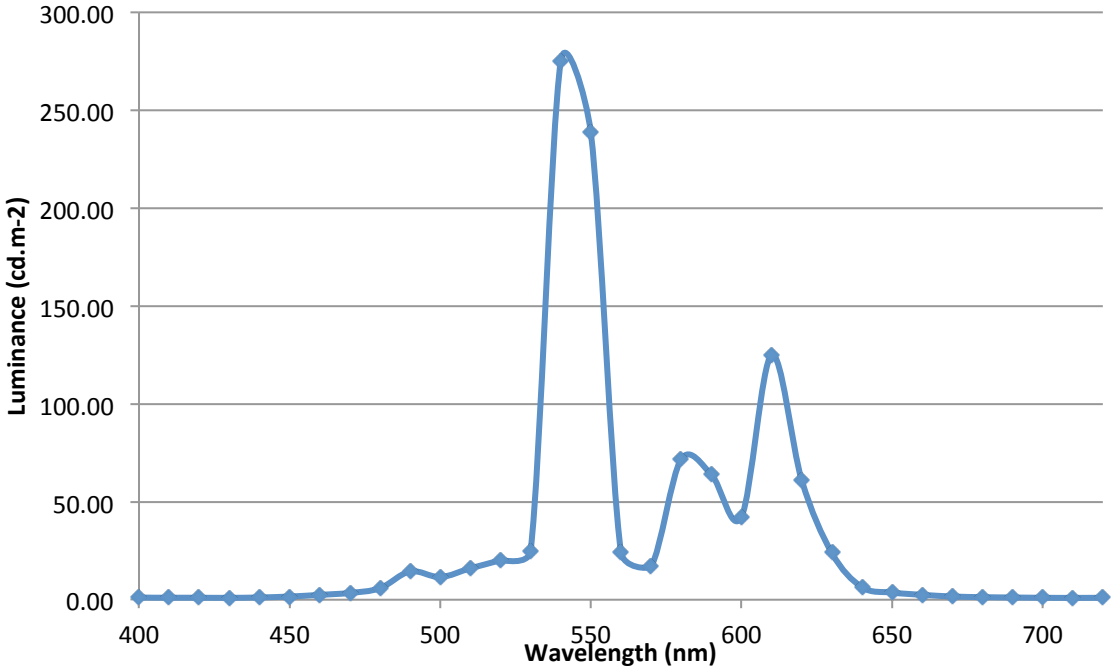

Figure 4.3.23 Luminance of light from Lamp 2 transmitted through the filter at 10 nm wavelength bands from 400 nm – 720 nm, measured by the PR-655

A more detailed analysis of the filter transmission is recorded in Figure 4.3.24, which displays the spectral data taken from the PR-655 of the same experiment. The transmission at every 4 nm from 380 – 780 nm was recorded for each 10 nm wavelength band from 400 – 720 nm. There is little transmission below 430 nm at any of the wavelength bands and little transmission above 660 nm, which means that it will be very difficult to collect colorimetric data at the ends of the spectrum. The issue of low transmission can be partially mitigated by using longer exposure times for imaging at these wavelength bands or by increasing the wavelength interval, to 20 nm for example, to increase the response.

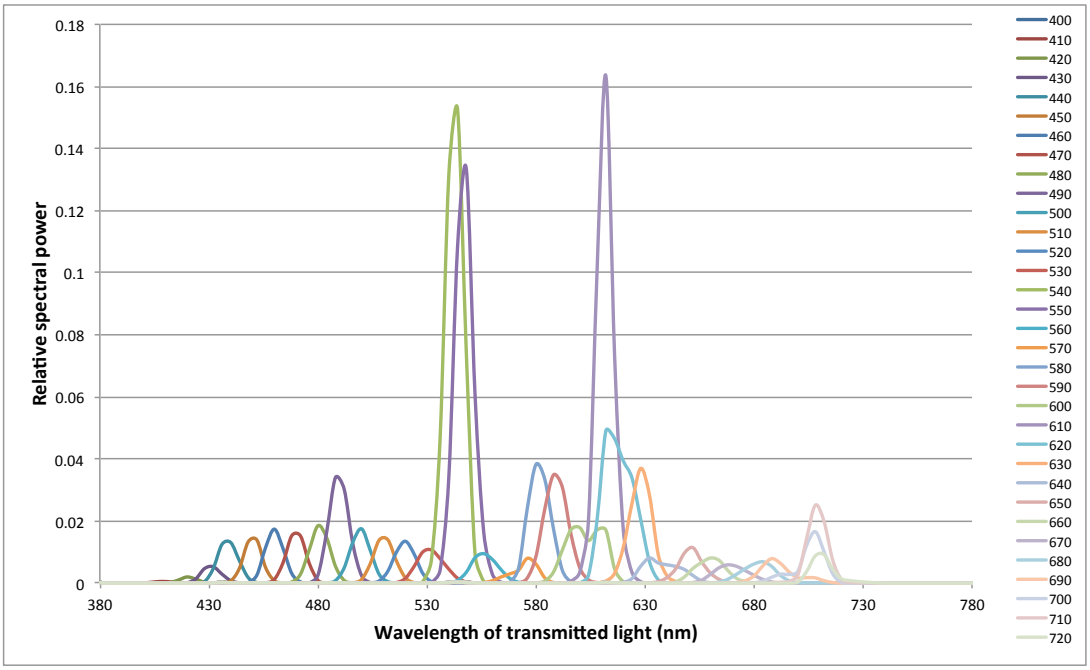

Figure 4.3.24 Transmission of the filter at 10 nm wavelength bands from 400 nm – 720 nm, measured by the PR-655 (FILTER-3 data)

The intensity of the light that passes through the filter varies from wavelength band to wavelength band. The chromaticity of the light that is transmitted can be determined from the PR-655 spectral data to give the gamut of light that can be transmitted. Figure 4.3.25 shows the gamut of the filter taken from the average of 3 datasets. The gamut of the filter closely matches the spectrum locus in some areas; however, it is deficient along the line of purples at the very short and very long wavelength bands, below 440 nm and above 630 nm. However, the colour gamut for the filter is still large enough to encompass a wide range of textile colours including, as will be noted later when colour measurements of the tapestry are reported, all of the colours of the tapestry. Therefore the filter can be used as part of the hyperspectral imaging system.

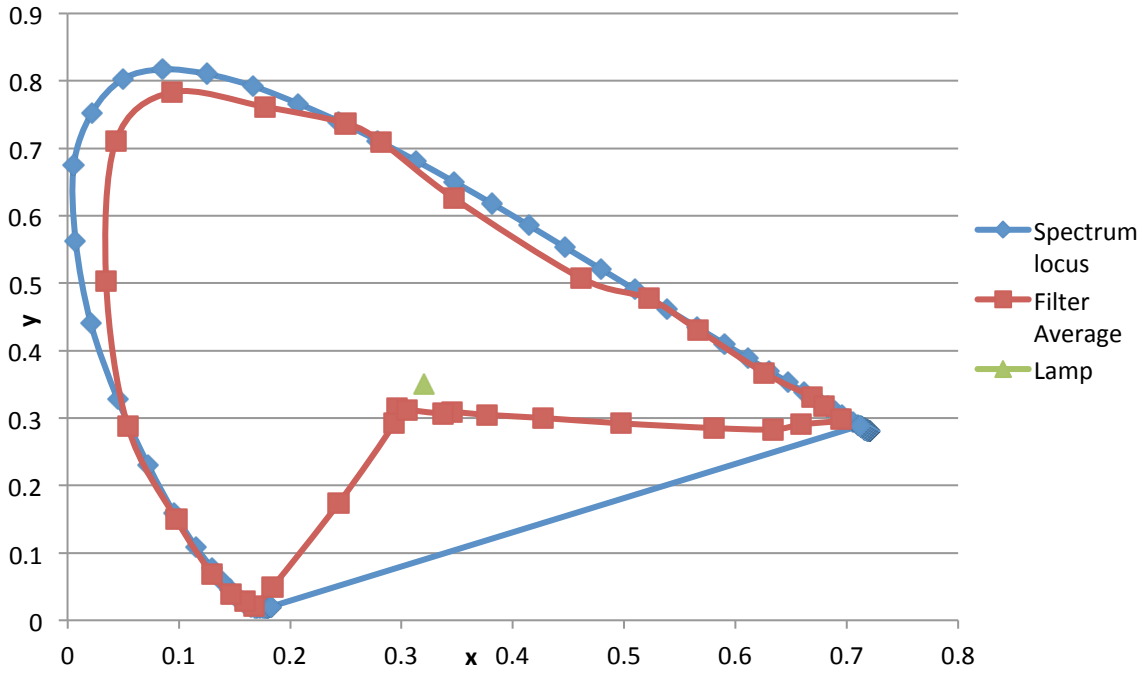

Figure 4.3.25 Chromaticity diagram showing the gamut of the filter transmission

4.3.4.6 Temporal stability of filter

The filter transmission was found during experimentation to vary due to the temperature of the filter; however, the readings were discovered to be stable when the filter temperature was between 19°C and 24°C. There were five sets of temporal stability measurements taken at different wavelengths at 10 second intervals for 5 minutes. The sets of luminance readings taken at the five different wavelengths had standard deviations of between 0.03 and 0.59 over the time period, which shows that the filter transmission is very stable when it has been warmed up to the correct temperature. The filter was connected to the PC and the software cycled the liquid-crystal filter through the full range of wavelengths for a minimum of 30 minutes until the temperature was within the acceptable range before any images were taken.

4.3.4.7 Spatial uniformity of filter

The spatial uniformity of the filter was determined from hyperspectral images of a white card, illuminated by the two studio lamps within the imaging set-up. The images in Figure 4.3.26 are the 31 intensity images taken through each filter wavelength band, cropped to show the 50 cm by 50 cm area at the centre of the image. This area is the size of the sections that the tapestry was segmented into.

Figure 4.3.26 Cropped hyperspectral images of a white card showing the central 50 cm by 50 cm area

4.3.5 Instrument characterisation conclusions

This section has outlined the components used to perform the hyperspectral imaging of the tapestry. The performance of each component has been quantified in terms of their spatial, temporal, spectral and colorimetric properties.

The lamps demonstrated Luminance stability after 15 minutes. Imaging of the tapestry occurred after, at least, 30 minutes of the warming up time. At this point the combined Luminance from the Lamps at a central location within the image was 306 $cd.m^{-2}$ plus or minus 1.22 $cd.m^{-2}$. The spatial distribution of the lamps was seen to reduce from the centre to the top left of the illuminated field. The Correlated Colour Temperatures of each lamp were, on average, 5767 K and 6020 K respectively. The CCT of the lamps together was 5831 K.

The spectral range of the transmitted light through the filter encompassed the gamut of dyed samples.

One limitation of working with valuable historic artefacts is to minimise any potential degradation caused by experimentation. In order to protect the tapestry from further photo-fading a decision was made to use a cool fluorescent light source. Although this was less harmful to the materials under investigation it compromised some of the colorimetric performance of the hyperspectral imaging system. The combination of fluorescent lighting and LCD filter meant that less light transmission was possible at the short and long wavelengths of the visible spectrum. This increased the signal-to-noise ratios in these areas and impacted on the spectral reconstruction. Nevertheless, the ΔE^*_{ab} of 2.17, for the reconstruction of the 24 patches of the X-Rite ColorChecker SG Chart, suggests a similar colorimetric performance of reconstruction as reported by previous workers. As the chromaticity coordinates of the dyes were encompassed by the gamut of colours from the ColorChecker Chart it was assumed that the system was suitable for purpose.

4.3.6 Imaging and image processing

The imaging method described below was followed systematically for hyperspectral imaging of the X-Rite Digital ColorChecker SG and the 170 sections of the front of the tapestry, as well as 6 areas of the reverse. The 'white template' was a 50 cm x 50 cm white card that was used for positioning the imaging system over the desired area of the tapestry, see Figure 4.3.27 (a), which had been divided into sections using threads. Monochromatic reference images of each section were captured using the camera and lens before the filter was attached, Figures 4.3.27 (a) and (b). The MiniColorChecker Chart was placed in the same location relative to the central section, marked by the white template, for each image. The periphery of the captured image, outside of the central area, overlapped the 4 adjacent images. The filter was then attached to the front of the lens and images were taken through the 31 filter wavelength bands, an example of one image is shown in Figure 4.3.27 (c).

Figure 4.3.27 (a) Monochromatic camera image of the white template marking the tapestry section D4, (b) Monochromatic camera image of the tapestry section D4 with the MiniColorChecker Chart in the periphery, (c) Intensity image of section D4, through the 550 nm wavelength band filter

4.3.6.1 Imaging methodology

1. Place the white template in a section of the grid
2. Place the Mini ColorChecker chart at the centre of the top edge of the template
3. Move the imaging system into the correct position so that the template is in the centre of the capture area
4. Set-up the light diffusing surround and the black-out curtain around the imaging area

5. Ensure the imaging system is level using the spirit level attached to the boom and that the camera is vertically aligned. Adjust position of imaging system if necessary
6. Ensure the lamps have been switched on for at least 30 minutes and are stable
7. Ensure the filter LCD is clear and it is warmed up to a temperature of around 20°C
8. Perform dark frame subtraction on the camera
9. Image the grid and white template without the filter, for 20 ms exposure
10. Remove the grid and template
11. Image the tapestry section with the Mini ColorChecker in the scene, without the filter, for 20 ms exposure
12. Attach the filter to the imaging system
13. Perform dark frame subtraction on the camera
14. Capture 31 intensity images at each 10 nm interval from 400 nm to 700 nm at exposure times stated in Table 4.3.4

Table 4.3.4 Exposure times for each of the hyperspectral images (seconds)

Wavelength (nm)	Exposure time (s)	**Wavelength (nm)**	Exposure time (s)	**Wavelength (nm)**	Exposure time (s)
400	180	**500**	2.399	**600**	2.152
410	153	**510**	2.399	**610**	0.909
420	45	**520**	2.399	**620**	1.590
430	13	**530**	2.251	**630**	3.732
440	5	**540**	0.386	**640**	9
450	5	**550**	0.431	**650**	15
460	3.629	**560**	2.576	**660**	26
470	3.385	**570**	3.282	**670**	52
480	2.742	**580**	1.479	**680**	87
490	1.519	**590**	1.570	**690**	139
				700	180

4.3.6.2 Test imaging of standard targets

The X-Rite Digital Colorchecker SG was imaged using the hyperspectral imaging system. The 31 intensity images of the X-Rite Digital ColorChecker SG chart were

loaded into MATLAB. The raw pixel values at one of the 2048 x 2048 pixel locations, for each of the 31 images, and therefore wavelength bands, were compiled into a spectral curve, shown in Figure 4.3.28.

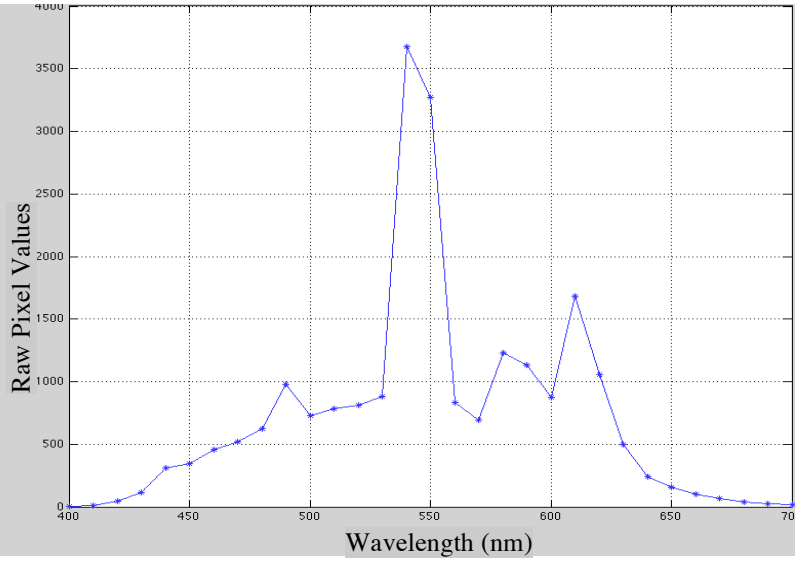

Figure 4.3.28 Reconstructed spectra for pixel location (200, 200) of X-Rite Digital ColorChecker SG (raw pixel values)

The raw pixel values were normalised using the spectra of the white point in the image, determined by calculating the maximum pixel value in each wavelength band. The relative reflectance spectra were reconstructed for each pixel, one of which is shown in Figure 4.3.29. The low responses at the short and long ends of the spectra are attributed to the low transmission of the filter that was reported in section 4.3.4.5.

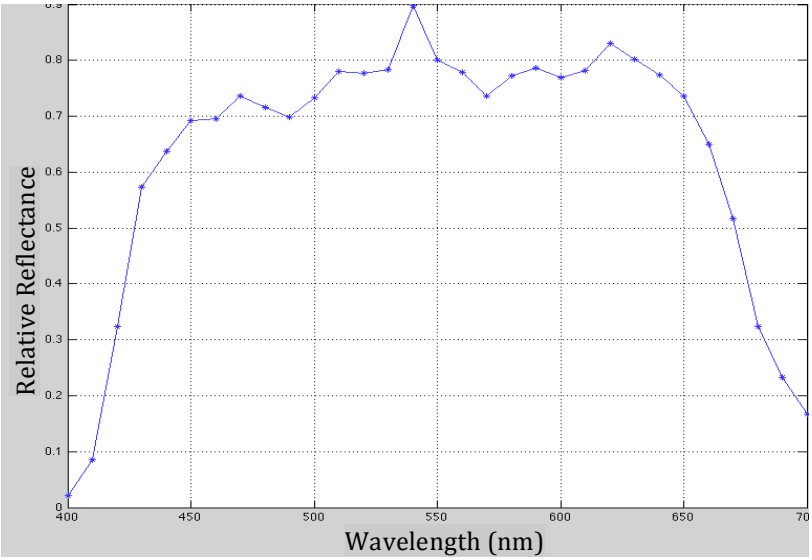

Figure 4.3.29 Reconstructed relative reflectance spectra for pixel location (200, 200) of X-Rite Digital ColorChecker SG (weighted by white point)

The reflectance data was converted to calibrated XYZ values and then to CIELAB colour coordinates. The reflectance data can be used to render images under different light sources, the reconstructed hyperspectral images in D65 (using the 1964 10° observer) and D50 (with the 1931 2° observer) are shown in Figures 4.3.30 and 4.3.31 respectively.

Figure 4.3.30 Reconstructed hyperspectral image of X-Rite Digital ColorChecker SG under D65 illuminant with 1964 standard observer

Figure 4.3.31 Reconstructed hyperspectral image of X-Rite Digital ColorChecker SG under D50 illuminant with 1931 standard observer

The performance of the hyperspectal imaging system was quantified by comparing the colour coordinates of the 140 patches of the ColorChecker SG to the standard values given by the manufacturer (under D50 2 Degree) and to SF600 measurements. This gave an average ΔE^*_{ab} value of 2.17 when a 4^{th} order polynomial transform was used.

4.3.6.3 Imaging the front of The Oath and Departure of Eliezer

The imaging methodology described in section 4.3.6.1 was used to image 170 overlapping sections of *The Oath and Departure of Eliezer*. Each of the 31 intensity images that were collected had the MiniColorChecker chart in a constant location in the periphery of the image, outside of the central 50 cm x 50 cm region. The white tile of the chart was taken as the white point in the image and used to normalise the raw pixel values to relative reflectance values. The MiniColorChecker chart was also used to normalise the reconstructed hyperspectral images of the 170 sections to one another. The overlapping areas between the sections were analysed for correlation and the images were mosaiced together.

The reconstructed hyperspectral image under illuminant D65 10 Degree, is shown in Figure 4.3.32 (a) with a compact camera image shown in Figure 4.3.32 (b) as a comparison.

Figure 4.3.32 (a) Reconstructed hyperspectral image of section D4 of *The Oath & Departure of Eliezer* (b) compact camera image of the same section of *The Oath & Departure of Eliezer*

4.3.6.4 Imaging the reverse of The Oath and Departure of Eliezer

Hyperspectral imaging of 6 sections of the reverse of the tapestry was performed, the sections chosen represented a range of features of the tapestry design including areas of metallic thread, areas containing different dyes, especially dyes that exhibit high levels of photo-fading, and sections of the highly detailed borders. The sections of the reverse corresponded to sections of the front so that comparisons of the reconstructed hyperspectral images could be made and colour differences

calculated. These images will also act as a digital archive that can be accessed in the future and analysed for further degradation. For this reason, the raw data collected by the imaging system should be retained so that the data will be compatible with future improvements in image analysis techniques and spectral reconstruction methods, which will no doubt improve the performance of this imaging system.

4.3.7 Conclusions

This chapter outlines the development, calibration and evaluation of a hyperspectral imaging system suitable for collecting both the spectral and spatial information of a historic tapestry.

The digital conservation of a colorimetrically accurate image of *The Oath and Departure of Eliezer* tapestry has produced an archive of images that contain colour information at every pixel location. The tapestry was laid flat for imaging and sectioned into regions of size 50cm by 50cm. A set of 170 sections of the front of the tapestry and 6 areas of the reverse were imaged at a wavelength resolution of 10 nm over a wavelength range of 400 – 700 nm to produce 31 dimensional hyperspectral images. Prior to image capture an X-Rite White Balance Card was placed in the centre of each section and imaged. Each section was also imaged with a mini X-Rite ColorChecker Chart in the periphery. The spatial uniformity of the light source was corrected by weighting the tapestry images by the corresponding intensity values of the White Balance Card in each dimension. The relative reflectance spectra at each pixel location were reconstructed and this data was converted to CIELAB colour coordinates. The imaging system was found to reconstruct the reflectance spectra of each pixel in the X-Rite ColorChecker Chart to an accuracy of approximately 2 ΔE^*_{ab} units, which is comparable to similar multispectral systems that have been developed.

This unique image archive of the tapestry allows the fine details of the tapestry to be studied by conservators from anywhere in the world with the knowledge that the colour is represented accurately. In addition the images of the reverse enable a new understanding of the original colours of the tapestry and the magnificence of the untarnished metallic threads. A simulation of how the tapestry would have originally appeared under historically relevant light sources could now be

generated. One advantage of capturing spectral data of the tapestry is that it could be used to reinterpret the tapestry and its history in further novel ways.

This project has advanced knowledge in the conservation of historic items through the application of scientific grade hyperspectral imaging systems and methodologies, generating precise spectral reflectance data of a textiles surface. The recording of the colour and condition of the tapestry at a specific moment during its lifetime will allow the further study of the lifecycle of the colorants used in the tapestry. Any changes in the materials can be recorded and are relatable to the time of capture, which may help to improve the conservation practices at Hampton Court Palace.

The system was developed within a set of physical constraints and requirements specified by the conservators at Hampton Court Palace for digitisation of such an important piece of cultural heritage. The imaging methodology was developed in a complex environment where the temperature, humidity and light conditions were subject to variability. The imaging system had to be portable as the tapestry was imaged in sections; in addition the components of the imaging system were to be non-destructive to the fragile tapestry. As such the methodology used for this project can be reproduced in many environments where historic collections are commonly on display.

5 Digital Recolouration

The aim of the digital recolouration of *The Oath and Departure of Eliezer* was to restore the tapestry to its original appearance using entirely non-invasive methods. The virtual restoration has integrated techniques from textile conservation, colour science and imaging science to simulate a realistic impression of the tapestry appearance during the reign of Henry VIII.

'Henry VIII's Tapestries Revealed' was launched in 2009 as part of Historic Royal Palaces' celebrations of the 500th anniversary of Henry VIII's accession to the throne. The show was conceived to raise public awareness of the important tapestry collections at Hampton Court Palace, their fragile state and the essential conservation work that is carried out to ensure their survival. The show involved projecting a recoloured calibrated image of *The Oath and Departure of Eliezer* onto the tapestry as it hung in the light controlled environment of The Queen's Guard Chamber of the palace. This digital restoration gave the visitors an impression of how the tapestry would have originally appeared before photo-fading of the dyes and tarnishing of metallic threads had occurred.

In order to determine the original colour appearance a variety of methods were used including colour measurement of the front and reverse of the tapestry and colour measurement of a set of model dyed fabrics and metallic threads both before and after accelerated photo-ageing, which was reported in Chapter 3. The reverse of the tapestry has suffered relatively low levels of photo-fading in comparison to the front due to the protection from light exposure by a lining material. Therefore the colours of the reverse are assumed to be representative of the original dye colours. Visual inspection of the tapestry determined the locations of areas of different dyes so that the full range of dye colours were measured using the PR-655 telespectroradiometer. Measurements of the progressive ageing of the model tapestry samples produced a dataset of fading profiles for each dye that was matched to the fading profiles of coloured regions of the tapestry.

Recolouration of an image of the tapestry involved segmenting the image into regions defined by the dye with which they were coloured. For each of these

regions there was a range of colour coordinates, resulting from texture of the woven material and shading in the design. This distribution was translated within colour space to a new range of coordinates that represented the original colour of the dye. Each natural dye demonstrates a unique fading profile that has led to a disparity in the colour balance of the tapestry design. This method of transforming each coloured region separately allows the colour ratios of the original design to be restored. The effect of the metallic threads was generated using texture mapping from areas of untarnished gold and silver threads on the tapestry reverse.

The recolouration process was developed during a pilot study on the *Lion* tapestry, a smaller tapestry fragment that exhibits similar photo-fading to *The Oath and Departure of Eliezer*. The dyed areas on the front of the *Lion* tapestry were recoloured using the RGB colour coordinates of the corresponding areas on an image of the reverse.

An image of the tapestry hanging in place in the Queen's Guard Chamber was captured using a calibrated Nikon D300 digital camera from a point as close to the projector's viewing angle as possible. The camera image size was 4288 x 2848 pixels. Deformation of this image was performed to account for the angle of imaging and projection. The final projected image size was 1920 x 1080 pixels. This image was modified using a combination of automated and interactive global and local image processing techniques so that the original colours of the dyed areas were reproduced. To achieve the effective recolouration on the tapestry surface the image was manipulated, taking into account the remaining colour and texture present on the tapestry to create a final image which when projected onto the tapestry produced the virtual restoration. The completed image was then modified by the appropriate linear transform for projection.

The resulting projected image forms the basis of the *Tapestries Revealed* show, which features a narrative explaining the history and significance of the tapestry, the role of the individual characters in the design and a virtual fading demonstration of the tapestry materials over its lifetime.

Recent research into digital restoration of cultural heritage has been focused on paintings (Berns, 2005. Cotte & Dupraz, 2006. Zhao *et al.,* 2008). Colour changes in pigments over time include fading, darkening or staining and the yellowing of varnish can result in dramatic colour changes in a painting. Colour measurements of areas of the painting that have been protected from degradation give an impression of the original colours. Spectral measurements of the painting can be used for pigment mapping whereby the constituent pigments in a coloured area are identified by spectral analysis (Zhao, 2008). When preserved pigments are not available, reproduction of the artist's materials provides a dataset of optical properties of the pigments. The spatial distribution of pigments in the paintings was determined from image segmentation using Photoshop (Berns, 2005) or clustering algorithms (Zhao, 2008) and the optical properties of the areas of pigment that had suffered colour changes were adjusted to those of the unaged pigments to replicate the original colour appearance. In addition to pigment recolouration, the removal of the yellowed varnish from the *Mona Lisa* was simulated by Cotte and Dupraz (2006).

5.1 Colour measurement of the tapestry

The tapestry was removed from display, laid out flat in the textile wash facility and the lining removed for the first time in around 70 years allowing the colourful reverse to be measured. Colour measurements were taken of the front and reverse of the tapestry using a portable Photo Research PR-655 telespectroradiometer so that no physical sampling of the tapestry was necessary. Measurements were taken of corresponding areas on the front and reverse to build up a database of the fading profiles of each of the dyes used in the tapestry.

1. Measurements were taken of the tapestry in the wash building using the imaging set-up described in Chapter 4
2. The tapestry was illuminated by both lamps which had been switched on for at least 30 minutes prior to measuring
3. Spectral data was collected by the PR-655 that was pointed directly at the tapestry surface, from a distance of 50 cm
4. Measurements were taken of 35 corresponding areas on the front and reverse of the tapestry and 10 additional reverse areas

5. Readings were taken for luminance ($cd.m^{-2}$), CIE x and y values and CCT from the PR-655 display
6. Spectral data was downloaded from the PR-655

Results are recorded in section 5.3.2

Measurements of the 24 patches of the X-Rite ColorChecker Chart and the X-Rite White Balance Card were taken using the same method as described above. The PR-655 results under the studio lamps were calibrated using Spectraflash 600 (SF600) measurements of the X-Rite ColorChecker Chart. A transform matrix was established for the conversion between the two instruments that was implemented on the PR-655 data for the tapestry front and reverse. This matrix converted the raw XYZ data to calibrated XYZ to L*a*b* values so that measurements from the PR-655 could be compared quantitatively with the dye colour coordinates measured using the SF600. This comparison was performed in CIELAB coordinates.

The entire front and areas of the reverse were imaged using a calibrated digital camera (Nikon D300), including areas of untarnished metallic thread on the reverse.

5.2 Imaging the tapestry

A high definition image of the tapestry hanging in place in the Queen's Guard Chamber was captured using a calibrated Nikon D300 digital RGB camera from a point as close to the projector's viewing angle as possible. Deformation of this image was performed to account for the angle of imaging and projection. The final image size was 1920x1080 pixels, which was determined by the projector resolution.

This image was processed using clustering algorithms in MATLAB to produce a series of masks that located each individual dye colour in the image. Although this procedure was automated some of the masks needed to be completed by hand. The spatial and colorimetric characteristics (in each plane of the CIELAB colour space) of pixel populations sampled from the reverse of the tapestry were then mapped onto the appropriately masked area of the image of the front of the tapestry. This

effectively shifted the L*, C* and h* distributions of individual colours to their unfaded counterparts. This image was manipulated, taking into account the remaining colour present on the tapestry to create a final image that when projected onto the tapestry produced the recoloured effect. The effect of the metallic threads was generated using texture mapping from detailed images of the tapestry reverse.

5.3 Production of recoloured images

5.3.1 Fading profiles of model dyed tapestry samples

The Datacolor SF600 spectrophotometer was used to measure the reflectance spectra of the dyed fabric samples before ageing and after 100 hours, 300 hours and 500 hours of photo-ageing. The samples were measured using a small aperture, Ultraviolet (UV) and specular excluded. Results shown in Table 5.3.1 are given as CIELAB values with ΔE^*_{ab} colour differences calculated using the dyed unaged fabric as the standard and the aged samples (after 100, 300 and 500 hours light exposure) as the batches. Cylindrical coordinates of colour difference in the CIELAB colour space, ΔL^*_{ab}, ΔC^*_{ab}, ΔH^*_{ab}, are quoted for the 500 hour aged samples. A negative ΔL^*_{ab} value signifies that the aged sample is darker than the original dyed colour, however, many of the dyes exhibit photo-fading so that the aged sample is lighter than the unaged. In fact, only the Undyed Silk sample and S Oakgall have darkened while the largest photo-fading effect was seen on W Brazil. A negative ΔC^*_{ab} value signifies that the aged sample has a lower chroma than the unaged sample, which indicates photo-fading, the strongest example of this effect is seen on W Weld. Undyed Wool and Silk samples have positive values due to the increase in chroma caused by photo-yellowing. Note the small shift in chroma of the W Brazil sample which exhibits the strongest photo-fading effect; this is due to the shift from a red colour to a yellow colour close to the chromatic coordinates of W Alum, which is the mordant used for dyeing W Brazil. This fading process is confirmed by the large value of ΔH^*_{ab}. Another notable sample is the fading profile of W Woad, which exhibits no change in hue, a very small decrease in chroma and only slight bleaching after 500 hours of photo-ageing. This confirms the light fastness of the woad dye.

Table 5.3.1 Colour difference of photo faded model dyed tapestry samples

	Unaged			100 hours				300 hours				500 hours						
Sample	**L***	**a***	**b***	**L***	**a***	**b***	**ΔE***	**L***	**a***	**b***	**ΔE***	**L***	**a***	**b***	**ΔE***	**ΔL***	**ΔC***	**ΔH***
W Undyed	77.9	-0.2	12.0	80.7	-0.6	12.7	2.9	81.1	-0.9	14.7	4.3	80.7	-0.7	14.6	3.8	2.7	2.63	0.47
W Alum	84.2	-0.2	12.7	86.4	-0.5	11.1	2.7	84.9	-1.3	15.1	2.8	84.9	-1.4	17.3	4.8	0.7	4.65	0.95
W Alder	54.8	5.7	23.4	60.7	5.6	24.1	5.9	64.2	4.6	23.4	9.5	67.2	3.7	22.1	12.6	12.4	-1.66	1.71
W Oakgall	63.8	2.9	23.5	62.8	5.0	30.2	7.1	64.3	4.5	27.9	4.7	66.5	4.0	25.9	3.8	2.7	2.52	0.72
W Iron	25.8	1.4	2.1	29.7	1.6	5.0	4.8	29.3	1.4	5.6	4.9	30.1	0.9	6.3	6.0	4.3	3.85	1.70
W Copper	32.2	1.1	12.6	36.8	1.2	15.3	5.2	37.8	0.9	17.0	7.1	40.9	0.6	17.9	10.2	8.7	5.22	0.75
W Madder	33.9	31.5	21.9	40.6	31.0	21.7	6.7	46.4	28.1	20.9	13.0	50.0	25.5	19.4	17.4	16.1	-6.30	1.51
W Madder2	39.6	23.6	22.9	46.1	21.4	22.9	6.9	52.5	15.9	20.9	15.1	55.2	13.8	20.5	18.6	15.6	-8.14	5.94
W Brazil	48.3	21.9	7.9	65.9	9.3	18.0	23.9	70.8	5.9	20.0	30.1	74.5	3.9	20.4	34.1	26.2	-2.51	21.74
W Coch	41.1	37.3	9.4	47.1	28.7	5.5	11.2	53.9	20.9	7.1	20.9	60.3	15.0	8.7	29.4	19.1	-21.2	7.18
W Weld	67.8	3.1	63.0	71.3	2.6	43.3	20.1	74.2	1.7	33.8	30.0	75.2	1.7	28.9	34.9	7.4	-34.1	0.45
W Gweed	58.3	1.8	40.1	63.1	2.1	32.0	9.4	66.2	1.7	27.6	14.8	68.6	1.5	23.2	19.8	10.3	-16.9	0.54
W Woad	28.0	-3.4	-13.8	31.4	-3.5	-13.4	3.4	29.3	-3.2	-14.4	1.4	29.5	-3.5	-14.5	1.6	1.5	0.66	0.00
S Undyed	84.7	0.8	8.4	84.0	0.6	11.9	3.6	83.2	0.8	16.3	8.1	82.9	1.2	18.3	10.1	-1.8	9.98	0.42
S Oakgall	72.8	2.4	18.4	68.9	3.6	27.1	9.6	70.6	3.4	27.2	9.2	68.9	4.1	27.2	9.8	-4.0	8.93	0.41
S Iron	20.9	1.1	-1.2	21.5	0.9	-0.9	0.7	21.3	1.0	-0.2	1.1	21.3	0.6	0.6	1.9	0.3	-0.82	1.68
S Brazil	56.2	15.5	0.9	68.2	5.9	14.9	20.8	73.4	3.8	16.5	26.0	76.1	2.6	16.7	28.5	19.9	1.30	20.4
S Madder	60.9	25.2	12.0	66.3	19.3	12.6	8.0	71.0	13.9	14.3	15.3	72.3	12.5	15.5	17.4	11.4	-8.03	10.4
S Coch	43.2	30.2	10.4	44.0	25.1	7.2	6.1	47.8	20.0	7.4	11.6	48.8	17.4	7.9	14.2	5.6	-12.8	2.27
S Weld	72.3	-3.0	51.5	71.2	1.1	42.3	10.1	73.0	1.0	33.9	18.0	74.2	1.1	30.8	21.1	1.9	-20.7	3.72
S Gweed	68.7	-0.8	41.8	69.7	1.8	32.7	9.5	71.9	1.9	27.2	15.1	72.5	2.1	24.3	18.1	3.8	-17.4	3.39
S Woad	41.7	-7.3	-9.1	44.2	-7.8	-8.7	2.5	48.0	-8.8	-6.0	7.2	49.7	-8.1	-4.7	9.1	8.0	-2.32	3.80

5.3.2 Fading profiles of coloured areas on the tapestry

The results of colour measurements of areas on the front and reverse of the tapestry, measured using the PR-655 and converted to D65_64, are given in Tables 5.3.2 and 5.3.3. Visual inspection of the reverse of the tapestry led to additional readings being taken of areas that were not measured on the front due to the presence of more unique colours than were predicted. The colour differences between the areas on the front and reverse are quoted as CIELAB colour space ΔL^*_{ab}, ΔC^*_{ab}, ΔH^*_{ab}, values. The dyed areas exhibit both lightening and darkening effects, the most significant of these is the change in lightness of the 'Tarnished background' sample of -36 ΔL^*_{ab}. This sample is an area of gold metallic thread, with a bright yellow colour, on the reverse that degrades to a darker grey, with a ΔC^*_{ab} value of -21.

Table 5.3.2 CIELAB values and colour difference of areas on the front and reverse of the tapestry

		Front			Reverse			Reverse - Front					
Sample		**L***	**a***	**b***	**L***	**a***	**b***	**ΔL***	**Δa***	**Δb***	**ΔE***	**ΔC***	**ΔH***
1	Blue Border	23.27	-3.74	-4.31	11.41	0.89	-2.67	11.86	-4.63	-1.64	12.83	2.90	3.97
2	Pinky Background	42.06	6.10	14.48	27.60	14.05	11.15	14.46	-7.95	3.33	16.84	-2.22	8.33
3	White flowers	52.39	5.33	15.63	39.50	2.19	14.87	12.89	3.14	0.77	13.29	1.49	2.87
4	Grey flower	39.34	2.17	12.24	31.65	1.14	9.19	7.70	1.03	3.05	8.34	3.17	0.56
5	Yellow leaf	41.07	4.97	20.22	32.03	3.31	19.65	9.04	1.65	0.57	9.21	0.89	1.50
6	Pale pinky border	44.84	5.68	12.51	33.73	3.47	13.63	11.11	2.21	-1.12	11.39	-0.33	2.46
7	Beige in geo border	32.66	3.28	11.59	26.07	6.67	16.90	6.59	-3.39	-5.31	9.12	-6.12	1.48
8	Rusty red	24.23	14.24	11.04	17.18	16.53	11.15	7.05	-2.29	-0.11	7.41	-1.92	1.25
9	Orange/brown	17.41	9.79	9.97	36.86	21.25	23.22	-19.44	-11.46	-13.25	26.17	-17.51	0.73
10	Sandy border	34.00	3.59	12.15	45.52	5.17	15.07	-11.52	-1.59	-2.92	11.99	-3.27	0.62
11	Dk blue shadow	18.67	-1.22	-2.37	22.34	2.18	3.31	-3.67	-3.40	-5.69	7.57	-1.30	6.50
12	Green foliage	35.24	2.56	13.48	56.58	4.00	27.52	-21.34	-1.44	-14.05	25.59	-14.09	0.85
13	Dark red-brown	24.48	9.58	10.12	24.51	9.83	8.61	-0.03	-0.25	1.51	1.53	0.87	1.26
14	Tarnished background	29.99	2.47	7.51	66.09	8.56	27.75	-36.10	-6.10	-20.24	41.84	-21.14	0.27
15	Mid green (lion)	31.99	2.71	15.60	35.06	8.41	25.76	-3.07	-5.70	-10.17	12.05	-11.27	2.97
16	Dull green (lion)	27.27	3.10	13.17	31.30	5.67	19.60	-4.03	-2.58	-6.43	8.01	-6.87	0.84
17	Light brown (pillar)	27.27	6.34	11.56	31.76	22.13	15.26	-4.49	-15.79	-3.70	16.83	-13.69	8.69
18	Raspberry red (dress)	20.63	16.30	6.12	17.96	15.69	6.80	2.67	0.61	-0.68	2.82	0.31	0.86
19	Beige (dress)	39.43	-0.42	10.28	51.07	2.21	16.10	-11.64	-2.62	-5.81	13.28	-5.96	2.28
20	Pale blue (dress)	39.75	-1.87	8.09	57.24	-0.15	14.64	-17.49	-1.72	-6.56	18.76	-6.34	2.39
21	Pale green leaf (headdress)	33.50	-0.84	12.80	41.17	1.52	20.06	-7.67	-2.36	-7.26	10.82	-7.29	2.27
22	Light pink (cornice)	31.88	4.69	9.35	54.01	28.98	28.60	-22.13	-24.30	-19.25	38.09	-30.26	6.72
23	Dark grey	29.11	0.52	7.98	45.01	8.16	20.53	-15.90	-7.64	-12.55	21.65	-14.10	4.14
24	Deep orange	18.19	6.64	8.61	33.52	15.31	17.74	-15.33	-8.67	-9.13	19.84	-12.56	0.89
25	Light blue	29.66	-2.57	1.54	38.20	2.46	9.62	-8.54	-5.03	-8.09	12.79	-6.94	6.52
26	Light maroon	21.65	7.76	7.42	39.85	26.48	25.34	-18.20	-18.72	-17.92	31.67	-25.92	0.01
27	Mid Maroon	16.40	7.34	5.44	24.58	15.80	14.32	-8.17	-8.46	-8.88	14.74	-12.19	1.37
28	Dark maroon	13.11	3.32	1.06	24.89	7.29	8.67	-11.78	-3.98	-7.61	14.58	-7.85	3.48
29	Mid Blue	21.94	-4.36	-6.40	35.67	-4.81	-3.97	-13.73	0.45	-2.44	13.95	1.51	1.96
30	Orange/brown	23.03	6.97	9.42	25.01	11.22	12.91	-1.98	-4.25	-3.49	5.84	-5.38	1.11
31	Metallic gold	36.50	-0.16	12.41	46.50	1.63	20.96	-10.00	-1.80	-8.55	13.28	-8.61	1.47
32	Dark brown-purple	10.92	1.45	-1.33	17.37	1.75	0.79	-6.45	-0.31	-2.12	6.79	0.04	2.14
33	Deep orange	20.56	11.26	10.18	34.52	27.73	20.01	-13.96	-16.47	-9.83	23.73	-19.02	2.51
34	Yellow/cream	46.92	6.69	22.59	63.04	16.70	47.84	-16.12	-10.01	-25.25	31.58	-27.11	1.65
35	Light cream	65.80	8.49	20.62	51.63	5.22	20.93	14.17	3.26	-0.30	14.54	0.73	3.20

Table 5.3.3 CIELAB values of areas on the reverse of the tapestry

Sample		L*	a*	b*
36	Dark green	18.23	-3.44	4.95
37	Brown	26.82	17.52	17.63
38	Light orange	26.07	9.73	17.14
39	Dark red	14.90	11.97	7.58
40	Red	20.90	20.47	13.50
41	Dusky pink	22.30	11.40	9.53
42	Light blue	34.68	-2.87	5.00
43	Yellow	43.52	2.19	27.35
44	Dark blue	12.48	-0.98	-4.71
45	Sandy	34.90	7.83	21.80

The CIE chromaticity diagram (illuminant D65, 10 degree) is shown in Figure 5.3.1 with the coordinates of the dyed areas on the tapestry front and reverse plotted. The distribution of the colours of the front is smaller than that of the reverse with the deficiency being predominantly in the orange/red region. This correlates with the colour differences noticeable upon visual inspection of the tapestry; the blue shades are still present on the front while a large portion of the red, pink, orange and yellow shades have been lost.

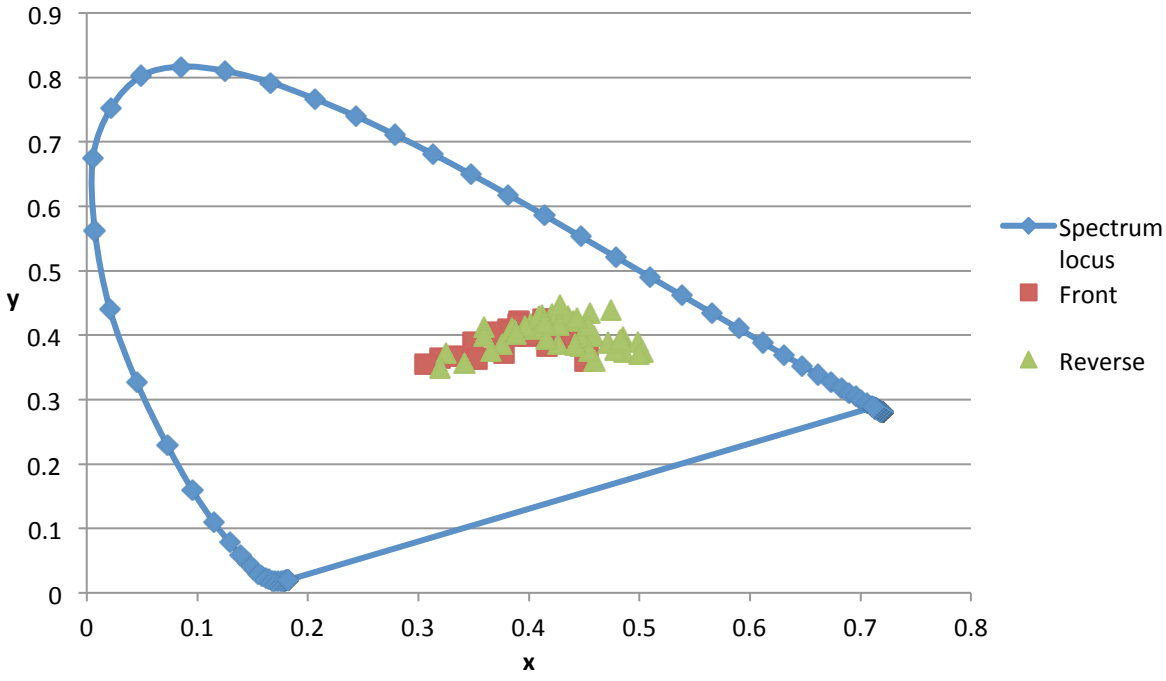

Figure 5.3.1 Chromaticity diagram of the dyed areas on the front and reverse of the tapestry

5.3.3 Matching the tapestry areas to model dyed tapestry samples

The areas of colour on the tapestry were matched to the natural dyes used for the model tapestry samples by comparing the colour difference between the front and

reverse to the gradual fading profiles of the dyes. This information was used in the recolouration process to identify distinct areas of dyes and to shift the colour distribution information of these areas towards the colours of the dyes. It was particularly important to identify those areas on the front of the tapestry that were completely photo faded and to recolour them according to the colour data of the corresponding dye.

The MATLAB function kNearestNeighbors.m was utilised for classification of the areas on the tapestry. The model dyed tapestry a* and b* colour coordinates were assigned as cluster centres and the function determined the nearest cluster for each of the dyed areas of the tapestry measured using the PR-655. The function returned the 3 nearest neighbours and the most suitable match was verified based on visual inspection of the tapestry. This method was used for matching the reverse areas to the unaged samples and the front areas to the 500 hour aged samples, then the classification that best represented the fading profiles of the dyes was selected. The lightness information was excluded from the matching process as it is the chromatic element of the tapestry areas that indicates the dye used. The lightness information is contained in the shading and texture of the dyed regions that forms the distribution of pixel values in the masks. The shape of the distribution is retained in the recolouration process while the location of the distribution in colour space is transformed. This ensures that the shading and texture of the dyed areas are preserved, which results in a natural recolouration effect.

5.3.4 Pilot study: Recolouration of *Lion* tapestry

The *Lion* tapestry is a fragment of a tapestry, which was produced around the same time as the *Abraham* set that was provided by Historic Royal Palaces for a pilot study of the hyperspectral imaging system and digital recolouration. The small size of the tapestry meant it could be imaged in the conservation studio at Hampton Court Palace. The tapestry has suffered similar levels of photo-fading as the *Abraham* tapestries whereby some dyes have remained fast and others have faded completely to a neutral shade, which makes it a suitable representative for the pilot study. One notable exception is that the *Lion* tapestry does not contain any metallic threads whereas the *Abraham* tapestries contain large areas of metallic threads that

have tarnished. Images of the front and reverse of the *Lion* tapestry are shown in Figure 5.3.2.

Figure 5.3.2 Images of the front and reverse of the *Lion* tapestry used in the recolouration pilot study

The methods for identifying the regions of different dyes on the image of the front of the tapestry, and recolouring them, have been tested and optimised during this pilot study and were subsequently applied to *The Oath and Departure of Eliezer* for the 'Tapestries Revealed' show. The digitally recoloured image of the *Lion* tapestry was printed onto fabric at full scale to create a replica of the original tapestry fragment that was employed at Hampton Court Palace to educate the visitors and stimulate interest in the upcoming exhibition.

The recolouration of an image of the *Lion* tapestry was achieved by segmenting the image into areas defined by the dyes used to colour them and then recolouring these areas with the shade of the corresponding areas on an image of the reverse of the tapestry. The image segmentation was performed primarily in MATLAB and it involved writing new MATLAB scripts and implementing existing functions of the software in order to successfully segment the image by dyes. The different methods used to achieve this result are described in the following sections.

5.3.4.1 Methods of identifying pixel populations, clustering and producing masks

The segmentation of the image by coloured regions involved obtaining a set of sample colours, identified by their pixel states in RGB or CIELAB colour space, and then determining which of these sample colours best represents each pixel in the image. Identifying each unique pixel state and its frequency in the image was the

first operation in the spatial segmentation process. The texture of the woven material results in many different pixel states in areas of similar colour in the image, which leads to a large number of unique pixel states being identified that all fall into a small range of actual shades. Filtering some of the texture out of the image can reduce this number of unique pixel states. The MATLAB function **`medfilt2`** is a 2-dimensional median filter where the value of a pixel is replaced by the median value calculated over an M x N neighbourhood surrounding the pixel. This function was implemented on the image of the front of the *Lion* tapestry, using different sized neighbourhoods, 3 x 3, 5 x 5 and 7 x 7, to assess the affect of filtering on image segmentation. The results of median filtering were that the texture of the weaving in the image was reduced and therefore the number of unique pixel states was lowered. However, this operation leads to blurring at the edges of different coloured areas and therefore loss of detail within the image. Median filtering was not found to improve the overall results of recolouration of the *Lion* tapestry.

Segmentation of monochromatic images is generally based on either partitioning the image by abrupt changes in intensity values i.e. edges, or by partitioning the image by regions of similar intensity values (Gonzalez *et al* 2004). For the segmentation of colour images, the intensity values in each and all planes of the colour space are considered. Edges are detected by finding discontinuities in intensity values. The MATLAB function **`edge`** finds places in an image where the intensity values change rapidly by analysing the gradient wherein the gradient is zero in areas of constant intensity. If the gradient is greater than a specified threshold value, the edge detection returns a value of 1 at that location in the outputted binary image. The threshold value is specified by the user or can be determined automatically by the function. The *Canny* method of edge detection uses two threshold values to detect strong and weak edges, and includes the weak edges only if they are connected to strong edges.

The *Sobel* and *Canny* methods of edge detection were performed on an RGB image of the front of the *Lion* tapestry and on the image after it had been converted to CIELAB colour space. The colourspace transformation was completed using the **`makecform`** and **`applycform`** functions with transform '**`srgb2lab`**'.

In the following section the function **edge** was applied to each plane of the image and the three resulting binary images were compiled into a single logical array with 1s where edges have been detected and 0s elsewhere. This was achieved by adding together the three edge images, dividing by 3 and then converting the resulting image to a logical array wherein all pixels that had been marked as an edge in any of the three planes are given a value of 1, with 0s elsewhere. The following commands were implemented on each of the edge images shown in this section; however, the process is not discussed at each stage to improve readability:

```
>> flat=(edge_red + edge_green + edge_blue) / 3;
>> edges = im2bw(flat, 0.1);
```

Figure 5.3.3 shows the edge image obtained using the default syntax for the Sobel option whereby the threshold value is determined automatically.

```
>> [sobel1, t] = edge(lion, 'sobel');
t =   0.0967 (Red)
      0.0930 (Green)
      0.0826 (Blue)
```

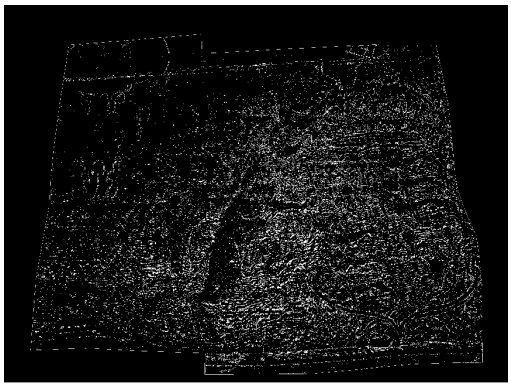

Figure 5.3.3 Result of Sobel edge detection on image of front of *Lion* tapestry in RGB colour space with the threshold determined automatically

As Figure 5.3.3 shows, the principal edges of the image have been detected as well as much of the texture of the woven material. Filtering the original image to reduce some of the texture can improve the edge detection result. Median filtering was implemented on the three planes of the original image using function `medfilt2` with a 5 x 5 neighbourhood.

```
>> for i =1:3
```

```
>> Filter(:,:,i)=medfilt2(lion(:,:,i), [5 5]);
>> end
```

Sobel edge detection was repeated using the default syntax to obtain the threshold values tred = 0.0436, tgreen = 0.0401 and tblue = 0.0341. Further edge detection was performed using a variety of threshold values to obtain a clean edge image. Figure 5.3.4 was generated from the edge images obtained using the following commands:

```
>> sobel6(:,:,1) = edge(Filter(:,:,1), 'sobel', 0.050);
>> sobel6(:,:,2) = edge(Filter(:,:,2), 'sobel', 0.045);
>> sobel6(:,:,3) = edge(Filter(:,:,3), 'sobel', 0.040);
```

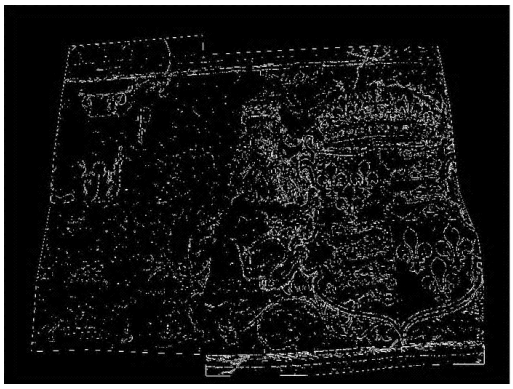

Figure 5.3.4 Result of Sobel edge detection on a 5 x 5 median filtered image of front of *Lion* tapestry in RGB colour space with specified threshold values

Figure 5.3.4 shows the predominant edges around the outside of the tapestry and many of the principal features in the right hand side of the tapestry image, however, much of the background pattern has not been detected and this edge image would not be adequate for segmenting the image by colour regions. Investigations into the results of Sobel edge detection on the transformed CIELAB image did not improve on the results obtained in RGB colour space.

Figure 5.3.5 shows the edge image obtained using the default syntax for the Canny option on the image of the front of the *Lion* tapestry in RGB colour space whereby the threshold values were determined automatically.

```
>> [canny1, t] = edge(lion, 'canny');
t = [0.0375 0.0938]
```

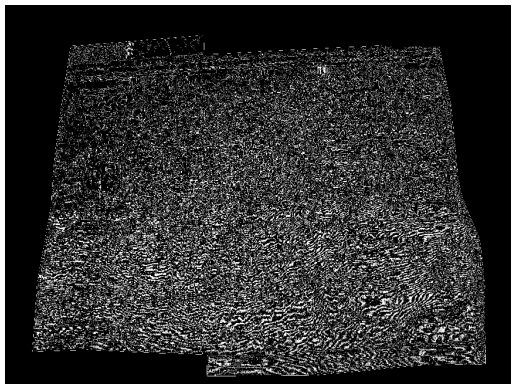

Figure 5.3.5 Result of Canny edge detection on image of front of *Lion* tapestry in RGB colour space with the thresholds determined automatically

The high and low threshold values used were the same in all three planes. The default value for the standard deviation of the smoothing filter used by the function is 1. As can be seen from Figure 5.3.5, this result does not produce the desired clean edge map. Starting with the default values for the threshold, the parameters were varied interactively with the objective of bringing out the principal features in the image, while reducing irrelevant detail as much as possible. Figure 5.3.6 shows the best edge detection result generated in RGB colour space, which was obtained using t = [0.100 0.2500] and a standard deviation of 1.5.

```
>> canny3 = edge(lion, 'canny', [0.1 0.25], 1.5);
```

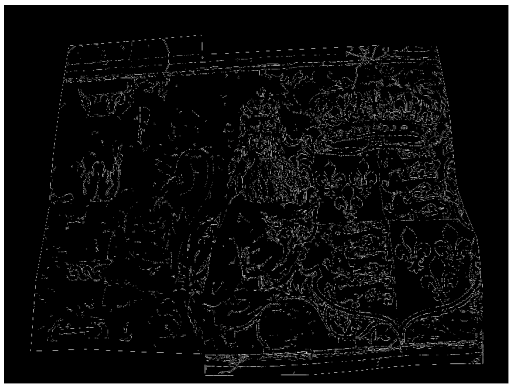

Figure 5.3.6 Result of Canny edge detection on image of front of *Lion* tapestry in RGB colour space with specified threshold and standard deviation values

As Figure 5.3.6 shows, the edge image produced in RGB colour space by the Canny method is inferior to the results obtained using the Sobel method as many of the primary features of the tapestry image have been poorly identified and most of the

detail on the left hand side of the image has not been detected. Converting the image to CIELAB and repeating Canny edge detection resulted in far superior results. The default values for the thresholds in each plane were determined by implementing the default syntax of the Canny method and found to be tL* = [0.0375 0.0938], ta* = [0.0312 0.0781] and tb* = [0.0375 0.0938]. The threshold values were varied interactively to obtain a clean edge image that highlighted the principal features of the tapestry. The best result found, which picks out much of the detail in the image including the pillar on the left hand side and the background pattern, is shown in Figure 5.3.7 and was obtained using t = [0.075 0.200] and a standard deviation of 2.2.

```
>>lab_canny6 = edge(lab_lion, 'canny', [0.075 0.2], 2.2);
```

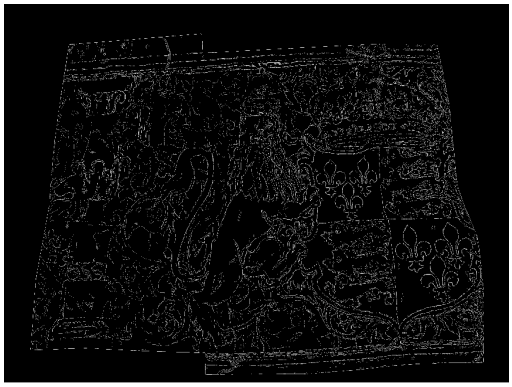

Figure 5.3.7 Result of Canny edge detection on image of front of *Lion* tapestry in CIELAB colour space with specified threshold and standard deviation values

Although this edge image successfully defines much of the details in the image, the lines formed are often fragmented and therefore do not isolate the coloured regions. Dilation of the edge image is performed in order to connect the edge lines and to improve their definition. The function **`imdilate`** is implemented with a structuring element array that consists of a horizontal and a vertical line of length 2. The following commands create the structuring element array and apply it to the best edge image generated in the previous section:

```
>> se1 = strel('line', 2, 0);
>> se2 = strel('line', 2, 90);
>> dEdges = imdilate(edges, [se1 se2]);
```

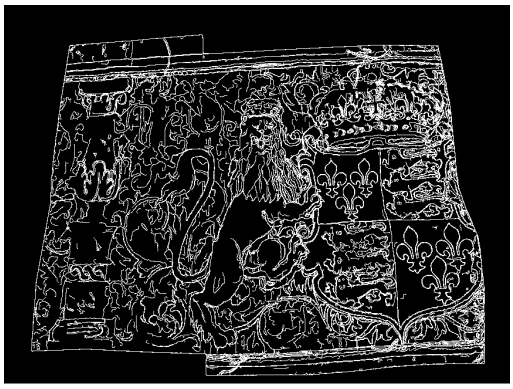

Figure 5.3.8 Result of dilating the edge image using two perpendicular linear structuring elements of length 2

Figure 5.3.9 Section of the image of the *Lion* tapestry overlaid with the dilated edge image visible as white lines

As Figure 5.3.8 shows, dilating the edge image produces continuous edge lines that are thicker and better define the separate coloured regions. Figure 5.3.9 shows a section of the *Lion* tapestry image that has been overlaid with the dilated edge image **`dEdges`** that is visible as white lines. The segmentation of different coloured regions in the background pattern on the left hand side of the image is not complete; however, the principal features of the design are very well defined. The dilated edge image has been utilised later in the pilot study to visually assess and consequently refine the masks created during image segmentation.

The creation of a set of masks that segment the image of the tapestry by coloured regions was based on locating pixels with similar sets of intensity values. The first objective was to define a set of sample colours that represent the range of different coloured regions in the image. This was carried out in one of two ways; by automatic selection based on the most frequently occurring unique pixel states; or by manual selection of a discrete number of regions of the image from which the

mean pixel values were calculated. This sample set of pixel values were defined as the centre points of clusters in the 3-D colour space around which all the other pixel states in the image were located. The process of assigning all of the pixels in the image to one of these cluster centres involved determining the cluster that was the smallest Euclidean distance from the pixel in colour space and labelling the pixel accordingly. From this information, a set of masks was produced as binary images in which pixels with similar intensity values in RGB or CIELAB colour space were grouped.

This method of image segmentation is based on the principals of k-means clustering whereby the data is partitioned into k clusters in which each data point belongs to the cluster with the nearest mean (Webb 2002). This assumes that the different colours in the image form distinct clusters in colour space and that each pixel in the image is associated with its nearest cluster. Another method of partitioning the data in colour space is to analyse the colour histogram for modes of high density and threshold the data at the valleys that separate the modes (Gonzalez *et al.,* 2004). Image segmentation by colour information alone is a global operation and can result in poor segmentation when the pixels do not form distinct clusters or the different colours in the image are similar to one another and overlap. Specification of the colours in an image by more than three components will help to distinguish the different coloured regions. Zhao (2008) segmented an image of the van Gogh painting *A Starry Night* into regions with different paint compositions. The classification was performed using k-means clustering in the six-channel camera space, which was linearly related to spectral reflectance space. Clustering based on the reconstructed spectral reflectance curves for each pixel from hyperspectral imaging is not viable due to the inhibitive computer processing power and time.

The automatic selection of the sample colours first implements a global clustering algorithm on the list of unique pixel states, starting with the most frequently occurring, which is defined as the first cluster centre. The list of unique pixel states is tested for similarity to this cluster centre if the Euclidean distance between them is less than a specified threshold. The threshold values used during the pilot study were 15 in RGB colour space and 5 in CIELAB. A solid sphere around the cluster centre with a radius equal to the threshold value defines the points that belong to

the first cluster. If the pixel state is not located within this sphere, the pixel state is defined as a new cluster centre. This process is repeated so that all unique pixel states are either accepted into an existing cluster or form a new cluster. New clusters are formed until a specified maximum number of clusters are reached or until the number of pixels in a new cluster falls below a specified level. The values of the cluster centres define the set of sample colours, which should represent the full range of different coloured regions in the image.

Manually sampling by visually inspecting the image and then selecting regions of different colours ensures that the set of sample colours is representative of the range of colours on the tapestry. A discrete number of colours were sampled using the function **`roipoly`** to select interactively each region of interest on the image of the tapestry. The mean values of the pixels located in each region were calculated for each colour plane to give a set of pixel states that defined the sample colours. The number of sample colours was determined by inspecting the number of distinct dyed areas on the front and reverse images of the tapestry and the shade variations in each of these areas.

Spatial segmentation of the tapestry image utilised a further clustering algorithm: Each pixel in the image was clustered to the sample colour with the nearest centre point and the pixel was labelled with an integer that represents its cluster. A binary mask for each cluster is produced which denotes the pixels belonging to that cluster by 1s, with 0s elsewhere. The sum of all of these masks encompasses every pixel in the original image.

Global segmentation of the image does not take into account the spatial information, which resulted in noisy masks and incorrect classification of pixels. Recent research in image analysis has developed segmentation algorithms that classify pixels based on colour and location (Chen and Lu, 2002. Botte-Lecocq *et al.,* 2007. Zhao *et al.,* 2008) or shape (Le Moan *et al.,* 2010). All of these methods involved testing for connectivity and similarity among neighbouring pixels.

Local segmentation algorithms in MATLAB software were explored, however, it was not the objective to develop an unsupervised method of image segmentation due to

the complexity of the tapestry subject. For the recolouration project, the classification of the pixels of the front of the tapestry was also influenced by the characteristics of the tapestry reverse. Interactive modification of the region masks was necessary to distinguish the dyed areas that had completely photo faded from each other. Adobe Photoshop image processing software was used for removing the noise from the masks produced by MATLAB and for localised segmentation into regions of different dyes.

5.3.4.2 Transforming population distributions of masks

The objective of this pilot study was to recolour the image of the front of the *Lion* tapestry so that the colours matched those of the corresponding areas on the reverse of the tapestry. The recolouration was achieved by transforming the distributions of the colours on the front to match target distributions selected from the reverse.

The set of masks described in the previous section defined the locations of the pixels that belong to a set of coloured regions. Each of these coloured regions contained a distribution of pixel values in each colour plane that was represented by the mean, minimum and maximum values.

Target colours were manually sampled after visually inspecting each of the masks of the front image and determining an area of the reverse image that best represented the required target colour. The target colours were sampled using the function **`roipoly`** to select interactively each of the chosen areas of interest on the image of the reverse. The mean, minimum and maximum values of the pixels located in each region were calculated for each RGB colour plane. This set of data represented the distributions of the target colours from the tapestry reverse.

Each mask was assigned a target colour. The transformation of the distribution of the pixel values in each mask was performed in each of the RGB colour planes. The mean of the front (sample) distribution was shifted to match the mean of the target distribution and the range of the sample distribution was transformed to match the range of the target distribution using the mathematical operation given in Equations

15-17. The recolouration of the image of the front of the tapestry was complete after the distributions of each mask had been transformed.

$Let\ P_S\ be\ a\ pixel\ value\ in\ the\ sample\ image$

$Let\ P_N\ be\ the\ new\ pixel\ value\ in\ the\ sample\ image$

$Mean_S = mean\ of\ the\ pixel\ values\ in\ the\ sample\ image$

$Mean_T, Min_T, Max_T = mean, minimum, maximum\ of\ the\ target\ values$

$Mean_N, Min_N, Max_N = mean, minimum, maximum\ of\ the\ new\ pixel\ values$

$$\boldsymbol{P_N = P_S + (Mean_T - Mean_S)} \qquad \textbf{Equation 15}$$

$if\ P_N < Mean_N$

$$\boldsymbol{P_N = Mean_T - \left(\left(\frac{Mean_N - P_N}{Mean_N - Min_N}\right) * (Mean_T - Min_T)\right)} \qquad \textbf{Equation 16}$$

$if\ P_N \geq Mean_N$

$$\boldsymbol{P_N = Mean_T + \left(\left(\frac{P_N - Mean_N}{Max_N - Mean_N}\right) * (Max_T - Mean_T)\right)} \qquad \textbf{Equation 17}$$

5.3.4.3 Summary of functions utilised during recolouration

MATLAB functions	Input	Output
medfilt2.m Median filter used to reduce the texture in the tapestry image	• 2D matrix (single plane of sample image) • Size of neighbourhood	• Median value of the M-by-N neighbourhood
edge.m Sobel and Canny methods used to detect edges in the image	• Intensity image (single plane of sample image) • Method of edge detection e.g. ('sobel','canny') • Sensitivity threshold value(s) • Standard deviation of Gaussian filter (Canny method)	• Binary image of the same size as the sample image with 1s where the edges are found and 0s elsewhere • Threshold value(s)
makecform.m Creates the colour transformation structure	• Type of colour space conversion i.e. 'srgb2lab'	• Colour transformation structure
applycform.m Applies the colour space transformation specified in makecform	• Image • Colour transformation structure	• Converted colour image

Custom functions	• Input	• Output
clusty.m Locates cluster centres based on unique pixel states in the image, clusters the pixels to the nearest cluster centre and produces masks of coloured regions	• Image • Specify clustering in RGB (0) or L*a*b* (1) • Show patches of cluster colour (1)	• RGB or L*a*b* values of cluster centres • Binary masks of the segmented image
Recolouration.m Semi-automated function to recolour the coloured regions of an image to a set of target colours. Masks of coloured regions are produced by automatic selection of clusters	• Sample image (front) • Target image (reverse) • Specify clustering in RGB (0) or L*a*b* (1)	• RGB or L*a*b* values of cluster centres • Binary masks of the segmented image • List of mean, min, max values of target colours • Target colour assignments • Recoloured image
Recolouration3.m Function to recolour the coloured regions of an image to a set of target colours. Masks of coloured regions are produced from a set of manually selected sample colours	• Sample image (front) • Target image (reverse) • Number of target colours • Filter the image (1)	• Pixel values of cluster centres • List of mean, min, max values of target colours • Image with pixels labelled with the nearest cluster • Binary masks of the segmented image • Recoloured image
selcols.m Function to find the distribution of pixel values in a region of interest	• Image • Number of colours to select	• List of mean, min, max values of each selected area
fn_popshift.m Recolours mask regions by shifting the distribution of pixel values to a target distribution	• Population distribution of target colour • Sample image • Binary mask of sample colour	• Recoloured image
imcolcount.m Lists the values and frequency of each unique pixel state in the image	• Image	• Unique pixel states in the image • Frequency of each pixel state
labelclusts.m Labels each pixel by its nearest	• Image • Pixel states of cluster centres	• Image with pixels labelled with the nearest cluster

cluster		
kNearestNeighbours.m Finds the nearest cluster centre for each pixel	• Pixel states of cluster centres • Image • Number of nearest neighbours	• Image with pixels labelled with the nearest cluster

5.3.4.4 Semi-automated method of recolouration

The following section describes a semi-automated method used to recolour both a test image and the image of the front of the *Lion* tapestry. The function **`Recolouration.m`** follows the concepts described in the previous sections of image segmentation and recolouration, implementing MATLAB and custom written functions to produce a recoloured image. This method is described as semi-automated due to its use of the automatic selection of clusters described in 5.3.4.1 and performed by the subfunction **`clusty.m`**.

The **`clusty`** function is implemented to create masks of the segmented sample image. The results can be controlled in a number of ways; by limiting the number of clusters that are defined; by specifying the minimum number of pixels that constitute a new cluster; and by specifying the threshold value for the Euclidean distance that determines if a unique pixel state belongs to a cluster. The clustering can be implemented in RGB or L*a*b* colour space.

The **`selcols`** function is used to select colours from the target image; the number of target colours is variable. An area of the target image is selected interactively by drawing a rectangle, then the mean, minimum and maximum pixel values are calculated in each RGB colour plane of the image. These values represent the distribution of each target colour and are listed in the output of the function.

The regions of the masks are then visually inspected to assign a target colour to each of the masks of the sample image. This part of the process must be performed interactively and the results are entered manually into a 1 x M array, **`assoc_cols`**, where M is the number of masks.

The recolouration of each mask region of the sample image is executed in the **fn_popshift** function. The distribution information of the target colour assigned to the mask, the mask itself, and the sample image are sent to the function. **fn_popshift** calculates the population distribution of the pixels in the sample image that are contained in the mask. The mean is calculated in the three planes and then shifted to the mean of the target distribution in each plane. The mean is recalculated with the shifted distribution along with the minimum and maximum values. The range of the sample distribution is adjusted to match the range of the target distribution. This operation is carried out for each of the masks and once all of the masks have been recoloured, the complete recoloured image is returned.

a.

b.

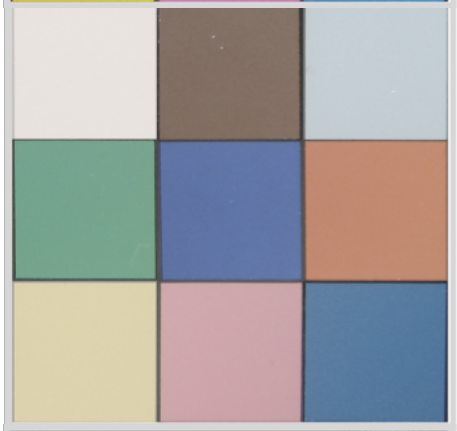

c.

d.

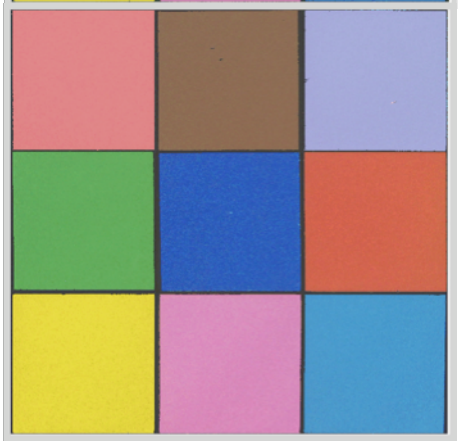

Semi-automated method used for recolouration of a test image

A target image (a) was created by copying patches from an image of the X-Rite ColorChecker Chart in Photoshop.

Each of the patches was adjusted to varying degrees in Hue, Saturation and Lightness to simulate the colour changes due to photo-fading in the tapestry. This created the sample image (b)

The **`Recolouration.m`** function was implemented using the sample image (b) and the target image (a).

The **`clusty`** subfunction automatically creates masks of the popular colours in the sample image (b) up to a maximum of 100. The minimum size of cluster was set to 50 pixels. The function returned 24 masks when clustering in RGB color space and 48 masks when clustering in L*a*b*.

The target colours were selected from the target image (a) using the **`selcols`** subfunction by drawing rectangles in areas of different colour. 11 target colours were selected including the 9 coloured patches, the black borders around the patches and a white border at the edge of the image. The mean, maximum and minimum values, in each of the three planes of the target colours were stored in **`list`**

The masks of the sample image were viewed and assigned one of the target colours. This data was stored in **`assoc_cols`**

The values of the target colour assigned to each of the masks of the sample image, the sample image itself, and the masks were sent to the **`fn_popshift`** subfunction. This function calculates the distribution, in each plane, of the pixels in each mask and shifts them to the distributions of the target colours. The recoloured image is returned to the main function. Images (c) and (d) were produced from clustering in RGB and L*a*b* respectively

Figure 5.3.10a Test target image of coloured squares, 5.3.10b Test sample image of faded coloured squares, 5.3.10c Result of recolouration.m in RGB 5.3.10d result of recolouration.m in L*a*b*

a.

b.

c.

d.

The **`Recolouration.m`** function was carried out on a tapestry fragment that had suffered similar photo-fading to the *Abraham* tapestry. The *Lion* tapestry fragment was used in pilot studies due to its more manageable size.

Images of the front and reverse of the tapestry were sent to the function **`Recolouration`**

Clustering of the front image (a) was carried out by the **`clusty`** subfunction in both RGB and L*a*b* colour spaces. The minimum number of pixels that constitute a cluster was set to 50, the maximum number of clusters was 100. The subfunction returned 43 masks when clustering in RGB and 100 masks for L*a*b*.

The target colours were selected from the reverse image (b) using the **`selcols`** subfunction. The user inputs the number of target colours into a dialog box. 24 target colours were used for the first recolouration (RGB) and 26 were chosen for the second recolouration (L*a*b*). The mean, maximum and minimum values, in each of the three planes of the target colours were stored in **`list`**

The masks of the front image (a) were viewed and assigned one of the target colours. This data is entered by the user into a dialog box and stored in the variable **`assoc_cols`**

Each mask, the target distribution for that mask (**`list(assoc_cols(:))`**) and the front image are sent to the **`fn_popshift`** subfunction. This function calculates the distribution, in each plane, of the pixels of the front image defined by each mask and shifts them to the distribution of the target colour. The recoloured image is returned to the main function. Images (c) and (d) were produced from clustering in RGB and L*a*b* respectively

Figure 5.3.11a Sample image of front of *Lion* tapestry, 5.3.11b Target image of reverse of *Lion* tapestry, 5.3.11c Result of recolouration.m in RGB 5.3.11d result of recolouration.m in L*a*b*

Clustering of the image was automatically performed first in RGB then in L*a*b* colour space by the **`clusty`** function that bases the cluster centres on the unique pixel states present in the image. This method of segmentation is a global operation whereby the locations of the pixels is not considered when creating regions of similar colour. The recoloured images that are the result of the recolouration.m function using the RGB and L*a*b* clusters are shown in Figures 5.3.11c and 5.3.11d respectively. Both of the recoloured images are clearly an improvement on the colour range of the faded tapestry front. The image obtained using the RGB clusters better matches the colour range of the tapestry reverse than the image obtained using the L*a*b* clusters. The recolouration of the background pattern in the RGB result is better than that in the L*a*b* result, however, a larger portion of the pillar in the RGB result has been incorrectly recoloured using the purple shade. Both images also show pollution by the purple shade of the green strips at the top and bottom of the tapestry. However, the recolouration of the right hand side of the image and the reproduction of the red, orange, yellow and blue shades are well executed by both methods.

As Figure 5.3.11a shows, the front of the tapestry is heavily faded in areas, particularly in the background pattern, which results in a large portion of the pixels having a neutral colour. When the reverse of the tapestry, shown in Figure 5.3.11b, is compared to the front, it is clear that several different coloured regions, purple, yellow, pink and neutral that are distinct on the reverse are indistinguishable on the front image. The pixel states that define these now neutral areas all fall into a small range so that when segmentation of the image into regions of similar colour is performed, the neutral pixels are clustered to the same colour. This leads to creation of masks that do not distinguish between some grey and purple pixels for example so that when either of these target colours is assigned to the mask, a number of pixels will be misrepresented. The incorrect recolouration of the grey pillar and the green strips to the purple shade in Figure 5.3.11c is a result of this issue as is the presence of yellow and grey pixels in the background pattern in Figure 5.3.11d.

The global segmentation of the image by the recolouration function can be improved by performing spatial modifications on the masks. The masks are visually

inspected to determine the areas of the image that they cover. Improvement of the recolouration of the faded areas, achieved after modification of the masks is discussed further in section 5.3.4.6.

There were the maximum number of 100 masks created by clustering in L*a*b* colour space; however, visual inspection of the masks found that some areas of distinctly different colour i.e. dark blue and brown, on the front image were clustered to the same mask. This is attributed to the clustering algorithm being based on unique pixel states and the lower threshold value assigned to clusters in L*a*b* than in RGB. The clusty function selects the clusters from the most frequently occurring pixel states first, however, the large areas of lots of neutral shades on the tapestry will contain many different pixel states that would be perceived as the same colour. Given the low threshold value for the Euclidean distance between clusters, this results in many clusters being created with similar shades rather than the areas of different colour that are of interest.

The texture of the woven material is represented in the image by variations in the intensity of the pixel values. The texture in the image of the front of the tapestry is very distinct since the dyes have faded and the colours are lighter therefore the contrast between the light and dark areas caused by the weave is large. In the image of the reverse of the tapestry the colour of the dyes is deeper than on the front so the contrast is smaller and the texture is less visible. Consequently the range of the distributions of areas on the front will be greater than those on the reverse. The texture of the tapestry also affects the results of image segmentation based on similar pixel values whereby the darker shades of the texture are masked as a different colour to the surrounding area. The texture may be labelled as a darker shade of the colour or even a completely different hue. This means that when recolouring, the texture on the image of the front is conspicuous and is often detrimental to the overall recolouration effect.

Visual inspection and modification of the masks to remove the noise in the binary images improves the performance of the recolouration function. This process is discussed further in section 5.3.4.6.

5.3.4.5 Manual method of recolouration

The following section describes a function **Recolouration3.m** that performs image segmentation using a set of clusters that are sampled manually using the subfunction **selcols.m**. The subsequent sampling of target colours and recolouration of the sample colours in the image is carried out using the same method as in **Recolouration.m.** This method of manually selecting the sample colours by visually inspecting the image of the front of the tapestry ensures that the sample colours represent the full range of coloured regions in the image.

The function **Recolouration3.m** allows the option for removing some of the texture in the image by implementing a median filter at the beginning of the process. The sample colours are selected from the filtered image and the clustering algorithm is performed on the filtered image, however, the recolouration is carried out on the original, unfiltered, image.

The subfunction **selcols** is implemented to select regions of colour on the image as described in the previous section, however, in the manual method the sample colours are selected from the image of the front of the tapestry and the corresponding target colours are selected from the image of the reverse. Visual inspection of the tapestry images determines the number coloured regions required to cover the full range of different dyed areas. The mean values of the pixels in the regions selected for the sample colours form the cluster centres. The distributions of pixel values in the target regions are used for recolouration.

Clustering and labelling of the pixels in the front image is performed by the **labelclusts.m** function that implements the subfunction **kNearestNeighbours.m** to calculate Euclidean distances between a pixel and each cluster centre and label pixel with the number of the nearest cluster. The binary masks of the coloured regions associated with each cluster are then produced.

The recolouration of the pixels in the mask regions is carried out by the function **fn_popshift.m** using the same method described in the previous section; the

distributions of the pixels on the front are shifted to the target distributions. The recoloured image is returned once all of the masks have been recoloured.

a.

b.

c.

d.

The **`Recolouration3.m`** function was carried out on the *Lion* tapestry fragment. Images of the front (sample) and reverse (target) of the tapestry were sent to the function **`Recolouration3.m`**

Median filtering of the sample image (a) was performed using a [5 5] neighbourhood if the filtering option was chosen. The filtered image was used for sample colour selection and for clustering. The original unfiltered image was recoloured by the function.

The user determines the number of sampling colours after visual inspection of the sample image (a) and the target image (b). 38 coloured regions were chosen.

The 38 sample colours were selected from the front image (a), or the filtered front image, using the **`selcols`** subfunction. The cluster centres were calculated from the mean pixel values of the sample areas.

Clustering of the front image (a), or the filtered front image, was carried out by the **`labelclusts`** subfunction The 38 masks, representing the locations of the pixels belonging to each cluster, were produced.

The areas of the 38 corresponding target colours were selected on the reverse image (b) using the **`selcols`** subfunction. The mean, maximum and minimum values, in each of the colour planes, of the target colours were stored in **`list_targ.`**

Each mask, the corresponding target distribution and the front image (a) were sent to the **`fn_popshift`** subfunction. This function calculates the distribution, in each plane, of the pixels of the front image defined by each mask and shifts them to the distribution of the target colour. The recoloured images (c) and (d) were returned to the main function. Image (d) was generated by masks created from the filtered image.

Figure 5.3.12a Sample image of front of *Lion* tapestry, 5.3.12b Target image of reverse of *Lion* tapestry, 5.3.12c Result of recolouration3.m on sample image 5.3.12d Result of recolouration3.m using filtered image

Figures 5.3.12c and 5.3.12d show the recoloured images produced by the recolouration3.m function. The method used to create the second image differs from the first in that it uses a filtered image of the front for selection of the sample colours and clustering of the pixels to those sample colours. The effect of the filter can be seen in Figure 5.3.12d on the body of the lion for example; the coloured regions are distinct and form patches rather than the gradual shading present on the reverse image and in Figure 5.3.12c. However, the effect of filtering the image has improved the recolouration of the background pattern, this is attributed to the removal of the texture in the image. The texture is clearly evident in the background pattern of Figure 5.3.12c due to the over-segmentation of pixel states in this area that leads to incorrect recolouration; the areas of the background pattern that should be purple have been coloured with both purple and grey shades. The removal of some of the texture using a median filter results in better region segmentation.

The manual sampling of the coloured regions produces a better range of sample colours than was produced by automatic selection. Visual inspection of the front and reverse images of the tapestry indicates several shades of brown and a distinct tan shade that can be individually selected. There is also a subtle variation in the shades of red present on the tapestry that is not detected with the automatic method. Many of the deeper shades in the tapestry such as the dark brown and dark blue areas were clustered to the black border by the automatic method so that these areas were recoloured as solid black. This mistake ruins the subtle colour balance present in the tapestry. The manual method of sampling proved to be superior to the automatic method in this aspect.

As can been seen from the incorrect recolouration of some areas of the pillar in Figures 5.3.12c and 5.3.12d, an issue that was previously noted in the recoloured images produced by the semi-automated method, the masks produced by this method are insufficient in region segmentation. This issue is especially consequential in those areas of different dyes that have faded to a similar neutral shade.

5.3.4.6 Improving the recolouration by spatial segmentation

The semi-automated method of recolouration produced a good representation of the original appearance of the *Lion* tapestry, however, there were some areas that were inaccurate. Figure 5.3.13 shows the image **`rgb2`** that was produced using the **`recolouration.m`** function that utilised 43 masks and 24 target colours to recolour the tapestry front image in RGB colour space. The background colour has not been reproduced accurately due to automatic clustering of the pixels. The automatic clustering method cannot distinguish between pixels that are located in the pillar, which were originally grey, and pixels located in the background, which were originally purple, due to the complete photo-fading of the purple dye. This causes these two areas to be grouped together into the same clusters that must be recoloured to either grey or purple. Therefore areas on the pillar are incorrectly recoloured as purple and similarly areas in the background are incorrectly recoloured as grey. This issue is also evident in the green strips at the top and bottom of the tapestry. The problem of incorrect recolouration is extended all across the image of the tapestry: due to the texture of the woven material there are many unique pixel states that contribute to a single dyed area and these pixel states are often clustered to a mask that is not representative of their original colour. This is evident from the noise that is present in all of the masks. The texture on the front of the tapestry is more noticeable than on the reverse due to the photo-fading of the dyes to lighter shades, which increases the contrast of the woven material.

Figure 5.3.13 Result of recolouration.m function on *Lion* tapestry image in RGB colour space

In order to distinguish the separate areas of dyes, each of the masks were inspected visually and modified in Photoshop. The edge detection image **dEdges**, Figure 5.3.8, was layered with the image of the front, the recoloured image **rgb2**, and each of the 43 masks. The masks were inspected for spatial correlation with the edges and with the correct target colour. A new set of masks was produced that coordinated with an optimal set of target colours that had been determined by visual inspection of the tapestry and experience of the recolouration process. Some of the 43 masks were spatially partitioned into separate areas where the pixels contained in the mask belonged to areas of different dyes. These were then grouped together to create a set of 27 new masks that were recoloured to the set of 27 optimal target colours. The recoloured image that was produced is shown in Figure 5.3.14. This is the best result obtained for the recolouration of the *Lion* tapestry, which is due to the spatial segmentation of the masks. The colours in the pillar, which had proven problematic to recreate with the recolouration functions has been rendered correctly. In addition the red area that is visible at the top of the crown on the right hand side of the image, has been generated for the first time due to the creation of a specific mask for this area.

Figure 5.3.14 Optimal recoloured image of *Lion* tapestry generated as a result of spatial segmentation of masks

5.3.4.7 Discussion of the recolouration pilot study

The recolouration of the *Lion* tapestry has been successfully accomplished using a combination of image segmentation methods; Global segmentation operations

based on pixel properties partitioned the image into regions of similar pixel values; Global thresholding based on discontinuities in the pixel values detected edges in the image; and Local operations on the masks produced by the global method were performed that improved the region-based segmentation of the image.

A combination of these different methods was necessary to produce good results due to the complex nature of the image that was being recoloured. The texture of the woven material and the photo-fading of different dyed areas to similar neutral shades present a unique set of challenges for image segmentation. The recolouration method developed on the pilot study was fairly time-consuming due to the manual manipulation of masks; however, it has proven very successful. The process of shifting the distributions of pixel values restores the colour in the area while maintaining the texture and shading variations of the design. This results in a very realistic impression of the original colour appearance.

5.3.5 Recolouration of *Abraham* tapestry

The recolouration method that was developed in the pilot study was applied to the high-definition (HD) image of *The Oath and Departure of Eliezer* that was captured with the calibrated RGB camera (Nikon D300). Segmentation of the image into different dyed regions was performed and the masks were adjusted manually to rectify any noisy or incorrectly segmented areas. The masks were visually inspected with images of the front and reverse of the tapestry to ensure that each different dyed area was correctly partitioned.

The areas of tarnished metallic threads on the *Abraham* presented a challenge that had not been approached in the pilot study, as the *Lion* tapestry did not contain any metallic threads. Masks were created specifically for areas of gold and silver threads. The locations of these areas were determined by thorough visual examination of the tapestry reverse with guidance from the experienced conservators at Hampton Court Palace. A large portion of the background in the tapestry border and large areas on the figures in the design were found to consist of metallic threads, either gold or silver in colour. These areas were digitally restored using texture mapping from images of the untarnished gold and silver areas on the reverse. The masks of the gold and silver regions were populated using the *clone* tool of Adobe Photoshop, from the calibrated images of the reverse.

The masks of the different dyed regions were recoloured using the method developed in the pilot study whereby the distributions of pixels in the sample (front) image are transformed to match the coordinates of target colours. The target colours were retrieved from the colorimetric data collected of the model dyed tapestry samples. The recolouration was performed in CIELAB colour space using the L* C* h values of the target colour assigned to each mask and the HD image of the front of the tapestry. The camera RGB values were first converted to XYZ values that were then transformed to CIELAB L* a* b* coordinates using the *xyz2lab* function in the Colour Toolbox written by Westland and Ripamonti (2004). The C* and h* values are easily computed from a* and b*. After image processing is complete, the image is converted back to RGB values that are required for the projection.

The use of the model dyed tapestry samples as the target colours for the recolouration allows the gradual fading of the tapestry to be simulated from the gradual fading profiles of the dyes. The dyed samples were photo-aged for a total of 500 hours, which equates to 500 years of museum light exposure, and colour measurements taken after 100 hours, 300 hours and 500 hours of exposure. The data was interpolated using polynomials to predict the colour coordinates of the dyed fabric after 200 hours and 400 hours of exposure. As discussed in Chapter 3, the tarnishing of metallic threads on the different dyed tapestry samples occurred at variable rates, which suggests the tarnishing process over the whole tapestry, as a function of time, was extremely complex. In order to simulate the gradual tarnishing of the metallic thread on the tapestry, the colour difference between the front and reverse metallic areas was assumed to be a linear process and the colour coordinates for the intervening time periods were estimated. This led to the creation of a set of 5 recoloured images that predicted the appearance of the tapestry at 100, 200, 300, 400 and 500 years after its manufacture.

5.4 Projector characterisation

The projector that was used for the virtual restoration of the tapestry was a Panasonic PT-DW10000 DLP (Digital Light Projector), which had a high-definition resolution of 1920 x 1080 pixels.

Device calibration attempts to set an imaging device to a known state and ensures that the device is producing consistent results. Characterisation is the relationship between device-dependent coordinates usually RGB and some device independent colour space such as CIE XYZ. The Gain-Offset-Gamma (GOG) model is a physical model of a visual display unit based on a cathode ray tube (CRT) that has been used for the characterisation of many display devices (Berns et al. 1993a, 1993b). The GOG model linearises the relationship between the voltage applied to the CRT's phosphors and the displayed luminance. Once the GOG model has linearised the DAC values linear transformations can be applied to generate a linear mapping between device dependent (RGB) coordinates and device independent coordinates (XYZ).

$$R = \left(\frac{ad_r}{\left(2^N - 1\right)} + \left(1 - a\right) \right)^{\gamma}$$ **Equation 18**

Equation 18 shows a GOG model equation used to normalise and linearise the red channel where the system gain and offset are assumed to be unity.

Once the GOG model has been used to linearise the DAC values, the values can be related to CIE tristimulus values using a simple linear transform as seen in Equation 19.

$$\begin{bmatrix} X \\ Y \\ Z \end{bmatrix} = \begin{bmatrix} X_{r,\max} & X_{g,\max} & X_{b,\max} \\ Y_{r,\max} & Y_{g,\max} & Y_{b,\max} \\ Z_{r,\max} & Z_{g,\max} & Z_{b,\max} \end{bmatrix} \begin{bmatrix} R \\ G \\ B \end{bmatrix}$$ **Equation 19**

Although the GOG approach has been adopted in the literature when characterising projectors (Kwak & MacDonald, 2000) more recent work suggests that including the white CIE Tristimulus values when calculating the transfer matrix may be beneficial

when attempting to characterise a DLP based projector (Wyble & Rosen, 2002; Wyble & Rosen, 2006).

$$\begin{bmatrix} X \\ Y \\ Z \end{bmatrix} = \begin{bmatrix} X_{r,\max} & X_{g,\max} & X_{b,\max} & X_{w,\max} \\ Y_{r,\max} & Y_{g,\max} & Y_{b,\max} & Y_{w,\max} \\ Z_{r,\max} & Z_{g,\max} & Z_{b,\max} & Z_{w,\max} \end{bmatrix} \begin{bmatrix} R \\ G \\ B \end{bmatrix} \qquad \textbf{Equation 20}$$

The Wyble model (see Equation 20) uses RGBW basis vectors in order to calibrate DLP projectors.

5.4.1 Analysis of temporal stability of the projector

The temporal luminance stability of the projector was determined by measuring the projector output reflected off a white screen using the following method:

1. Measurements were taken in a darkened room at The University of Manchester to eliminate errors due to ambient light
2. The projector was controlled by a laptop on which MATLAB was used to produce a full screen white image (RGB 255, 255, 255) at 1080 x 1920 resolution
3. The projector was placed in front of a white screen
4. Measurements were recorded as a function of time from when the projector was switched on until a stable output was achieved
5. Two sets of spectral data were collected by the PR-655, pointed directly at the white screen, at a distance of 50 centimetres and 150 centimetres
6. Readings were taken every 30 seconds for 42 minutes: 30 seconds
7. Readings were taken for luminance ($cd.m^{-2}$), CIE x and y values and CCT from the PR-655 display

A graph of luminance as a function of time for the projector is given in Figure 5.4.1. The average luminance value was calculated from data collected after 15 minutes to eliminate errors from the initial warm up period.

Average luminance: 414.6 $cd.m^{-2}$ Standard deviation: 1.3

Reading 2:44:30 after projector was switched on:

Luminance:	414.9 $cd.m^{-2}$
CCT:	6595 K
x:	0.307
y:	0.352

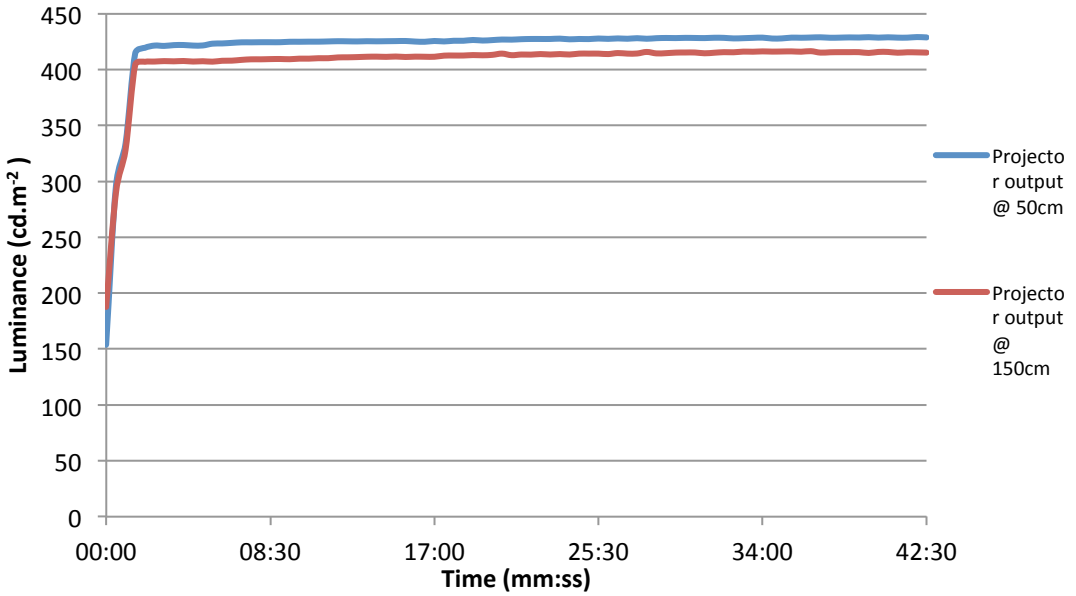

Figure 5.4.1 Graph of the temporal stability of the projector luminance

As seen from Figure 5.4.1, the luminance of the projector varied with time initially after the instrument was switched on; however, the output became relatively constant after approximately 5 minutes after which the values increased more gradually. The output of the projector, measured at a distance of 150 cm, stabilised at 416 cd.m^{-2} (±1 cd.m^{-2}) after 30 minutes of measurement.

5.4.2 Analysis of spatial uniformity of the projector

In order to correct for luminance differences across the image the spatial uniformity of the output from the projector was measured by taking reflectance measurements across the surface of a large white screen using the following method:

1. Measurements were taken in a lecture theatre at The University of Manchester
2. The ambient light in the room was measured
3. Spectral data was collected by the PR-655 which was pointed directly at a white screen, illuminated by the projector, at a distance of approximately 9 metres
4. The projector was outputting a full screen white image (RGB 255, 255, 255) at 1920 x 1080 resolution
5. The projector had been switched on for at least 10 minutes prior to measuring to allow the luminance values to stabilise

6. Readings were taken for luminance (cd.m^{-2}) from the PR-655 display
7. Measurements were taken at 17 positions across the white screen
8. Three sets of data were collected and the results averaged

The ambient light measured on the white screen in the room was 0.31 cd.m^{-2}. Figure 5.4.2 shows the luminance values across the whole of the projected image. The field was brightest in the bottom centre (40 cd.m^{-2}) and darkest in the top right corner (28.2 cd.m^{-2}). This information was used to modify the lightness values in the projected image.

Projector light reflected off a white screen				
30.9		31.1		28.2
	33.0	32.7	31.1	
31.5	34.2	35.0	31.8	28.6
	35.6	39.0	33.6	
32.5		40.0		31.3

Figure 5.4.2 Schematic of spatial uniformity of the projector: luminance measurements of reflected light across a white screen (cd.m^{-2})

5.4.3 Colorimetric performance of the projector

In order to determine the gamut of the projector a set of colour ramps were produced. Ten coloured patches were created, at equal intervals of intensity from 0 to 255, for each of the red, green and blue channels. These coloured patches were displayed full field and projected onto a white screen. Ten neutral patches were also created at equal intervals of RGB intensity from [0, 0, 0] to [255, 255, 255] and displayed for radiometric measurement with the PR-655. The projections were measured in a darkened room from a distance of 0.5 metres.

The chromaticities of the red, green, blue and white fields were measured by the PR655 and used to construct a transfer matrix, Equation 21, for the Panasonic PT-DW10000 DLP projector to convert XYZ tristimulus values to projector RGB.

$$\begin{bmatrix} X \\ Y \\ Z \end{bmatrix} = \begin{bmatrix} 0.6567 & 0.3306 & 0.1441 & 0.3102 \\ 0.3324 & 0.6408 & 0.0557 & 0.3523 \\ 0.0109 & 0.0286 & 0.8002 & 0.3375 \end{bmatrix} \begin{bmatrix} R \\ G \\ B \end{bmatrix} \qquad \textbf{Equation 21}$$

The chromaticities of the maximum red, green and blue channels were calculated and can be seen in Figure 5.4.3 along with the range of chromaticities of the model dyed tapestries. It can be seen that the chromaticities of the dyed fabrics fall inside the gamut of the projector, ensuring the projector is capable of reproducing the target colours.

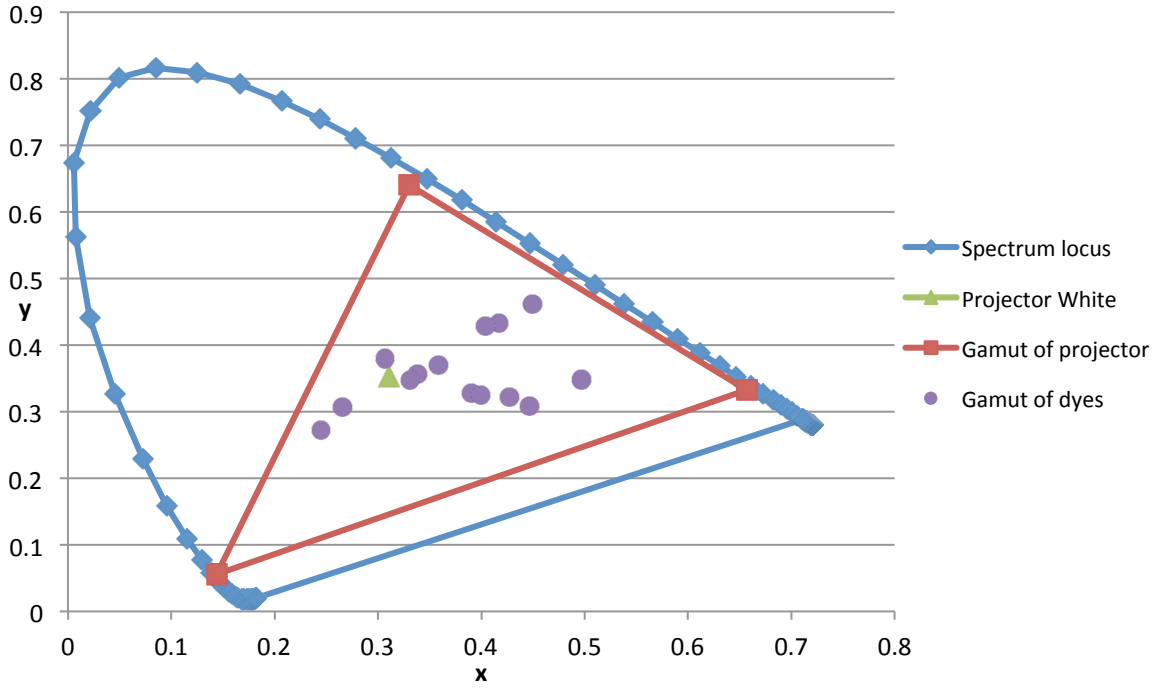

Figure 5.4.3 CIE Chromaticity diagram of the gamut of the Panasonic PT-DW10000 DLP projector and model dyed tapestry samples

Colour ramps were projected onto the tapestry. The PR-655 was used to capture radiometric measurements at specified points relating to particular dyed areas of the tapestry. Linear transformations were calculated based on these data and applied to the projected image.

5.5 'Tapestries Revealed' show

A display stand was specially constructed to hang the tapestry, which measures 8.4 x 4.8 metres, in the Queen's Guard Chamber for the recolouration show while the projector was mounted in a window recess opposite at a distance of around 13 metres. The display of the tapestry in a dedicated exhibition room has provided the opportunity to highlight the tapestry collection and has stimulated renewed interest in tapestries and their conservation. Visitors can appreciate the size and

magnificence of the tapestry when viewed in isolation as well as learning much more about the history and significance of Henry VIII's tapestries than is usually possible. The exhibition gives the viewer a realistic impression of how the tapestry would have appeared when first constructed and is virtually aged to show the effects of photo-ageing on the tapestry after 100, 200, 300 and 400 years. The 'Henry VIII's Tapestries Revealed' show was extremely popular with visitors; it was extended for nine months to a total of 18 months and was seen by over a million people.

The requirements for the show were a set of images that were displayed in conjunction with music and a voiceover commentary that tells the story of the tapestry's significance, its history of deterioration and the need for skilled and exacting conservation care. During the show the tapestry is illuminated with a series of images that recolour separate sections of the tapestry to highlight specific features and characters of the story. A gradual fading simulation was achieved by creating a set of recoloured images using the colour information of the 100, 300 and 500 hour photo-aged samples. The show took place five times during the day for an 18 month period and was presented at special evening events at the palace. At the back of the room there is an exhibition where visitors can learn about conserving tapestries and handle accurate replica samples of tapestry materials.

The conservators at Hampton Court Palace set an acceptable annual light dose for the tapestry of 150,000 lux hours. Calculations of the light budget ensured the annual light dose the tapestry would receive during the exhibition was within acceptable limits. The ambient light and the use of the Queen's Guard Chamber for evening functions and events were also taken into consideration. The show was scheduled five times per day, which amounted to no more than a few minutes of projector light exposure each day. Light monitoring showed that the total light dose was 100,000 lux hours for the period of April 2009 to January 2010, 50,000 less than the budgeted light level. The show's popularity and this lower-than-predicted exposure to light led to the exhibition being extended until the end of October 2010.

5.6 Discussion of the digital recolouration of the tapestry

The aim of the digital recolouration of *The Oath and Departure of Eliezer* was to restore the tapestry to its original appearance using entirely non-invasive methods. The virtual restoration has integrated techniques from textile conservation, colour science and imaging science to simulate a realistic impression of the tapestry appearance 500 years ago by projecting a calibrated image onto its surface. To achieve this firstly the current tapestry appearance was established by colorimetric analysis using the PR-655. Then the original appearance of the tapestry was predicted from two sets of data; fading profiles of replica tapestry materials in CIELAB colour coordinates and colorimetric analysis of the tapestry reverse using the PR-655.

The data collected using the PR-655 was calibrated by the SF600, producing a transform matrix to convert its readings into a device independent colour space, CIELAB. This means that the dye data and the tapestry data are comparable.

The calibrated CIELAB values of areas on the reverse of the tapestry were compared with the dye colours of replica samples, and classification of the tapestry areas by dye was determined from proximity in CIELAB colour space.

An image of the tapestry front was captured using a calibrated digital camera. RGB values were converted to XYZ tristimulus values and subsequently into CIELAB. A variety of global and local segmentation techniques were used to determine regions of similar colour in the image and masks were produced that specified the locations of the individual colours. The original, unfaded, colour of each of these regions was determined by the dye classification given to the corresponding area of the reverse of the tapestry. The lightness (L*), chroma (C*) and hue (h) distributions of each mask region were shifted in colour space to the coordinates of the original dye shade. The recoloured image exhibits much improved colour balance and is comparable to the appearance of the tapestry reverse.

Calibration of the recoloured image was performed to ensure colorimetric accuracy when projected onto the tapestry surface. The performance of the recolouration was limited by the resolution of the projector in that each pixel covered several threads of the tapestry, so that the projector could not resolve the details and

texture of the tapestry design. However, the composite effect of the projection onto the tapestry meant that the tapestry itself provided the detail and the projected image contained the colour components that are missing from the faded tapestry.

6 Conclusions and Further Work

6.1 Conclusions

This thesis has demonstrated the application of scientific research in a cultural heritage application to develop an exciting and entertaining way of communicating the important work of conservators to the public.

This research has achieved its aims to virtually restore a historic tapestry back to its original appearance, and to digitally conserve a colorimetrically accurate image of the tapestry. The research has also characterised tapestry materials and their photo- and thermal degradation properties, providing a valuable novel dataset for conservators that formed the basis of the digital recolouration of the tapestry.

The principal outcomes of this research are:

1. A better understanding of the ageing characteristics of tapestry materials. The data archive on historic dyestuffs for wool and silk has been expanded, providing a range of colour measurements of unfaded and photo-faded natural dyes. In addition, new information on the corrosion of metallic threads within the tapestry environment has been collected. The research into the fading characteristics of historic tapestries and their materials has led to increased knowledge and understanding of these complex processes.
    a. The creation of a novel dataset of the photo-fading profiles of natural dyes available in the 16th century. This will be an important resource for textile conservation and has been a critical component in predicting the original appearance of the 16th century tapestry *The Oath and Departure of Eliezer.*
        i. Colour measurement of the gradual photo-fading of dyed samples showed that undyed wool and silk samples increased in chroma after exposure to radiation, the photo-yellowing effect caused by the oxidation of amino acids.

ii. Identification of areas of the tapestry that exhibit similar fading characteristics to the natural dyes has allowed the classification of the tapestry into regions by dye.
iii. The original appearance of the tapestry was modelled on the photo-fading of natural dyes. The image was then recoloured to the colour coordinates of the newly dyed samples.

b. An investigation of the formation of corrosion on metallic threads
   i. EDX and XPS analysis shows the growth of corrosion products at the surface of the metal filament, which occludes the gold layer, forming Ag_2S, AgCl, Cu_2S, $CuSO_4$, metal oxides at the surface.
   ii. The SEM micrographs show the formation of corrosion products of various shapes, principally at the edges of the metal filament where the gold layer is thinner.
   iii. The corrosion rates of metals in different dye and fabric environments are variable, however, it was not clear if any dyes had particularly corrosive effects.
   iv. XPS analysis showed that photo-ageing of wool fibres led to an increase in sulphur content at the fibre surface in its S^{6+} oxidation state, which signifies the breaking of disulphide bonds in cystine to form cysteic acid.
   v. Photo-oxidation of sulphur in wool led to the formation of corrosion products on the metal surfaces during photo- and thermal ageing. Sulphur content at the surface of the samples was shown to correlate with the visual degradation of the metallic threads and coupons, which is attributed primarily to the formation of silver sulphide, which is black.
   vi. Sulphur content was higher on wool samples than on silk and visual degradation was worse on wool samples.

2. The development of a hyperspectal imaging system that collects the spectral and spatial information of the tapestry in a multidimensional image. This system was found to reconstruct the spectra of each pixel in an image to an accuracy of approximately 2 ΔE^*_{ab} units and produced more complete and

detailed set of data than is possible using a three-channel RGB system. This project has advanced the conservation application of scientific grade hyperspectral imaging systems and methodologies, generating precise spectral reflectance data of a textiles surface. The imaging methodology was developed in a complex environment where temperature, humidity and light conditions were uncontrolled and variable. As such the methodology can be reproduced in many environments where historic collections are commonly on display.

3. The digital conservation of a colorimetrically accurate image of *The Oath and Departure of Eliezer* tapestry. 170 sub-images of the front of the tapestry and 6 areas of the reverse were reconstructed. These images archive the colour information at every pixel location and will be used in future studies of studying the colour change of materials in the tapestry.
4. A digitally "virtually" restored a 16th century tapestry using a projected colour-calibrated image, for the 'Tapestries Revealed' exhibition at Hampton Court Palace:
    a. The restoration recreated, as closely as possible with the equipment available, the original appearance of the tapestry using non-invasive measurement methods.
    b. The show proved to be very popular with the public and has stimulated renewed interest in tapestries and conservation science.
5. The development of a recolouration algorithm that has different functionality for calculating the target colours and for use in different colour spaces. The algorithm uses global and local segmentation techniques to map the original dye colours to areas of the image where the dyes have been photo-faded.

6.2 Further work

- An investigation of the corrosion products of metallic threads and coupons could be extended with the use of other analytical methods such as ToFSIMS or X-Ray Diffraction.

- An investigation of the spectral characteristics of wool and silk dyed with natural dyes could be used to spectrally match areas of the tapestry to natural dyes. This dye mapping could be used on other historic textiles that have been profiled using spectral imaging, to predict the dye composition.

- An improvements to the performance of the hyperspectral imaging system could be made by using different calibration techiniques for example non-linear transformations or by adjusting the wavelength bands of the filterbank to increase the light transmission response in the poor signal regions.

- Colour measurements of the tarnishing of aged metallic threads could be modelled onto the tapestry where the different dyes are located to predict the gradual degradation of the tapestry.

- An improvement to the automation of the recolouration algorithm using different segmentation methods.

References

Abdel-Kareem, O. and Al-Saad, Z., 2007. Conservation strategy of metal embroidery threads in textile objects in Museum of Jordanian Heritage. *Proceedings of the International Conference on Strategies for Saving Indoor Metallic Collections*, pp. 23-30

Bamberger, J. A., Howe, E. G. and Wheeler, G., 1999. A variant Oddy test procedure for evaluating materials used in storage and display cases. *Studies in Conservation 44,* pp 86-90

Band, J., The survival of Henry VIII's *History of Abraham* tapestries: an account of how they were perceived, used and treated over the centuries. In: Lennard, F. and Hayward, M., 2006. *Tapestry Conservation: Principles and Practice.* Oxford: Butterworth-Heinemann. Ch. 3

Bearman, G.H. and Spiro, S.E., 1996. Archaeological applications of advanced imaging techniques. *The Biblical Archaeologist 59 (1),* pp. 56–66

Becker, M. A. and Tuross, N. C., 1993. Initial changes found in bombyx mori silk fibroin. In: D. Kaplan *et al* eds. *Silk Polymers: Materials Science and Biotechnology.* Charlottesville, Virginia: American Chemical Society, pp. 252-269

Berns, R. S., 2000. *Billmeyer and Saltzman's principles of color technology.* New York: Wiley

Berns, R. S., 2004. *Roy S. Berns, Ph. D. Research: Seurat.* [online] Available at: <http://www.cis.rit.edu/people/faculty/berns/seurat/meas_23.html> [Accessed 22/02/2011]

Berns, R. S., 2005. Color-accurate image archives using spectral imaging. *Scientific Examination of Art: Modern Techniques in Conservation and Analysis, National Academies Press,* pp. 105-119

Bowens, 2011. *Bowens continuous lighting: Unilite*. [online] Available at: <http://www.bowens.es/content/pages/unilite.html> [Accessed 9/02/2011]

Bradley, R. H. and Mathieson, I., 1997. Chemical interactions of ultraviolet light with wool fiber surfaces. *Journal of Colloid and Interface Science 194 (2),* pp. 338-343

Brosens, K. and Delmarcel, G., 2003. *Flemish tapestry in European and American collections: Studies in honour of Guy Delmarcel*. Turnhout, Belgium: Brepols

Cakir, A. F., Simsek, G. and Tezcan, H., 2006. Characterisation of gold gilt silver wires from five embroidered silk Qaaba curtains dated between the 16th and 19th centuries. *Applied Physics A – Materials Science & Processing 83,* pp. 503-511

Campbell, T., 2003. The *Story of Abraham* tapestries at Hampton Court Palace. In: Brosens, K. and Delmarcel, G., 2003. *Flemish tapestry in European and American collections: Studies in honour of Guy Delmarcel.* Turnhout, Belgium: Brepols. pp. 59-85

Candee, H. C. M., 1935. *The tapestry book.* New York: Tudor

Carr, C. M., Ho, S. F., Lewis, D. W., Owen, E. D. and Roberts, M. W., 1985. Photoelectron spectroscopy and the surface chemistry of wool. *Journal of the Textile Institute 76 (6),* pp. 419-424

Carr, C. M., Mitchell, R. and Howell, D., 2004. Surface chemical investigation into the cleaning procedures of ancient tapestry materials. Part 1. *Journal of Materials Science* 39, pp. 7317-7318

Carr, C. M., Mitchell, R. and Howell, D., 2004. Surface chemical investigation into the cleaning procedures of ancient tapestry materials. Parts 1 & 2. *Journal of Materials Science* 39

Cotte, P. and Dupraz, D., 2006. Spectral imaging of Leonardo Da Vinci's Mona Lisa: A true color smile without the influence of aged varnish. *Proceedings of Third European Conference on Color in Graphics, Imaging, and Vision*, pp. 311–317

CRi, 2011. *Products – Components – VariSpec: CRi*. [online] Available at: <http://www.cri-inc.com/products/varispec.asp> [Accessed 9/02/2011]

Daniels, V. and Ward, S., 1982. A rapid test for the detection of substances which will tarnish silver. *Studies in Conservation 27,* pp 58-60

Fischer, C. and Kakoulli, I., 2006. Multispectral and hyperspectral imaging technologies in conservation: current research and potential applications. *Reviews in Conservation* 7, pp. 3-16

Foster, D. H., Amano, K., Nascimento, S. M., and Foster, M. J., 2006. Frequency of metamerism in natural scenes. *Journal of the Optical Society of America A, Vol 23 (10),* pp. 2359-2372

Geijer, A., 1979. *A history of textile art.* London and Totowa N.J.: Pasold Research Fund in association with Sotheby Parke Bernet; distributed by Biblio Distribution Center

Gillespie, J. M., Broad, A. and Reis, P. J., 1969. Further study on the dietry-regulated biosynthesis of high-sulphur wool proteins. *Biochemical Journal 112,* pp. 41-49

Gonzalez, R. C., Woods, R. E. and Eddins, S. L., 2004. *Digital image processing using MATLAB.* New Jersey: Pearson Prentice Hall

Hacke, A. M., 2006. *Investigation into the Nature and Ageing of Tapestry Materials.* Ph. D. University of Manchester

Hacke, A. M., Carr, C. M., Brown, A. and Howell, D., 2003. Investigation into the nature of metal threads in a Renaissance tapestry and the cleaning of

tarnished silver by UV/Ozone (UVO) treatment. *Journal of Materials Science* 38

Hallett, K., Thickett, D., McPhail, D. S. and Chater, R. J., 2003. Application of SIMS to silver tarnish at the British Museum. *Applied Surface Science 203-204,* pp 789-792

Haneishi, H., Hasegawa, T., Hosoi, A., Yokoyama, Y., Tsumura, N. and Miyake, Y., 2000. System design for accurately estimating the spectral reflectance of art paintings. *Applied Optics 39 (35)*, pp. 6621-6632

Hayward, M., 2006. Fit for a king? Maintaining the early Tudor tapestry collection. In: Lennard, F. and Hayward, M., 2006. *Tapestry Conservation: Principles and Practice.* Oxford: Butterworth-Heinemann. Ch. 2

Hoke, E. and Petrascheck-Heim, I., 1977. Microprobe analysis of gilded silver threads from mediaeval textiles. *Studies in conservation 22,* pp. 49-62

Howell, D., Mitchell, R. and Carr, C. M., 2007. Surface chemical investigation into the cleaning procedures of historic tapestry materials. Part 2. *Journal of Materials Science* 42, pp. 5452-5457

Hunt, R. W. G., 1995. *The reproduction of colour.* Kingston-upon-Thames: Fountain Press

Hunter, G. L., 1925. *The practical book of tapestries.* London: J. B. Lippincott Co

Imai, F.H., Rosen, M.R. and Berns, R.S., 2000. Comparison of spectrally narrow-band capture versus wide-band with a priori sample analysis for spectral reflectance estimation. *Proc. of Eighth Color Imaging Conference: Color Science and Engineering, Systems, Technologies and Applications, IS&T/SID, Color Imaging Conference, Scottsdale, AZ, United States,* pp. 234-241

Imai, F. H., Rosen, M. R. and Berns, R. S., 2001. Multispectral imaging of Van Gogh's self-portrait at the National Gallery of Art, Washington, D.C. *Proceedings of PICS 2001: Image Processing, Image Quality, Image Capture Systems Conference, Montreal Quebec, Canada.* Society for Imaging Science and Texhnology, Springfield 185-189

Indictor, N., Koestler, R. J., Wypyski, M. and Wardwell, A. E., 1989. Metal threads made of proteinaceous substrates examined by scanning electron microscopy – energy dispersive x-ray spectrometry. *Studies in Conservation 34,* pp. 171-182

Jaro, M., 2009. Metal thread variations and materials. In: *Conserving Textiles: Studies in honour of Agnes Timar-Balazsy*. ICCROM Conservation Studies 7. Ch. 8

Járó, M., Gál, T. and Tóth, A., 2000. The characterization and deterioration of modern metallic threads. *Studies in conservation 45,* pp. 95-105

Johansen, K., 2009. Assessing the risk of wet-cleaning metal threads. In: *Conserving Textiles: Studies in honour of Agnes Timar-Balazsy*. ICCROM Conservation Studies 7. Ch. 9

Jones, L. N., Rivett, D. E. and Tucker, D. J., 1998. Wool and related mammalian fibres. In: M. Lewin and E. M. Pearce, eds. *Handbook of Fibre Chemistry.* New York: Marcel Dekker Inc, p 378

Karatzani, A., 2008. Study and analytical investigation of metal threads from Byzantine/Greek ecclesiastical textiles. *X-Ray Spectrometry 37,* pp.410-417

Launer, H., F. and Black, D., 1971. Gases produced from wool by light and heat. *Applied Polymer Symposium 18*, pp. 347 - 352

Leeder, J. D. and Marshall, R. C., 1982. Readily-extracted proteins from merino wool. *Textile Research Journal 52 (4),* pp. 245-249

Lennard, F. and Hayward, M., 2006. *Tapestry Conservation: Principles and Practice*. Oxford: Butterworth-Heinemann

Live Production, 2010. *The future of the living past. LIVE-PRODUCTION.TV.* [online] Available at <http://www.live-production.tv/news/cultural-events/future-living-past.html> [Accessed 18/08/2010]

Maclaren, J. A. and Milligan, B., 1981. *Wool Science – The Chemical Reactivity of the Wool Fibre.* Science Press

Marillier, H. C., 1931. *The tapestries at Hampton Court Palace.* London: Published for the Ministry of Works by H.M. Stationery Office

Martinez, K., Cupitt, J., Saunders, D. and Pillay, R., 2002. Ten years of art imaging research. *Proceedings of the IEEE 90 (1),* pp. 28–41

MIT, 2001. *Lecture 2 – 6.837 Fall '01.* [online] Available at: <http://groups.csail.mit.edu/graphics/classes/6.837/F01/Lecture02/Slide29.html> [Accessed 22/02/2011]

Nord, A. G. and Tronner, K., 2000. A note on the analysis of gilded metal embroidery threads. *Studies in Conservation 45,* pp. 274-279

Odlyha, M., Wang, Q., Foster, G. M., de Groot, J., Horton, M. and Bozec, L., 2005. Thermal analysis of model and historic tapestries. *Journal of Thermal Analysis and Calorimetry Vol 82,* pp 627-636

Photo Research, Inc., 2010. *Photo Research, Inc. - PR-655 SpectraScan Spectroradiometer.* [online] Available at: <http://www.photoresearch.com/current/pr655.asp> [Accessed 9/02/2011]

Pretzel, B. and Shibayama, N., 2003. Standard materials for corrosiveness testing. *V&A Conservation Journal 43*

QImaging, 2011. *QImaging Cameras: Retiga-4000R.* [online] Available at: <http://www.qimaging.com/products/cameras/scientific/retiga_4000r.php > [Accessed 9/02/2011]

Rice, D. W., Peterson, P., Rigby, E. B., Phipps, P. B. P., Cappell, R. J. and Tremoureux, R., 1981. Atmospheric corrosion of copper and silver. *Journal of the Electrochemical Society: Electrochemical Science and Technology Vol. 128, No. 2*, pp. 275-284

Rippon, J. A., 1992. The structure of wool. In: D. M. Lewis, ed. *Wool Dyeing.* Society of Dyers and Colourists, pp. 1-51

Robinet, L. and Thickett, D., 2003. A new methodology for accelerated corrosion testing. *Studies in Conservation 48*, pp 263-268

Robson, R. M., 1998. Silk: Composition, structure and properties. In: E. M. Pearce, ed. *Handbook of Fibre Chemistry.* New York: Marcel Dekker Inc, pp. 415-464

Rogerson, C. and Garside, P., 2006. Instrumental analysis of metal threads as an aid for interpretation and preservation of a fifteenth-century tapestry altar frontal and super frontal. In: *Tapestry Conservation: Principles and Practice.* Oxford: Butterworth-Heinemann. Ch. 6

Rosen, M.R., Imai, F.H., Jiang, X. and Ohta, N., 2001. Spectral reproduction from scene to hardcopy II: Image processing. *Proceedings of the SPIE, SPIE, SPIE, 4300, San Jose, California, United States,* pp. 33-41

Saunders, D., 1997/8. High-Quality Imaging at the National Gallery: Origins, Implementation and Applications. *Computers and the Humanities, Vol. 31, No.3*, pp. 153-167

Sease, C., Selwyn, L. S., Zubiate, S., Bowers, D. F. and Atkins, D. R., 1997. Problems with coated silver: Whisker formation and possible filiform corrosion. *Studies in Conservation 42,* pp. 1-10

Shao, J., Liu, J., Zheng, J. and Carr, C. M., 2002. X-ray photoelectron spectroscopic study of silk fibroin surface. *Polymer International 51 (12),* pp. 1479-1483

Swift, J. A. and Smith, J. R., 2001. Microscopical investigations on the epicuticle of mammalian keratin fibres. *Journal of Microscopy 204 (3),* pp. 203-211

The Rylands Cairo Genizah Collection, 2010. *Hyperspectral Imaging - The Rylands Cairo Genizah Collection.* [online] Available at <http://rylandsgenizah.wordpress.com/2010/12/07/hyperspectral-imaging/> [Accessed 24/03/2011]

The Rylands Collection, 2011. *Rylands Collection.* [online] Available at <http://enriqueta.man.ac.uk:8180/luna/servlet/Manchester~91~1;jsessionid=76462A41F8A99D3101845E8AF44B2981?cic=Manchester~91~1> [Accessed 24/03/2011]

Tronner, K., Nord, A. G., Sjostedt, J. and Hydman, H., 2002. Extremely thin gold layers on gilded silver threads. *Studies in Conservation 47,* pp.109-116

Westland, S. and Ripamonti, C., 2004. *Computational colour science using MATLAB.* Chichester: J. Wiley

Wyszecki, G. and Stiles, W. S., 1982. *Colour science : concepts and methods, quantitative data and formulae.* New York; Chichester, Wiley

Yanagi, Y., Kondo, Y. and Hirabayashi, K., 2000. Deterioration of silk fabrics and their crystallinity. *Textile Research Journal 70 (10),* pp. 871-875

Yang, C. J., Liang, C. H. and Liu, X., 2007. Tarnishing of silver in environments with sulphur contamination. *Anti-Corrosion Methods and Materials Vol. 54 Issue 1*, pp. 21-26

Zahn, H., Wortmann, F. J. and Hocker, H., 1997. Chemistry and the structure of wool. *Chemie in Unserer Zeit 31 (6),* pp. 280-290

Zhao, Y., Berns, R.S., Okumura, Y. and Taplin, L.A., 2005a. Improvement of Spectral Imaging by Pigment Mapping, *IS&T/SID, Thirteenth Color Imaging Conference, Scottsdale, Arizona, United States,* pp. 40-45

Zhao, Y., Taplin, L.A., Nezamabadi, M. and Berns, R.S., 2005b. Using the Matrix R Method for Spectral Image Archives. *Proc. of the 10th Congress of the International Colour Association, International Colour Association, 10th Congress of the International Colour Association, Granada, Spain,* pp. 469-472

Appendices

Appendix A The Story of Abraham tapestries as told in the Book of Genesis

1. God commands Abraham to lead the Israelites into Canaan, promising to bless him and his people (Genesis Book 12, versus 1-8). *The Departure of Abraham*
2. The Return of Sara by the Egyptians, following the discovery of the Pharaoh that she was Abraham's wife and not his sister as he had been led to believe (Gen 12:15-20)
3. The Separation of Abraham and Lot, to prevent further fighting among their tribesmen (Gen 13:8-9)
4. The Meeting of Abraham and Melchizedek, following Abraham's victory over the Elamites who had defeated and captured Lot (Gen 14:15-20)
5. God Appears to Abraham and promises him a son, he also warns him of the destruction of Sodom and Gomorrah. The escape of Lot and his daughters appears in the background (Gen 18:2-33)
6. The Circumcision of Isaac and the Expulsion of Hagar and Ishmael, symbolising the continuation of God's covenant with Abraham through his son Isaac and Abraham's dismissal of his concubine Hagar and their son into the dessert (Gen 18:1-21)
7. The Sacrifice of Isaac, according to God's command (Gen 22:5-18)
8. Abraham purchases the Field of Ephron, as a burial site for Sarah and himself (Gen 23:10-16)
9. The Oath and Departure of Eliezer, Abraham's faithful servant goes in search of a suitable wife for Isaac (Gen 24:1-10)
10. Eliezer and Rebekah at the well, when he recognises the qualities of a wife for Isaac, for which he was searching, in Rebekah (Gen 24:15-18)